Polymer Nanocomposite Foams with Enhanced Thermoelectric Efficiencies

Mohammadmehdi Aghelinejad

A DISSERTATION SUBMITTED TO

THE FACULTY OF GRADUATE STUDIES

IN PARTIAL FULFILLMENT OF THE REQUIREMENTS

FOR THE DEGREE OF

DOCTOR OF PHILOSOPHY

GRADUATE PROGRAM IN

MECHANICAL EGINEERING

YORK UNIVERSITY

TORONTO, ONTARIO

August 2019

Abstract

Over the past decades, alternative sources of energy have been the subject of extensive research due to the scarcity of fossil fuels and international concerns on greenhouse gas emission. Considerable efforts have been focused on developing thermoelectric (TE) materials and their applications in waste heat recovery, power generation, and refrigeration. Thermoelectric generators (TEGs) can harvest energy by converting waste heat into electricity. The advantages of TE power generators include solid-state operation, maintenance-free with long life-span, and negligible emission of greenhouse gases. Conventional semiconducting TE materials, as today's TE materials of choice, have many disadvantages such as high cost, scarcity, and toxicity.

In recent years, organic TE materials have attracted more attention because of their various advantages, such as light weight, low cost, flexibility, and simple synthesis. However, compared with their semiconducting counterparts, polymers have lower TE efficiencies, which have limited their applications. A fundamental challenge to improve the efficiency of polymeric TE materials is to simultaneously enhance their Seebeck coefficient and electrical conductivity while suppressing their thermal conductivity. In this context, the materials would have the electrical properties of a crystalline material and the thermal properties of an amorphous or glass-like material.

The proposed research aims to develop micro-and-nano structuring strategies, as novel processing techniques, to design and fabricate organic materials with promising TE efficiencies for future TEGs. Achieving this objective requires decoupling the highly interconnected TE parameters. The main idea of this research is to decrease the thermal conductivity of the material system by introducing a cellular structure in the bulk of material. Furthermore, incorporating

carbon nanoparticles as conducting fillers will help to improve the electrical conductivity of polymeric materials. As a result, the thermoelectric performance of the material system would be significantly enhanced.

This study showed that microcellular foaming is highly effective in enhancing the TE efficiency of polymer nanocomposites. The result of this research suggests micro/nano-cellular foaming as a novel fabrication method to promote the TE efficiency of polymeric materials. The proposed method provides an opportunity to develop polymer-based materials, as an environmentally friendly alternative for their semiconducting counterparts, for green energy harvesting.

Dedication

To my beloved wife, Laya, for her endless love and great support. I could never accomplish my PhD without her encouragement.

To my lovely son, Pedram, for coming into my life.

To mom and dad for their continuous love, care and support. Those who made me what I am today.

Acknowledgements

I would like to thank my supervisor, Prof. Siu Ning Leung for his kind support and valuable guidance during my entire PhD studies.

I am thankful to Prof. George Zhu, Prof. Alex Czekanski, and Prof. Roger Kempers for their recommendations on my thesis and their consideration as being my committee members. Special thanks to Prof. Patrick Lee and Prof. John Lam for their feedbacks and advices on my dissertation as my examiners.

Also, I would like to thank all my colleagues and friends at York university for their wonderful friendship and support. These people made my life and PhD studies enjoyable during the past few years.

Table of Contents

List of Tables

List of Figures

List of Abbreviations

CNT	Carbon nanotube
D.I.	Deionized
DSC	Differential scanning calorimetry
DC	Direct current
DWCNT	Doublewalled carbon nanotube
FLG	Few-layer graphene platelet
GF	Glass fiber
GnP	Graphene nanoplatelet
HDPE	High density polyethylene
ICP	Intrinsically conducting polymer
LBL	Layer by layer
MFP	Mean free path
MO	Methyl orange
MTPS	Modified transient plane source
MWCNT	Multiwalled carbon nanotube

NW	Nanowire
1D	One dimensional
PGEC	Phonon-glass electron-crystal
PA	Polyacetylene
PANI	Polyaniline
PC	Polycarbazole
PDMS	Poly(dimethylsiloxane)
PCDTBT	Poly[N-9’-heptadecanyl-2, 7-carbazole-alt-5, 5-(4’,7’-di-2-thienyl-2’,1’,3-benzothiadiazole)]
PPy	Polypyrrole
PS	Polystyrene
PSS	Polystyrene sulfonate
PEDOT	Poly(3,4- ethylenedioxythiophene)
P3OT	Poly(3-octylthiophene)
P3HT	Poly(3-hexylthiophene)
PTh	Poly-thiophene
PVAc	Polyvinyl acetate
PVA	Poly(vinyl alcohol)

PVDF	Polyvinylidene fluoride
PF	Power factor
SEM	Scanning electron microscopy
SWCNT	Singlewalled carbon nanotube
DOC	Sodium deoxycholate
SDS	Sodium dodecyl sulfate
Sc	Supercritical
TE	Thermoelectric
TEG	Thermoelectric generator
TCPP	Tetra(4-carboxyphenyl) porphine
3D	Three dimensional
2D	Two dimensional

List of Symbols

K_B	Boltzmann constant
ε_c	Carnot efficiency
n	Carrier charge concentration
μ	Carrier charge mobility
N_o	Cell population density
T_c	Cold-side temperature
ρ	Density
m^*	Effective mass of charge carriers
η	Efficiency
σ	Electrical conductivity
k_e	Electronic thermal conductivity
e	Electron charge
T_h	Hot-side temperature
k_l	Lattice thermal conductivity
L	Lorenz number
h	Planck's constant

PF	Power factor
S	Seebeck coefficient
T	Temperature
ΔT	Temperature difference
k	Thermal conductivity
ZT	Thermoelectric figure of merit
ΔV	Voltage difference

Chapter 1. Introduction

1.1 Preamble

Over past decades, considerable efforts have been made on developing thermoelectric (TE) materials and their utilization for energy-related applications such as waste heat recovery, power generation, air-conditioning, and refrigeration. Thermoelectric materials are designed to convert waste heat into electrical energy as a result of the Seebeck effect. They can also be used in solid-state refrigeration devices due to their Peltier effect. TE materials are most beneficial in fabricating thermoelectric generators (TEGs), where they can be utilized for green energy harvesting. The advantages of thermoelectric power generators include solid-state operation, silence in operation, absence of toxic residuals, environmentally friendly with negligible direct emissions of greenhouse gases, vast scalability, maintenance-free operation with the lack of moving parts or chemical reactions, and long lifespan of reliable service. However, because of the low energy conversion efficiencies of TE materials, current TEGs have found limited commercial application.

Semiconducting-based TE materials such as bismuth telluride alloys are current TE materials of choice. These materials provide superior TE efficiencies, which can be characterized by the dimensionless figure of merit (*ZT*). However, conventional semiconducting TE materials have several drawbacks such as high cost, scarcity, rigidity, high density, and toxicity. Moreover, because of their instability, they cannot be used at high temperatures in air. In recent years, organic materials have become attractive alternatives for TE applications despite their lower *ZT* values. Unlike semiconducting TE materials, polymers have various advantages such as lightweight, low

cost, flexibility, and simple synthesis. The potential to tailor the versatility of polymeric TE materials also represent another critical advantage, especially for wearable electronics.

1.2 Technology Gaps and Challenges

Polymers have very low TE efficiencies compared to their semiconducting counterparts. To improve the TE performance of polymeric materials, their electrical conductivity and Seebeck coefficients should be enhanced without compromising their low thermal conductivity. Developing TE materials with superior performances needs tailoring their inherent TE parameters. However, these three properties of materials are highly interrelated, which make it virtually impossible to increase the TE efficiency above certain level. An ideal TE material should have the electrical properties of crystalline materials and the thermal properties of glass-like materials.

Polymeric materials are intrinsically poor thermal conductors, which makes them excellent choices for TE applications. However, typical polymers have low electrical conductivities and low Seebeck coefficients, which adversely affects their TE performances. Intrinsically conducting polymers (ICPs) are mostly suggested by researchers for TE applications. ICPs provide high electrical conductivities and relatively good Seebeck coefficients, especially at high doping levels. However, their properties usually change over time due to oxidization in air. Their complicated synthesizing techniques are also considered as their disadvantages for any commercial applications.

A few studies have suggested the utilization of conventional non-conducting polymers for TE applications. The electron transport properties of polymer matrices can be significantly enhanced by adding conducting nanoparticles. Creating conductive filler networks within the polymer nanocomposite can potentially promote the electrical conductivity and the Seebeck coefficient of

the material. However, the introduced electrical contact resistance at a multitude of filler-filler junctions as well as at filler-polymer interfaces adversely affect the final electrical conductivity of the nanocomposite sample. Moreover, the incorporation of conducting fillers will increase the thermal conductivity of the polymer, which is detrimental for its TE efficiency.

A fundamental challenge in developing organic TE materials is to promote their electrical conductivity and Seebeck coefficient without compromising their low thermal conductivity. To achieve this aim, a new processing technique should be introduced to decouple their TE parameters to be able to tune them simultaneously. Consequently, the energy conversion efficiency of the fabricated material system will be effectively enhanced.

1.3 Research Goals and Objectives

The long-term goal of this study is to suggest a novel processing technique to develop new polymeric TE material systems that have improved TE efficiency, reduced weight, tailored multifunctionality, and simple manufacturability. To achieve this goal, the following short-term objectives are defined in the current dissertation:

i) to design and fabricate super thermal insulating polymeric samples. For this aim, different foaming strategies were introduced in this study.

ii) to design and fabricate polymer nanocomposite samples with high electrical conductivities and low percolation threshold values. To achieve this purpose, great control over the distribution of conducting fillers within polymer matrices is required. Therefore, a three dimensional (3D) conducting network throughout the bulk of polymeric samples can be created.

iii) to integrate and combine the suggested processing techniques in the previous phases of this research and fabricate polymer nanocomposite foams with improved TE conversion efficiencies.

The main idea of this study is to apply both foaming and micro-nanostructuring to simultaneously tune TE parameters and enhance the TE efficiency of organic materials. By introducing cellular structure within polymeric samples, their thermal conductivity will be significantly suppressed. Incorporating carbon nanoparticles as conducting nanofillers inside the polymer matrices will result in simultaneously promoting their electrical conductivities and Seebeck coefficients. This approach will potentially result in a remarkable improvement in the *ZT* value as a measure of the TE energy conversion efficiency.

With the aid of foaming techniques, super thermal insulating polymeric materials with nano/micro-cellular structures can be fabricated. By utilizing different foaming methods such as supercritical carbon dioxide foaming and salt leaching method, polymeric porous templates with both types of open-cell and closed-cell foam structures can be fabricated to provide high thermal insulation. In order to overcome low electrical conductivity of polymers, nanocomposite samples with low percolation threshold will be developed by arranging a conductive network of nanofillers throughout polymeric matrices. Consequently, novel polymer nanocomposite foams with high TE efficiency, high flexibility, and lightweight can be developed.

Incorporating hybrid 1D and 2D carbon nanoparticles within the polymeric foam samples will result in simultaneously promoting their electrical conductivity as well as Seebeck coefficient, and thereby enhancing their *ZT* values. The synergistic effects arising from the interaction among different conducting fillers can potentially facilitate the charge carrier transportation within their

networks. Using conducting types of polymers in combination with conducting nanofillers will also help to maximize the TE properties of organic materials. The effects of different processing parameters on the TE efficiency of the fabricated samples will also be investigated and optimized in this study. Different types of polymers and nanofillers, along with multiple foaming conditions will be examined to achieve the best thermoelectric efficiency.

1.4 Overview of the Thesis

This manuscript is organized in eight chapters covering different experimental studies on the design and fabrication of organic thermoelectric materials with enhanced energy conversion efficiencies. The research mainly focused on utilizing non-conducting polymers for TE applications due to their excellent mechanical features and good processability for fabricating thermoelectric generators.

Chapter two provides a brief review on the thermoelectric phenomenon, its applications, and different types of thermoelectric materials. This chapter reports a more in-depth study on polymer-based TE materials and various strategies to promote their efficiencies. Moreover, the physical properties of TE materials, their interrelation, and different parameters that can affect the carrier transport properties of these materials are discussed. This part of the dissertation aims to review the most recent research and developments in thermoelectric polymer nanocomposites, to better understand different challenges that impede the advancement of their TE properties.

In the third chapter, polypyrrole (PPy)/multiwalled carbon nanotubes (MWCNT) nanocomposite samples were fabricated, and their potential for TE applications was explored. PPy was used as a conducting type of polymer to provide good electron transport properties. A systematic experimental study was performed to investigate the effects of different processing

parameters on the TE performance of PPy/MWCNT nanocomposites. The effect of using different dopants on the morphology and TE properties of the nanocomposite samples were also examined in this phase of the research.

In chapter four, physical foaming is suggested as an innovative and effective processing strategy to simultaneously tune the TE properties of nanocomposite materials. The results of this phase of studies showed that incorporating thermally insulating air voids in nanocomposite foams significantly suppresses their thermal conductivities. Moreover, creating cellular structures within polymer nanocomposites helped to alter the localization of nanofillers and thereby control the formation of electrically conductive pathways in the polymer matrices. Consequently, this fabrication method led to a significant improvement in the TE efficiencies of the nanocomposite materials.

Freeze-drying method was utilized in chapter five to fabricate nanocomposite foams with improved TE properties. By in-situ polymerization of PPy, as a conducting type of polymer, within freeze-dried PVA foams, conducting networks for electron transferring through the insulative polymer matrices were created. The addition of graphene nanoplatelets throughout the material system helped to further promote the electrical conductivity and Seebeck coefficient and thereby the *ZT* value of the material. The effects of different processing parameters on the TE properties of the fabricated foams were investigated to optimize their properties. This study suggested a new technique to develop organic TE materials by using insulating polymer matrices to overcome the processing challenges and poor mechanical properties of conducting polymers as current polymeric TE materials of choice.

In chapter six, a simple and efficient processing technique is proposed to fabricate TE polymer nanocomposites with enhanced energy conversion efficiencies. This approach uses macroporous polymer foams with open cellular structures as templates to assist the formation of conductive filler networks within polymer matrices. As a case study, polyvinylidene fluoride (PVDF) foam templates were fabricated and coated with MWCNTs using deep coating method. The created 3D network of MWCNTs and the macro-porosity of the foam substrates helped to simultaneously promote the electrical conductivity and suppress the effective thermal conductivity of organic thermoelectric materials, and thereby enhance their TE efficiencies. In-situ polymerization of PPy during the template-assisted nanotube coating process, also promoted the Seebeck coefficient of the polymer nanocomposites, while suppressing their electrical conductivity. A series of parametric experiments were performed in this study to investigate the effects of open-cell morphology, nanotubes content, and PPy-MWCNT interfaces on the TE properties of organic materials.

The effects of filler hybridization (i.e., using one-dimensional and two-dimensional conducting nanofillers) on TE properties (i.e., electrical conductivity, thermal conductivity, and Seebeck coefficient) of nanocomposite foams have been thoroughly investigated in chapter seven. Layer by layer (LBL) deposition of MWCNTs and graphene nanoplatelets (GnPs) throughout the cellular structures of PVDF foams, resulted in a segregated network of conducting fillers. The results showed that the synergistic effects of the filler-filler junctions and filler-polymer interfaces help to simultaneously promote the electrical conductivity and the Seebeck coefficient of the material system without compromising its low thermal conductivity.

The last chapter (i.e., chapter eight) reports some concluding remarks and key contributions of different phases of the study. Several research strategies are also proposed, as potential future

plans, to enhance the TE performance of organic materials and make them viable for industrial applications in power generation.

Chapter 2. Literature Review

2.1 Thermoelectric Phenomenon

Global warming and energy crisis are the main concerns of human beings in 21st century. The environmental impacts and lack of resources of fossil fuels require developing new technologies to utilize different renewable energy sources such as solar, wind, and geothermal. On the other hand, the dissipation of a vast amount of energy in the form of waste heat from power plants and industries necessitates utilizing new techniques for thermal management. The statistics show that more than 60 percent of the produced energy is usually wasted to the environment in the form of heat (Figure 2.1) [1]. Recovering this enormous amount of waste heat would significantly save money while being beneficial for the environment in terms of reducing greenhouse gases. Recycling this excessive waste heat in another form of energy has recently been considered as an alternative low cost, environmentally friendly source of power.

During the last decades, thermoelectric phenomenon has drawn broad interests from researchers in two contexts: thermal management and energy harvesting. These two applications are based on the Peltier effect and the Seebeck effect, respectively. The schematic illustration of a TE module in both power generation and refrigeration modes is shown in Figure 2.2 [2]. When an electric current, flows through a junction of two dissimilar materials, it will either absorb or reject heat. This phenomenon occurs due to the Peltier effect and can be utilized for cooling applications such as for air-conditioning or in refrigeration [3]. The reverse phenomenon, the Seebeck effect, is related to the generation of electricity when a temperature gradient is imposed through a thermoelectric material [4]. In other words, TE materials can produce an electric potential when

they are exposed to a temperature gradient due to the material's Seebeck effect. The generated electric voltage is directly related to the temperature difference and the Seebeck coefficient of the material, as shown in Equation (2-1):

$$\Delta V = S\Delta T \tag{2-1}$$

where ΔV is the generated electric potential (μV), ΔT is the temperature difference (K), and S is the Seebeck coefficient (μVK^{-1}).

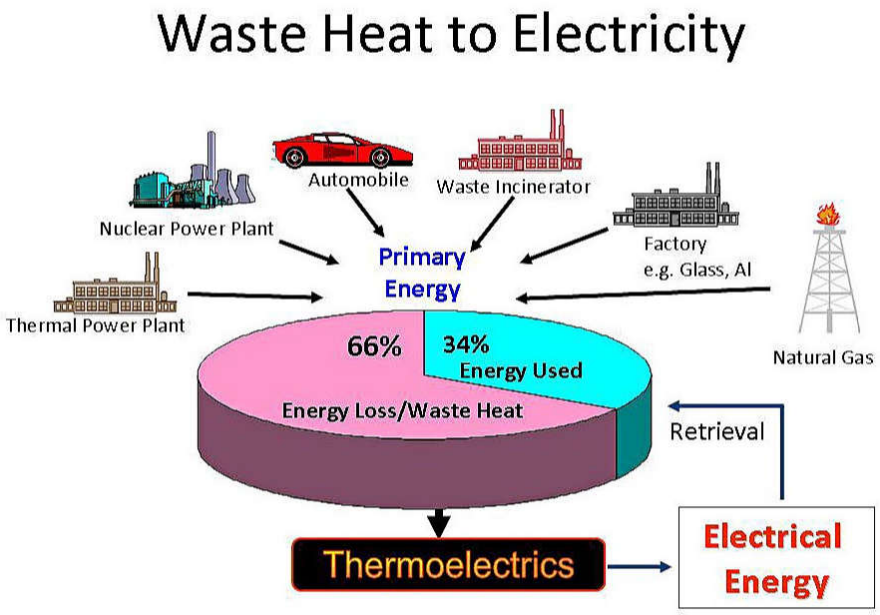

Figure 2.1 Potential sources of waste heat in real life for the application of thermoelectric materials. Adapted with permission from Ref. [1]

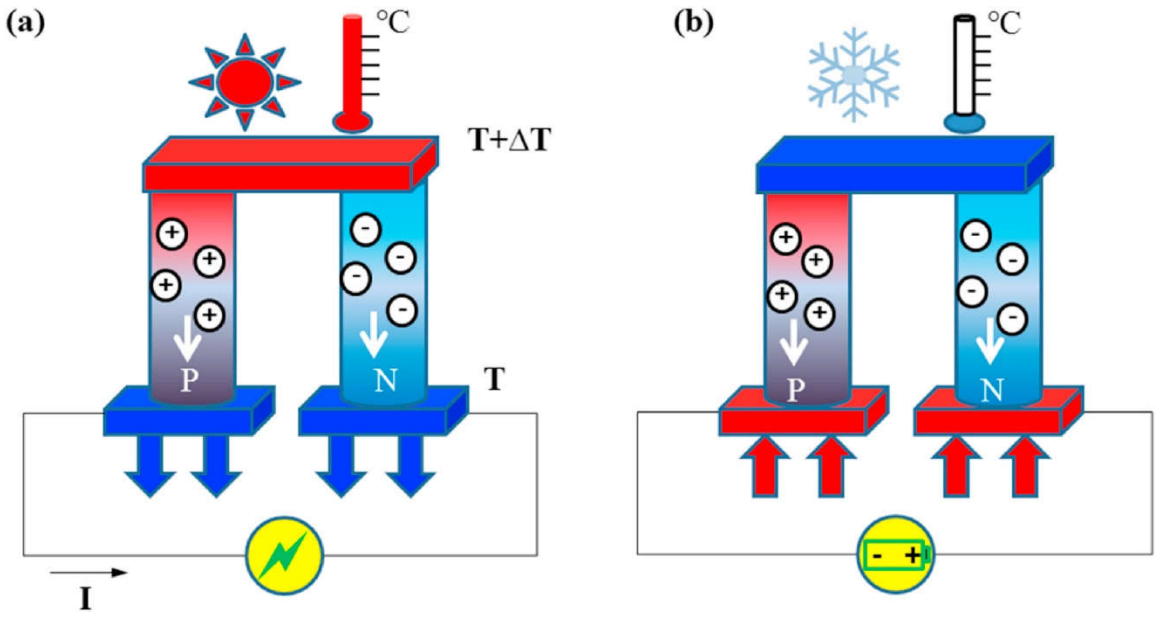

Figure 2.2 Displaying a thermoelectric module operating in: (a) power generation; and (b) refrigeration modes. Adapted with permission from Ref. [2]

2.2 Thermoelectric Application

Over the past decades, thermoelectric materials have attracted significant research interests for green energy harvesting and waste heat recovery [5–8]. These materials can directly convert thermal energy into electricity. This phenomenon can be utilized to harness energy from various heat sources such as automobiles or solar cells and to improve the efficiency of many power generating systems [9–11]. It also opens new routes for extracting small amounts of waste heat from the human body where it can be applied to provide power for wearable or portable biomedical devices (e.g., pacemakers) and electronics (e.g., smartphones) [12].

Considering the large number of available heat sources, thermoelectric generators can be an alternative source of electrical energy in the future [13]. Thermoelectric generators have many advantages over conventional power generators (i.e., combustion engines and turbines) such as

solid-state and silent operation, scalability, maintenance-free with lack of moving parts or chemical reactions, long life-span and high reliability, absence of toxic residuals, lack of pollution and negligible emission of greenhouse gases. TEGs can be utilized in remote areas and spacecrafts because of their light weight and high reliability. Despite all these advantages, TE modules have found limited commercial applications due to their low energy conversion efficiencies.

A TEG consists of several pairs of n-type and p-type thermoelectric elements which are arranged electrically in series and thermally in parallel to give high voltage output. The semiconducting elements are usually sandwiched between two ceramic plates which are maintained at two different temperatures. The hot side is considered as heat source, and the cold plate works as heat sink in the TE module. The absorption and rejection of heat at ceramic plates induce a temperature gradient across TE elements [14]. The temperature difference causes diffusion of charge carriers, that were initially uniformly distributed, from the hot side to the cold side of TE elements. This flow of charge carriers in TE couples results in a potential difference across the TE module [15]. In p-type semiconductors, positively charged holes are the majority of charge carriers, while in n-type semiconductors, negatively charged electrons are the main contribution in charge transportation. Figure 2.3 schematically illustrates the typical structure of a TE module [15].

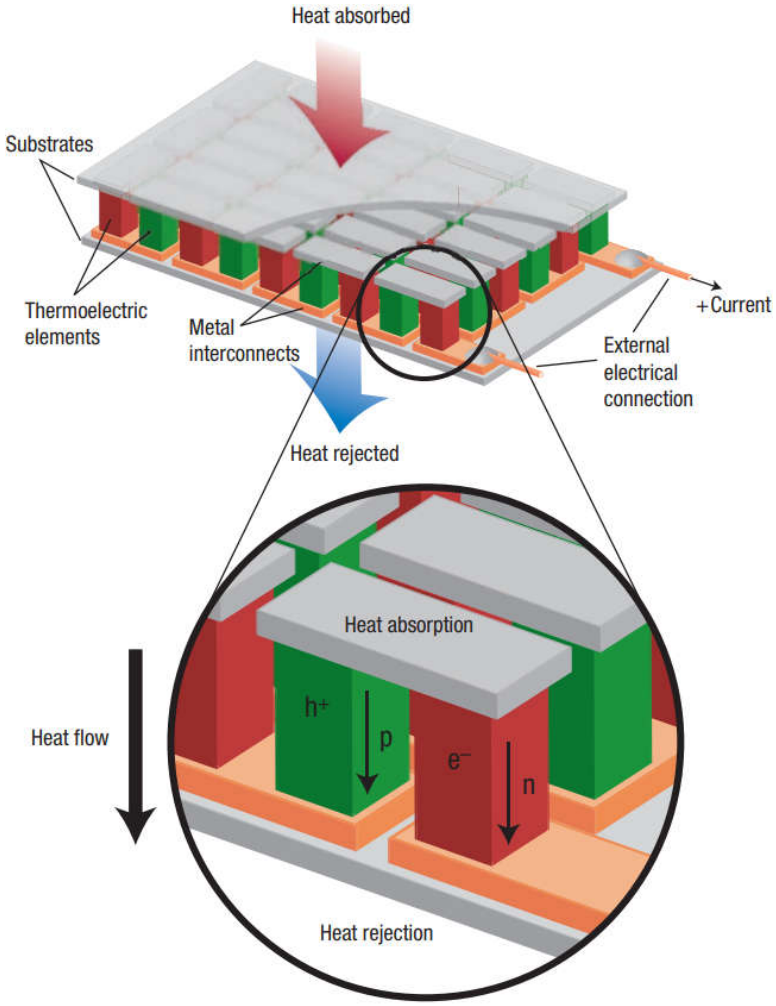

Figure 2.3 A thermoelectric module consisting of multiple couples of n-type and p-type TE elements. Adapted with permission from Ref. [15]

Statistics show that more than 50 percent of the fuel energy in automobiles is usually wasted in the form of heat while being escaped to the environment. TEGs have already been implemented in the automobile industry (e.g., BMW) to recover the exhaust heat and reduce fuel consumption. TEGs have potential usage in the aerospace sector as well, due to the remote locations which require reliable sources of electrical energy to run autonomous systems. These generators have been utilized by NASA, for more than 50 years, to provide power for spacecrafts [16]. Radioisotope TE generators (RTGs) are another example of practical application of TEGs, which

have long been used to produce electricity in space probes and satellites. Figure 2.4 summarizes multiple applications of TE devices in industry. It also plots a typical value of the energy conversion efficiency (*ZT*) for different types of TE materials with respect to their operating temperature range.

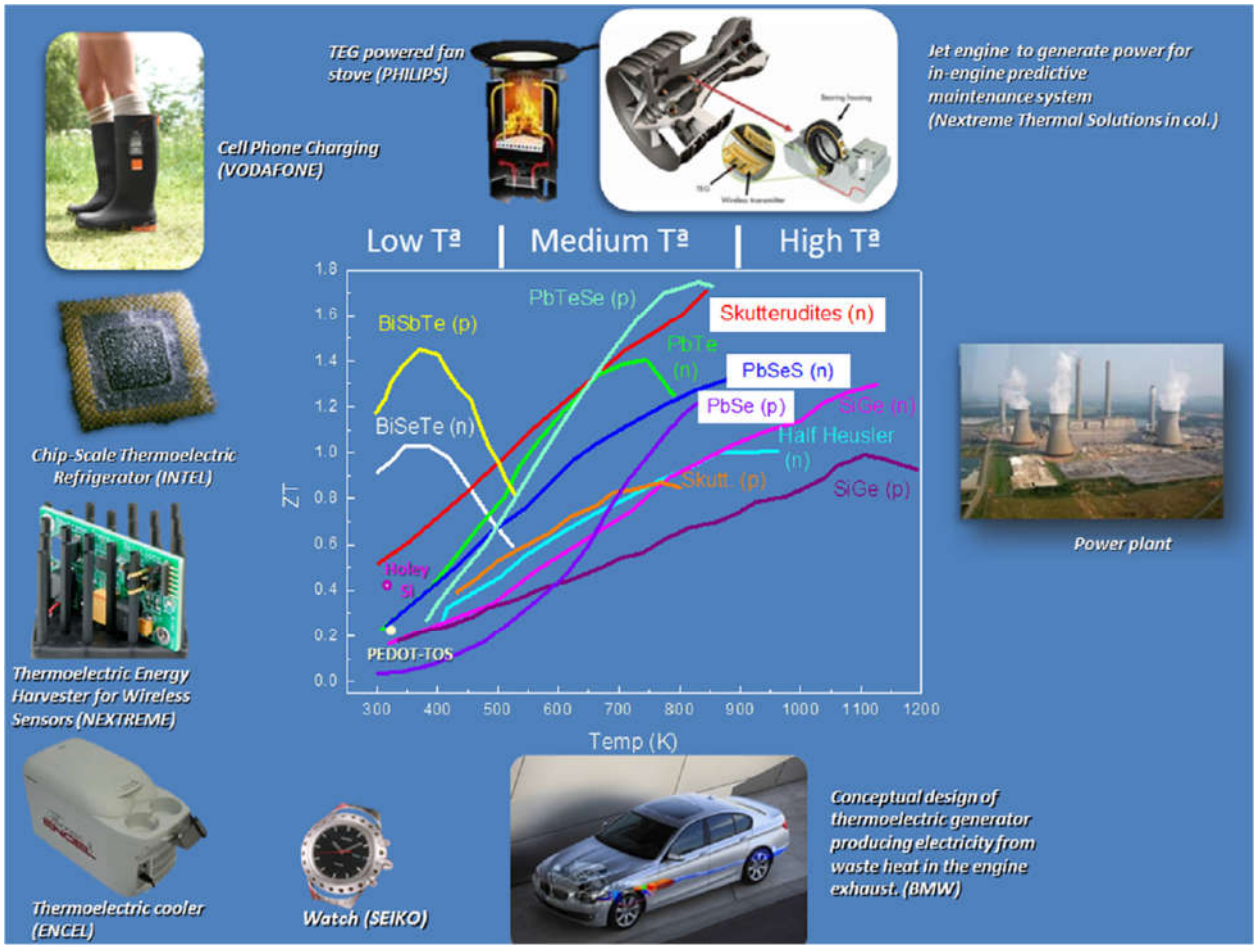

Figure 2.4 Various applications of thermoelectric modules. The graph shows different TE materials and their typical *ZT* values based on their working range of temperature. Adapted with permission from Ref. [17]

The energy conversion efficiency of thermoelectric devices is usually less than 10 percent, which has limited their applications. Aside from the impacts of fabrication techniques and the

temperature difference on the performance of TEGs, the TE properties of the material have a crucial contribution in this regard. Therefore, a significant improvement in the efficiency of TE materials is required to make TEGs competitive with industrial power generating or refrigerating systems.

2.3 Thermoelectric Efficiency

The energy conversion efficiency of TE materials is usually characterized by the dimensionless figure of merit (*ZT*) as expressed in Equation (2-2):

$$ZT = \frac{\sigma S^2 T}{k} \tag{2-2}$$

where σ is the electrical conductivity (Scm^{-1}), S is the Seebeck coefficient (μVK^{-1}) which is also known as thermopower, k is the thermal conductivity ($Wm^{-1}K^{-1}$), and T is the absolute temperature (K).

The power factor (*PF*), expressed as (σS^2), is another parameter that is frequently used in the literature to measure the TE performance of materials. Materials with high TE conversion efficiencies (i.e., high *ZT* value) should have high Seebeck coefficients, high electrical conductivities, and low thermal conductivities. These materials should also withstand high operating temperatures to provide maximum TE efficiencies.

The efficiency of a thermoelectric device in cooling applications is given by Equation (2-3):

$$\eta_c = \frac{T_h}{T_h - T_c}\left(\frac{\sqrt{1 + ZT_{avg}} - {T_h}/{T_c}}{\sqrt{1 + ZT_{avg}} + 1}\right) \tag{2-3}$$

where, T_h and T_c are the temperature of hot and cold sides of the module (K), respectively. ZT_{avg} is the average figure of merit for both p-type and n-type TE elements. The energy conversion efficiency of a TE generator is usually calculated through the following Equations [18]:

$$\eta = \varepsilon_c \left(\frac{\sqrt{1 + ZT_{avg}} - 1}{\sqrt{1 + ZT_{avg}} + {T_c}/{T_h}} \right) \tag{2-4}$$

$$\varepsilon_c = \frac{T_h - T_c}{T_h} \tag{2-5}$$

where ε_c represents the Carnot efficiency of the system.

Like all heat engines, the maximum efficiency of TEGs for power generation is thermodynamically limited to the Carnot efficiency. It should be noted that the efficiency of a TE generator depends on the operating temperature, as the TE properties of materials can vary at different temperatures. Therefore, to achieve the highest efficiency for TEGs, thermoelectric parameters of materials (S, σ, k) should be optimized in the specific operating range of temperature.

There are some limitations and challenges related to the fabrication and commercialization of TEGs. The synthesis of TE materials with high efficiencies is time-consuming and mostly not reproducible. Furthermore, their TE properties may change over time, which provides insufficient accuracy of the estimated efficiency of TE modules. Due to the uncertainty of the measurement methods and thereby lack of repeatable experiments, many lab-made materials with claimed high *ZT* values were not considered for real applications [16]. Current commercial TE materials have a relatively low figure of merit, which is about unity. For fabricating an ideal TEG, there should be a perfect electrical and thermal contact between TE elements to reduce the joule heating and to provide continuous heat flow throughout the TEG. Therefore, the average efficiency of existing

TEGs is approximately five percent, which is pretty small compared to conventional power generating systems [19]. Considering the relatively low efficiency of current TEGs compared with typical power generating systems, they are potentially useful for small scale applications, where the thermal energy input is provided by waste heat.

2.4 Improving TE Efficiency

A fundamental challenge to increase the TE efficiency of materials is to simultaneously enhance their electrical conductivity and Seebeck coefficient while suppressing their thermal conductivity. In this context, Slack suggested that the best TE material should have "phonon-glass electron-crystal" (PGEC) behavior, which means it should have the electrical properties of crystalline materials (i.e., high electrical conductivity) and the thermal properties of amorphous glass-like materials (i.e., low thermal conductivity) [20]. In this situation, electrons will carry charges freely but phonons, as heat carriers, will be scattered and disrupted within the atomic structure. However, in most materials, high electrical conductivity usually comes with high thermal conductivity. The electrical conductivities of materials, on the other hand, typically have an inverse relationship with their Seebeck coefficients [21,22]. The three TE properties of materials (i.e., S, σ, and k) are intrinsically interrelated as a function of carrier concentration, carrier mobility, electron energy bands, and many other factors [23]. Therefore, the critical limitation to improve a material's TE efficiency is the need to decouple the TE parameters [24].

For electrically conductive materials, their thermal conductivity generally comprises of two parts as a contribution of electronic and lattice thermal transport effects:

$$K = K_e + K_l \tag{2-6}$$

where K_e is the electronic thermal conductivity and K_l is the lattice thermal conductivity of the material ($Wm^{-1}K^{-1}$). The electronic part of thermal conductivity is the heat transportation from charge carriers (electrons and holes), and the lattice part is the result of heat transfer from moving phonons through the crystal lattice vibration [19]. Based on the Wiedemann-Franz law, the electronic thermal conductivity is correlated with the electrical conductivity of material [15]:

$$K_e = \sigma LT \tag{2-7}$$

where L is the Lorenz factor, which is equal to 2.4×10^{-8} $J^2K^{-2}C^{-2}$ for free electrons, and it varies depending on carrier concentration.

According to Equations (2-6) and (2-7), by increasing the electrical conductivity of material, its thermal conductivity will also increase. This interrelation of the properties adversely affects the *ZT* value. Consequently, decreasing the lattice thermal conductivity of TE materials is the best approach to suppress the k without compromising the σ to maximize their *ZT* value. In this approach, the flow of a spectrum of phonons with various wavelengths through the bulk of material should be scattered with different synthesizing techniques.

The electrical conductivity of materials is related to carrier concentration, carrier mobility, and electron charge through the following Equation [25]:

$$\sigma = ne\mu \tag{2-8}$$

where n is the carrier concentration (cm^{-3}), μ is the carrier mobility ($cm^2V^{-1}S^{-1}$), and e is the electron charge (1.602×10^{-19} C). The Pisarenko equation expresses the Seebeck coefficient of materials in terms of their transport properties [26]:

$$S = \frac{8\pi^2 {K_B}^2}{3eh^2} m^* T \left(\frac{\pi}{3n}\right)^{2/3} \quad (2\text{-}9)$$

where k_B is the Boltzmann constant (1.38×10^{-23} JK^{-1}), e is the carrier charge (the electron charge, C), h is the Planck's constant (6.626×10^{-34} Js), m^* is the effective mass of charge carriers (also known as the density of states effective mass, kg), and n is the carrier concentration (cm^{-3}).

According to Equations (2-8) and (2-9), by increasing the carrier concentration, the electrical conductivity of material will increase. However, the Seebeck coefficient will decrease, which adversely affects the TE efficiency. In order to get the best ZT value, charge carrier concentration and carrier mobility should be tuned to maximize the power factor ($S^2\sigma$). Simple models of electron transport in thermoelectric materials have proven that maximum ZT value typically occurs at carrier concentrations of about 10^{19} to 10^{21} carriers per cm^3. This value of concentration is usually found in heavily doped semiconductors [15]. The interrelation between the electrical conductivity, thermal conductivity, and Seebeck coefficient of TE materials is illustrated in Figure 2.5 [27]. This plot also shows the variations in these parameters based on the free charge carrier concentration of the material. The maximum value of the power factor ($S^2\sigma$) curve happens at an optimum doping level of 10^{19} cm^{-3}.

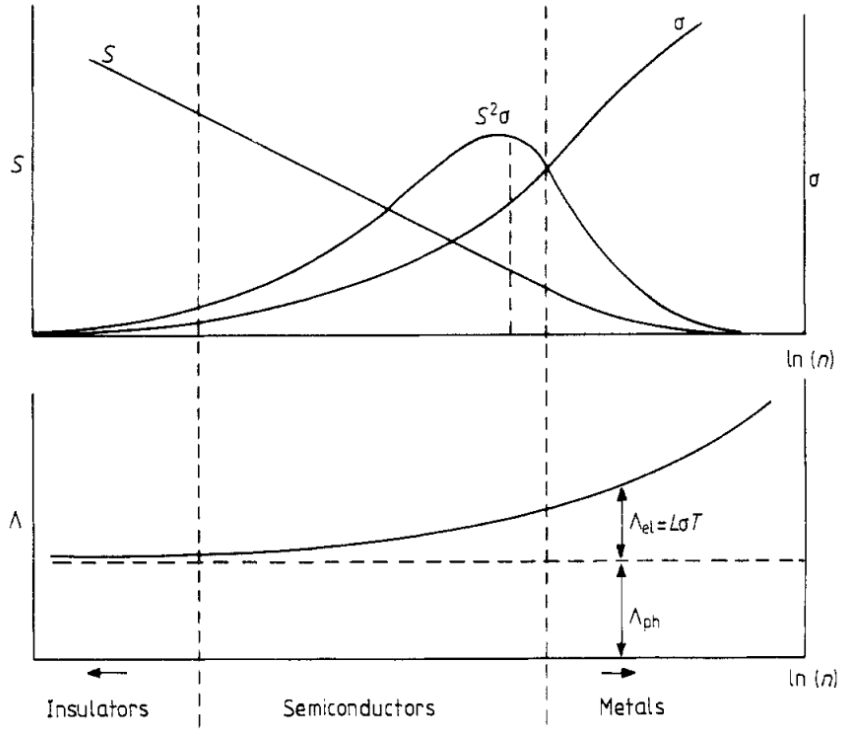

Figure 2.5 Variation in TE parameters of materials and their relations to the lattice (Λ_{ph}) and electronic (Λ_{el}) thermal conductivities as a function of their charge carrier concentration n. Adapted with permission from Ref. [27]

2.5 Processing Methods for Improving TE Performances

Over the past decade, considerable effort has been devoted on developing more efficient thermoelectric materials. Some of the research is focused on minimizing the lattice thermal conductivity, while others are working on materials which exhibit larger power factors ($S^2\sigma$). Investigating the potential of bulk materials for TE applications is an active area of research. Since the discovery of thermoelectric effect, various processing techniques have been developed to enhance the TE efficiency of different classes of materials [25,28]. Recent advances in nanotechnology have opened a new route to partially decouple the TE properties of materials

[17,19]. The introduction of nanostructures has become a potential strategy for decoupling the interrelated physical properties of TE materials by simultaneously increasing the Seebeck coefficient and suppressing the thermal conductivity. A big challenge on the development of nanostructured bulk TE materials is the electron scattering at their structural interfaces and boundaries, which reduce their electrical conductivity while suppressing thermal conduction. Nanostructured materials with various dimensions such as superlattices, nanowires, and nanodots have been recently developed with improved TE efficiencies [29].

Decreasing the lattice thermal conductivity of TE materials can potentially promote their TE efficiencies without compromising their electron transport properties. Several approaches have been successfully implemented in this regard such as creating rattling structures and point defects by alloying (e.g., clathrates and skutterudites), fabricating complex crystal structures to achieve a phonon-glass, and providing multiple interfaces for phonon scattering in multiphase composites [15]. An enhancement of TE properties is expected by nanostructuring of materials. Introducing nano-interfaces enhances interfacial reflection and scattering of phonons within the bulk of materials without significantly affecting the transport of charge carriers. Hierarchical complexities are required to scatter phonons within broad length scales which are involved in heat transfer through the material's structure.

The quantum confinement of electron charge carriers has been suggested as a successful technique to promote the TE efficiency of materials. As the confinement increases and the dimensionality of the material decreases, the energy bands get narrower in the material system, which provides higher Seebeck coefficients. In nanostructured materials, the quantum confinement effect helps to alter their electronic density of states, leading to enhanced Seebeck coefficients [30–32]. Fabricating small dimensional material structures such as quantum wells (two

dimensional), quantum wires (one dimensional), quantum dots (zero-dimensional), and thin films has been demonstrated as an effective strategy to promote the TE efficiency of materials. Electron transport regions with such low dimensions might enhance the Seebeck coefficient of the material through carrier confinement and electron filtering [15]. Moreover, phonons with short mean free paths will be scattered in regions with small dimensions (i.e., on the order of nanometer or angstrom scales).

Carrier energy filtering is an alternative strategy to improve the thermopower of TE materials. In this approach, charge carriers with lower energy levels can be blocked within the material system by introducing nanostructures and multiple interfaces in the bulk of material. As a result, lower charge carrier concentration with higher average energy level will provide high thermopower and thereby promote the *ZT* value [18,33].

2.6 Thermoelectric Materials

Thermoelectric materials comprise a broad family of materials from semimetals and semiconductors to ceramics and polymers. TE materials contain various structures from monocrystals and polycrystals to nanocomposites [25]. The following sections will provide a brief literature review on conventional and state-of-the-art TE materials. This part is specially focused on reviewing organic TE materials, which are the subject of this dissertation. The latest advancements in synthesizing techniques of TE materials will also be discussed in this section.

2.6.1 Semiconducting Thermoelectric Materials

Among different material families, semiconducting alloys have the best combination of properties (i.e., high Seebeck coefficients and good electrical conductivities) that lead to high TE efficiencies. Depending on the desired operating temperature range, TE semiconductors are mostly

alloys of Bismuth (Bi), Selenium (Sb), Tellurium (Te), Antimony (Se), Lead (Pb), Silicon (Si), and Germanium (Ge) elements. Conventional semiconducting TE materials (i.e., alloys of Bi_2Te_3 and Sb_2Te_3) have high Seebeck values, exhibiting superior thermoelectric efficiency of $ZT \approx 1$ at near-room temperature. Bi_2Te_3 and Sb_2Te_3 alloys can be applied for waste heat recovery at temperatures below 200°C.

Tuning of carrier concentrations alongside decreasing the lattice thermal conductivity is possible in these alloys, which has made them as most widely used TE materials within last decades. For power generation at mid-range temperatures (i.e., 500-900 K), alloys of PbTe, GeTe, and SnTe are typically used as TE materials with the highest efficiencies [15]. For high-temperature applications (i.e., >900 K), bulk materials such as skutterudites, clathrates, half-Heusler alloys, and complex chalcogenides are being investigated in recent decades [34]. Silicon-germanium (SiGe) alloys are also considered as high-temperature TE materials. Basic crystal structure of these materials ensures good electric properties. Also, spacious voids in their lattice structures reduce thermal conductivity by strong phonon scattering. Figure 2.6 shows the best *ZT* values achieved from different types of bulk thermoelectric materials (separated as n-type or p-type TE materials) at various working temperatures [35].

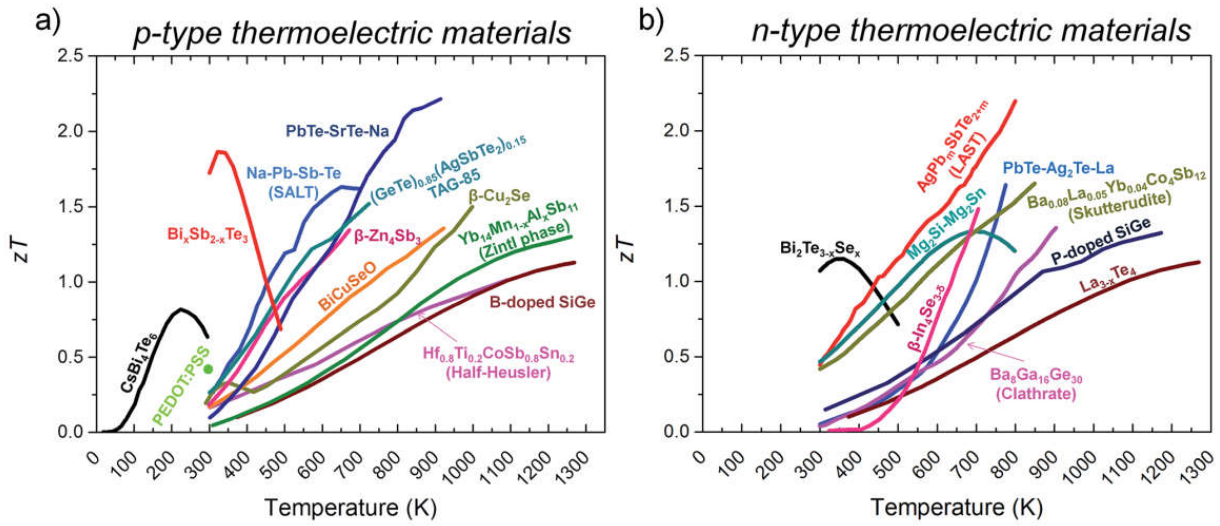

Figure 2.6 Variation of the *ZT* value of p-type and n-type bulk TE materials at different working temperatures. Adapted with permission from Ref. [35]

2.6.2 Polymer-based Thermoelectric Materials

Semiconductors (e.g., bismuth telluride alloys) are commonly used for TE applications due to their high Seebeck coefficients and relatively good electrical conductivities that result in their high *ZT* values (i.e., ~1 to 2) [36,37]; however, their toxicity for the environment, scarcity, high cost, and complexities of processing have restricted their widespread applications. Moreover, they are heavy and rigid. Recently, polymeric TE materials have become the subject of interest as potential alternatives for semiconductors for TE-related applications [38]. Unlike semiconducting TE materials, polymers are more readily available and possess many other advantages for TE applications [39]. These include low cost, light weight, flexibility, simple processability, and environmental sustainability [40,41]. The potential to tailor the flexibility of polymer-based TE materials also represent another critical advantage, especially for wearable electronics. The intrinsic low thermal conductivities of polymers are desirable to achieve high *ZT* values. In contrast, their electrical conductivities and Seebeck coefficients should be significantly improved

to make them viable options for TE applications. The low TE efficiency of polymeric materials is considered as their main drawback for their use in this area of research.

During past few years, researchers have achieved a significant improvement in TE efficiency of organic materials. Conjugated polymers have great potential for TE applications due to their relatively good electrical conductivities [42,43]. However, complexities of processing and unstable properties due to air degradation are some disadvantages of using conducting polymers for TE applications. Polymer nanocomposites, containing non-conducting polymers, have also been investigated for thermoelectric applications. Embedding conductive fillers such as metallic or carbon particles (i.e., carbon nanotubes (CNTs), graphene, graphite, carbon fiber, and carbon black) in polymer matrices can promote their electrical conductivities [44–48]. On the other hand, the addition of conducting fillers would compromise the material system's low thermal conductivity, which would negatively affect their TE efficiencies [49–53]. As for any TE material, the main challenge to improve the *ZT* value of polymeric materials is the needs to simultaneously tune their TE parameters (i.e., electrical conductivity, Seebeck coefficient, and thermal conductivity), which are usually highly correlated.

2.6.2.1 Conducting Polymers

Conjugated polymers or intrinsically conducting polymers (ICPs) are among the most investigated organic materials for TE applications, while many studies have recently focused on improving their TE performances [54]. The electrical conductivity of conjugated polymers can reach the levels of semiconducting materials through different doping mechanisms [42]. Among different types of conjugated polymers, poly(3,4- ethylenedioxythiophene) (PEDOT), polyaniline (PANI), poly-thiophene (PTh), polypyrrole (PPy) and their derivatives have attracted most

research interests in this area due to their high TE properties [54–61]. The molecular structure of some common conducting polymers is displayed in Figure 2.7 [62].

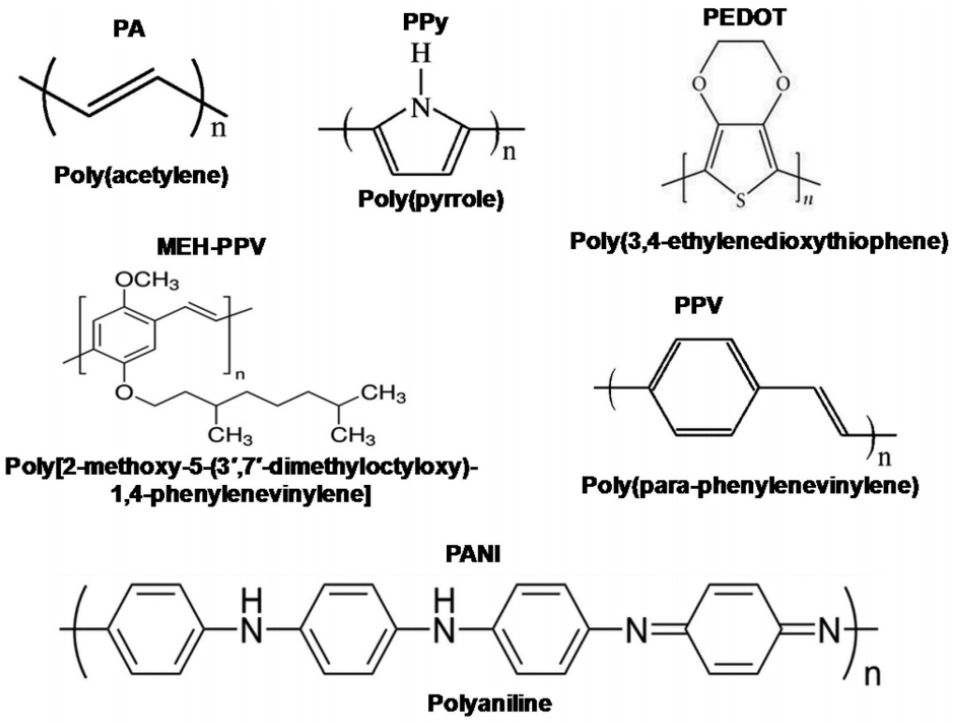

Figure 2.7 Chemical structure of common conducting polymers. Adapted with permission from Ref. [62]

A review on conducting polymers and their TE nanocomposites by Du *et al.* reported that their value of Seebeck coefficient ranges from -4088 to 1283 μVK^{-1}, σ ranges from 10^{-7} to 10^{4} Scm^{-1}, and k falls between 0.02 to 1.2 $Wm^{-1}K^{-1}$ [63]. Most researchers have tried increasing the power factor of conducting polymers while maintaining their thermal conductivity within the range of 0.2-0.6 $Wm^{-1}K^{-1}$ [64,65]. Zhang *et al.* investigated the TE transport in one-dimensional (1D) conducting polymers as organic TE materials [66]. They achieved an optimized *PF* value of 35.8 $\mu Wm^{-1}K^{-2}$ for PEDOT nanowires (PEDOT NWs) assembly.

The electrical conductivity of conductive polymers improves with high level of doping; however, their Seebeck coefficient decreases when doping increases as a result of increased charge carrier density. Recent study by Maiz *et al.* showed an improvement in TE properties of iron-doped poly[N-9'-heptadecanyl-2, 7-carbazole-alt-5, 5-(4',7'-di-2-thienyl-2',1',3-benzothiadiazole)] (PCDTBT) polymer film [67]. Using $FeCl_3$ as a doping agent, the electrical conductivity of PCDTBT polymer films was increased without significantly increasing their thermal conductivity. Consequently, an enhancement of two orders of magnitude in the *ZT* value of the polymer film was observed.

Wang *et al*. reported the highest power factor of 7.05 $\mu Wm^{-1}K^{-2}$ for poly(3-octylthiophene) (P3OT)/carbon fiber composites [68]. They solution casted P3OT, as a conducting polymer, on carbon fiber sheets to prepare the composite TE material. Meng *et al.* used CNT to improve the transport properties of polyaniline (PANI) [69]. Their results revealed that the TE performance of CNT/PANI nanocomposites was remarkably enhanced when compared with both of their bulk parent samples. The power factors of the CNT/PANI nanocomposites were still inferior to those of conventional semiconducting TE materials, mainly due to the poor absolute Seebeck coefficient of PANI. A study by He *et al.* revealed that adding Bi_2Te_3 nanowires in poly(3-hexylthiophene) (P3HT) polymer would effectively enhance the power factor of the polymer matrix from 3.9 $\mu Wm^{-1}K^{-2}$ to 13.6 $\mu Wm^{-1}K^{-2}$ [23]. The introduced organic-inorganic interfaces in the nanocomposite material system served as energy-filtering barriers, which increased the Seebeck coefficient without significantly suppressing the electrical conductivity.

2.6.2.2 Polymer Nanocomposites

Most developed conducting polymers for thermoelectric applications such as PANI, PEDOT, PTh, PPy, polyacetylene (PA), and polycarbazole (PC) have poor processability and low stability

especially at high temperatures, which has limited their widespread applications [70]. A few studies are available on developing organic TE materials using non-conducting polymers. Polymer nanocomposites have attracted much attention during the last decades in microelectronic industry and sensor applications. In addition to typical advantages of polymers (Such as light-weight, low cost, and good processability), the promotion of electrical properties (e.g., electrical conductivity) by the inclusion of a small amount of conductive fillers into polymer matrices have made polymer nanocomposites versatile multifunctional materials. Incorporating carbon-based, semiconducting, and metallic particles within polymer matrices along with hybridization of different types of fillers and polymers are among various strategies that have been investigated to develop polymeric TE materials [71–75].

Literature studies show that electrical conductivity and TE performance of polymeric materials strongly depend on their nanostructures [76–78]. By introducing nanostructured interfaces into the bulk material, the lattice thermal conductivity of the material will decrease because of phonon scattering. Incorporating different range of nanostructures will help to reduce the mean free path (MFP) of phonons in a broad range and effectively suppress the thermal conductivity, without affecting electron transport in nanocomposite materials [19]. Moreover, the mismatch between molecular vibration of polymer particles and nanofillers in polymer nanocomposites will help to filter phonon transport at the junction of polymer-filler, which results in suppressing thermal conductivity of the material system [79]. However, the constituent materials in nanocomposites should be selected in a way that their electronic mismatch would not adversely affect the electron transport properties of the material. The processing conditions of polymer nanocomposites can significantly affect the material system's morphology and structure. Therefore, it is essential to

determine the roles of different processing parameters in tuning the micro-and-nanostructures of polymer nanocomposites, which will influence their TE efficiencies.

Among different electrically conductive fillers, carbon nanotubes represent one of the best candidates for manufacturing conductive polymer nanocomposites because of their excellent electric properties. With an extremely high aspect ratio, uniform dispersion of a small amount of CNT can produce an efficient conductive network throughout the insulating polymer matrix. Many studies have investigated the electrical properties of polymeric composites and nanocomposites with multi-walled carbon nanotubes or single-walled carbon nanotubes (SWCNT). Nasr *et al*. showed that the DC electrical conductivity of MWCNT/Poly(vinyl alcohol) PVA nanocomposites increased by several orders of magnitude with the introduction of the conductive nanofiller into the PVA matrix [80]. Aguilar *et al.* studied the effect of CNT dispersion state (agglomerated vs. uniformly dispersed) on the electrical conductivity of CNT/polymer composite films [81]. They revealed that clustering of CNT, especially for CNT contents close to the percolation threshold, would promote the electrical conductivity of CNT/polymer nanocomposite films.

Many researchers have investigated polymer nanocomposites for TE applications. Carbon nanofillers such as CNTs and graphene nanoplatelets (GnPs) have shown promising TE efficiencies because of their high electrical conductivities and relatively high Seebeck coefficients [82–85]. By controlling the dispersion of carbon nanofillers within polymer matrices, continuous three dimensional (3D) networks can be created to facilitate electron transfer and promote the electrical conductivity of polymer nanocomposites [86,87]. Moreover, creating filler-filler junctions and organic-inorganic interfaces in polymer nanocomposites have demonstrated great potentials to increase their Seebeck coefficients through carrier filtering effect, while suppressing their thermal conductivity via phonon scattering [88,89].

Carbon nanotubes are promising candidates for developing lightweight and low-cost polymeric TE materials. Studies have demonstrated that CNT/polymer thin films with some degrees of heterogeneity allow for slight decoupling of TE parameters, leading to an increase in *ZT* value [90]. Yu *et al.* suggested polymer nanocomposites with segregated network of conductive fillers as possible replacement of semiconducting materials for thermoelectric applications [86]. They managed to develop an electrically connected and thermally disconnected network of carbon nanotubes around emulsion polymer particles, which resulted in a *ZT* value as high as 0.006 at 300 K. The effect of CNT's type on TE properties of Nafion polymer nanocomposites was investigated by Choi *et al.* [91]. They found that the CNT type has a significant effect on the electrical conductivity of polymer nanocomposites. However, their Seebeck coefficients were insensitive to the type of CNT, especially at high CNT loading. They achieved a maximum *PF* value of 1 $\mu Wm^{-1}K^{-2}$ for few-walled CNT/Nafion nanocomposites with approximately 30 wt.% filler loading.

Choi *et al.* studied the effects of CNT loading on TE properties of poly(dimethylsiloxane) (PDMS)/CNT nanocomposites [92]. They realized that by increasing the CNT content, the electrical conductivity and Seebeck coefficient of the polymer nanocomposite significantly improved without a remarkable increase in their thermal conductivity. With 10 wt.% loading of CNT, they measured a maximum Seebeck coefficient and *ZT* values of 10.4 μVK^{-1} and 7.7×10^{-7}, respectively, at 100 °C for fabricated nanocomposite samples. Liebscher *et al*. investigated the effects of differently functionalized MWCNTs on TE properties of polycarbonate (PC)/MWCNT nanocomposites [93]. Their results showed that by increasing the oxygen content of MWCNTs, the Seebeck coefficient of the nanocomposite samples improved. Their maximum reported electrical conductivity and Seebeck coefficient values were around 0.1 Scm^{-1} and 12 μVK^{-1}, respectively, for PC/MWCNT composites with 2.5 wt.% of filler content. In another study, the

effect of SWCNT loading on TE parameters of PVDF/SWCNT composite thin films was investigated [94]. Their results demonstrated that reducing the SWCNT content in PVDF/SWCNT nanocomposite films was beneficial to their TE efficiency, and the *ZT* value ranged from 7×10^{-6} for pure SWCNT film to 10^{-4} for PVDF-based nanocomposite film loaded with 5 wt.% SWCNT.

Sung *et al*. compared the TE properties of CNT/glass fiber (GF)/epoxy composites with carbon fiber (CF)/epoxy composites at various filler loadings [95]. They observed higher in-plane electrical and thermal conductivities than the corresponding through-thickness results for composite samples. The results of their study showed a maximum *ZT* value of 2×10^{-6} for CNT/GF/epoxy samples with 5 wt.% of CNT/GF loading. Recent research has demonstrated improvement in TE power output of an organic multilayered CNT-based TE module [96]. By selecting the appropriate type of CNT and dopant for the conducting layers (i.e., SWCNT for the p-type layers and polyethylenimine-doped SWCNT for the n-type layers) and using polyvinylidene fluoride as the base polymer, a single thermocouple Seebeck coefficient of $96 \pm 4\ \mu VK^{-1}$ was observed.

A study conducted by Hewitt *et al.* on TE properties of few-layer graphene platelet (FLG)/ PVDF composites revealed the importance of optimizing the trade-off between the electrical conductivity and the Seebeck coefficient of polymer composites to achieve high power factors [97]. They reported a maximum *PF* value of $0.52\ \mu Wm^{-1}K^{-2}$ for FLG/PVDF composites with 80 wt.% FLG content. A practical approach to improve *ZT* values of polymer nanocomposites is to increase their electrical conductivity by creating an efficient network of conductive fillers through the insulative polymer matrix. A study by Zhao *et al.* demonstrated the potential of graphene-CNT aerogels for thermoelectric application [98]. By fabricating a 3D porous structure of graphene and

CNT with ultra-low thermal conductivity, the electrical conductivity and the Seebeck coefficient of the nanocomposite aerogel was increased, which resulted in a *ZT* value of 0.001.

Moriarty *et al.* studied the effect of semiconducting (meso-tetra(4-carboxyphenyl) porphine (TCPP)) and insulative (sodium deoxycholate (DOC)) stabilizers on TE properties of polyvinyl acetate (PVAc)/CNT nanocomposites [99]. They reported an improvement in Seebeck coefficient of MWCNT:TCPP/PVAc compared to MWCNT:DOC/PVAc nanocomposites (up to five times) using two types of carbon nanotubes (double-walled and multi-walled CNTs). Chung *et al.* reported a significant enhancement in TE behavior of carbon fiber/epoxy composites by incorporating a combination of inorganic fillers (i.e., tellurium, bismuth telluride) and carbon black [100]. Their results showed an increase in thermoelectric figure of merit of the composite samples from 9×10^{-6} to 9×10^{-2} by adding multiple fillers. While tellurium increased the TE power, bismuth telluride increased the electrical conductivity and decreased the thermal conductivity. Moreover, carbon black improved the composite's electrical conductivity.

2.7 Foaming

Foaming is a process to create a porous structure within the material system. Plastic foaming is a processing technology that generates porous structure in polymer matrix for a variety of scientific and industrial applications such as insulation, cushioning, absorbents, filtering, tissue engineering, and scaffolds [101]. Introducing cellular structure will help to modify mechanical and transport properties of materials such as impact absorption, thermal insulation, and acoustic properties [102]. Porosity will also result in decreasing the density of samples, which means reducing the overall weight and saving the material usage.

Foam samples are generally divided into two groups based on their cellular structures; open-cell and closed-cell foams. Figure 2.8 demonstrates the morphology of polymeric foam samples with open-cell and closed-cell structures. In open-cell foams, the cells are not fully encapsulated while there are lots of ruptures on the cell-walls. Therefore, the pores are usually interconnected due to the openings on the walls of the adjacent cell. In closed-cell foams, however, the cells are fully enclosed by their walls. Consequently, the pores are mostly isolated from each other. Increasing demand for lightweight materials with improved mechanical and thermal properties has led to several foaming techniques for various material systems (i.e., one-step and two-step foaming, physical and chemical foaming). A variety of chemical and physical foaming methods have been developed in past decades to fabricate open-cell and closed-cell foams with different porous structures.

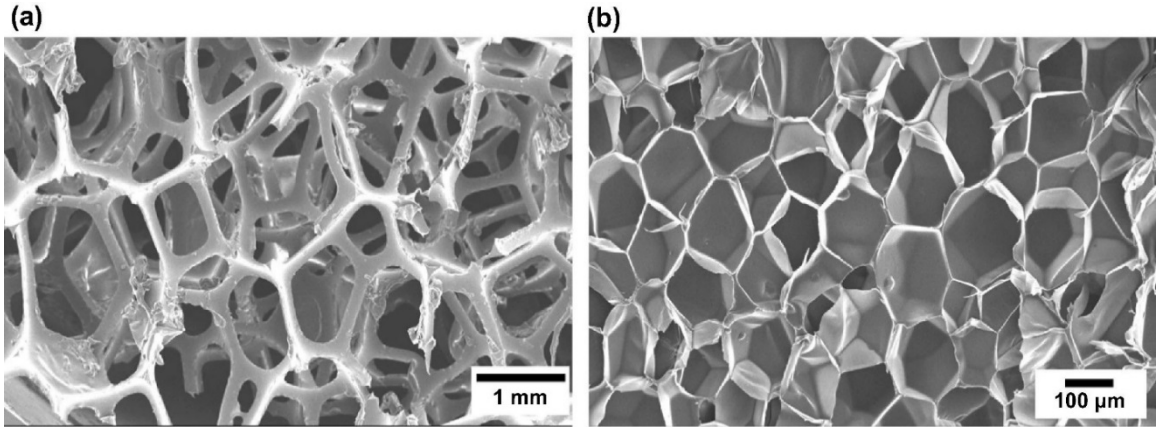

Figure 2.8 The morphology of polymer foams with: (a) open-cell; and (b) closed-cell structures. Adapted with permission from Ref. [103]

Environmentally friendly techniques have been adopted in industry using supercritical fluids (such as CO_2 and N_2) for polymer processing and foaming applications [104]. In this method, the polymeric sample is firstly saturated with supercritical fluid under high pressure. The polymer/gas

mixture is then supersaturated by bringing into a thermodynamically unstable state, which happens through reducing pressure or increasing temperature. This phenomenon results in the nucleation and growth of cells within the polymer matrix [105]. This method usually produces microcellular foams with average cell-sizes of 10 to 100 microns, depending on the foaming conditions. Supercritical carbon dioxide ($ScCO_2$) is most often used, because of its physical properties (i.e., non-toxic, non-flammable, abundance, and highly soluble).

2.7.1 Thermal and Electrical Conductivity of Polymeric Foams

Polymer foams are widely investigated for thermal insulating applications due to their low thermal conductivities. Generally, four different terms contribute in thermal conduction of foams:

$$k = k_s + k_g + k_r + k_c \tag{2-10}$$

In this equation, k_s, k_g, k_r, and k_c are solid phase conduction, gas phase conduction, radiation, and convection ($Wm^{-1}K^{-1}$), respectively. Foam samples with closed-cell structures have usually lower thermal conductivities in comparison with open-cell foams. This property is due to the negligible effect of convection mechanism in overall thermal conductivity of foams with closed-cell structures.

Studies have demonstrated that by decreasing the cell-size, the thermal conductivity of foam samples usually decreases [106]. In foam samples with small cell-sizes, the convection heat transfer mechanism can be ignored. Moreover, because of the Knudsen's effect, by reducing the cell-size around the mean free path value of gas molecules or smaller than that, the gas conduction term significantly decreases [107]. This phenomenon happens due to the increased number of collisions of gas molecules with the cell-walls, which results in lower gas mobility and thereby lower gas-phase thermal conduction [108,109]. In this context, nanocellular foaming has offered

significant improvement in thermal insulation of polymer foams [110]. However, fabrication of porous samples with nanocellular structures and controlling their cell structures are the main challenges that need to be resolved [111].

Alvarez *et al.* reported that the thermal conductivity of open-cell Polyolefin foams was slightly higher than the closed-cell ones with the same range of densities [112]. Their study also revealed that by decreasing the cell-size, the thermal conductivity of polymer foam decreases. Experimental studies have demonstrated that the thermal insulation property of materials with porous structures has a direct relation with their densities [113]. Aerogels are highly porous materials with ultra-low densities, which can provide extremely low thermal conductivities [114]. Aerogels have open-cell structures while their pore sizes are typically around 1 to 100 nm, which is close to the mean free path of gas molecules in the air (i.e., around 7 nm at 1 bar). This structure of aerogels provides a high suppression of the gaseous heat transfer (i.e., conduction and convection) through the sample [115].

Foaming has recently been applied to alter electrical and thermal conductivity of polymer nanocomposites. Inclusion of different nanofillers in polymer matrices, on the other hand, can help to control the morphology and cell structure of polymer foams [101,116]. A study by Baseghi *et al.* showed that CO_2 foaming of polymer nanocomposites could decrease the percolation threshold of the filler content [117]. As a result, introducing microcellular foam structures helped to promote the electrical conductivity of polymer nanocomposites by using lower amount of fillers. Yang *et al.* applied batch foaming with the aid of $ScCO_2$ to control the electrical conductivity and percolation threshold of MWCNT/Polystyrene (PS) nanocomposite [118]. By decreasing the cell-wall thickness, they were able to achieve higher electrical conductivity values. Jun *et al.* investigated the effect of graphene sheet size on the electrical conductivity of

graphene/Polydimethylsiloxane (PDMS) foam [119]. The results of their study revealed that by increasing the filler's aspect ratio, the electrical conductivity of the polymer nanocomposite foam increases because of enhanced interconnectivity among conducting fillers.

By simultaneously incorporating an electrically conductive network of fillers and creating a thermally insulating cellular structure through the polymer matrix, the TE efficiency of the polymer system will potentially enhance. Fabricating aerogel structures from conducting nanoparticles can help to simultaneously improve their electrical conductivity and suppress their thermal conductivity [120]. Zhao *et al*. managed to decouple the thermoelectric parameters of a hybridized aerogel made up of MWCNTs and carbonized resorcinol-formaldehyde (RF) resin [121]. Their results showed that by creating a porous structure within a conducting network of carbon nanotubes, three TE parameters (electrical conductivity, thermal conductivity, Seebeck coefficient) can be simultaneously tuned to maximize the *ZT* value.

2.8 Concluding Remarks

While extensive research has been conducted to investigate on the strategies to improve the TE conversion efficiencies of various material families, the success in developing polymer nanocomposites with high TE efficiencies was more limited. Because of several niche benefits of TE polymer nanocomposites (e.g., lightweight, flexibility, low cost), any new strategy that can significantly promote the TE efficiency of polymer nanocomposites would represent a significant technological breakthrough. Ongoing studies on TE materials are mainly focused on increasing the electrical conductivity and the Seebeck coefficient; because the thermal conductivity of polymer nanocomposites was found to moderately increase while increasing their electrical

conductivity. In this context, current study aims to investigate the potential of using different foaming techniques, as a novel strategy, to fabricate thermoelectric organic materials.

The suggested approach can potentially enhance the TE conversion efficiency of polymeric materials by not only promoting their electrical conductivity and Seebeck coefficient but also simultaneously suppressing their thermal conductivity. The effects of different processing parameters and material combinations on TE properties of nanocomposite samples were also studied in this research. The findings have proven that foaming can serve as an innovative technique to enhance the efficiency of various polymeric TE materials and make them viable as replacement of semiconductors for energy harvesting and waste heat recovery.

Chapter 3. Polypyrrole/Multi-walled Carbon Nanotubes Nanocomposites with Enhanced Thermoelectric Efficiencies[1]

3.1 Introduction

Charge transport properties of intrinsically conducting polymers (ICPs) is highly related to their microstructures. Processing conditions and material formulations can alter the morphology of ICPs and thereby their electrical and thermoelectric properties. In this chapter, the effects of different processing parameters on the electrical conductivity and TE performance of polypyrrole/multi-walled carbon nanotubes nanocomposites were investigated. PPy/MWCNT nanocomposite samples were prepared by in-situ oxidative polymerization method. The effects of polymerization time, oxidant-to-monomer ratio, filler-to-monomer ratio, and reaction medium on electrical conductivity and Seebeck coefficient of the fabricated PPy/MWCNT nanocomposite samples were explored to optimize their TE efficiencies. The results of this study revealed that the MWCNT-to-monomer molar ratios of 0.1 and 1 provided the highest electrical conductivity and the maximum power factor, respectively. Moreover, the addition of methanol to the reaction solution led to finer structures in the nanocomposites, and thereby enhanced their electrical conductivity as well as their TE efficiencies.

[1] This chapter is based on reference [171]

3.2 Experimental

3.2.1 Sample Preparation

PPy/MWCNT nanocomposites were fabricated using in-situ oxidative polymerization method. An aqueous solution of MWCNT (AQ0101, Nanocyl) was firstly prepared using deionized (D.I.) water. The solution was sonicated for one hour with an ultrasonic probe (Q700, QSonica) to ensure uniform distribution of carbon nanofillers. The pyrrole monomer (Py, reagent grade, 98%, Sigma Aldrich) was then added to the solution while the sonication was continued for 5 minutes. An aqueous solution of iron (III) chloride ($FeCl_3$, reagent grade, 97%, Sigma Aldrich) was separately prepared and added dropwise into the Py/MWCNT solution to initiate the polymerization of PPy. The pyrrole concentration in the final reaction solution remained constant at 0.04 mol/L for all composite samples. The solution's temperature was retained at 0 °C to 5 °C using an ice bath, for the duration of polymerization, to slow down the polymerization process. Decreasing the polymerization rate will result in longer conjugation, which would provide better electron transfer along the polymer's backbone [122,123]. The reaction solution was vigorously stirred for one hour to achieve a uniform distribution of MWCNTs within the PPy matrix.

Three reaction times (i.e., 1, 5, and 24 hrs) were selected to study its effects on the TE properties of the fabricated samples. Three types of additives (i.e., methanol, methyl orange (MO), and sodium dodecyl sulfate (SDS)) were separately added to the reaction mediums, and their effects on the PPy/MWCNT nanocomposite's morphology and TE efficiency were investigated. The selected concentrations of methanol and SDS in the final reaction solutions were 20 wt.% and 0.1 mol/L, respectively. The MO-to-Py molar ratio of 0.05 was selected for the samples prepared by using methyl orange. Upon the completion of polymerization, the precipitate was filtered and

rinsed with D.I. water and ethanol for multiple cycles to remove any remaining oxidants or impurities. The fabricated nanocomposites were then dried in an oven with air atmosphere at 60 °C for 12 hours, and the dried powders were weighed to determine the filler contents of PPy/MWCNT nanocomposites. Different oxidant-to-monomer molar ratios (R_1; ranged from 0.1 to 8) and filler-to-monomer mass ratios (R_2; ranged from 0.01 to 5) were used to investigate the effects of these processing parameters on the TE efficiency and morphology of the fabricated samples.

3.2.2 Characterization

The nanocomposite powders were cold pressed at 4000 psi into circular discs of 20 mm in diameter and 2 mm in thickness using a compression molding machine (Craver Press, 4386 CH). The microstructure of polymer nanocomposite samples was characterized using scanning electron microscopy (SEM: FEI Company, Quanta 3D FEG) with an accelerating voltage of 20 kV. The cross sections of samples were exposed by cryo-fracturing them within liquid nitrogen, following by gold coating using a sputtered coating machine (Denton Vacuum, Desk V Sputter Coater). The void fractions of the cold-pressed samples were estimated by calculating the density of the composite material using their mass and physical dimensions, and considering the densities of MWCNTs and PPy to be 1.75 gcm^{-3} and 1.5 gcm^{-3}, respectively [72,124]. The electrical conductivities of nanocomposite samples were measured by the four-point method using a multifunctional source meter (Keithley, SMU 2450) and a four-point probe (SP4 probe head) installed on a probing fixture (Signatone probe S-302-4). According to ASTM F84-02 standard, the samples' bulk electrical conductivities were calculated using the size and thickness correction factors. The Seebeck coefficient was determined using a custom-built analyzer, that measured the induced voltage across the surface of a sample once exposed to a temperature difference. Figure

3.1 shows a schematic picture of the equipment which was used for measuring the Seebeck coefficient of the composite samples during this study. All samples were subjected to temperature differences in the range of 2 K to 4 K by putting them between two copper blocks. One of the blocks was embedded with a heating module while the other embedded with a cooling module. A thin layer of glass was used as a contact medium between the nanocomposite sample and the copper blocks to limit the current flow through the sample. The temperature difference across the sample was measured using two thermocouples. The Seebeck coefficient was calculated as the slope of the linear change in measured voltage versus the temperature difference across the sample's surface.

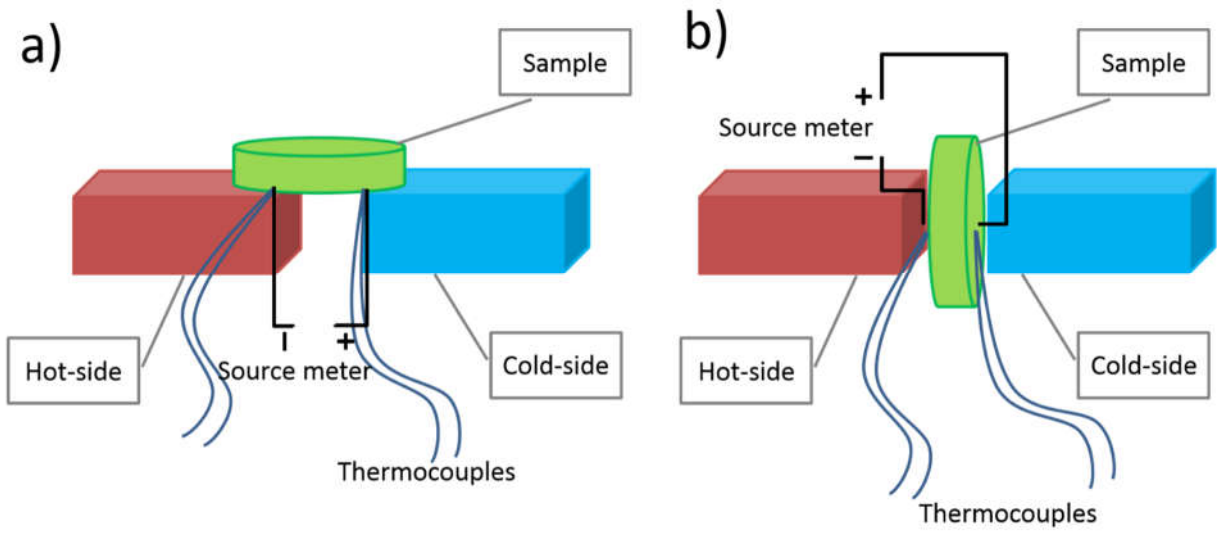

Figure 3.1 The custom-build unit for measuring the Seebeck coefficient of the fabricated samples in: (a) through-surface direction; and (b) through-thickness direction

3.3 Results and Discussion

3.3.1 Effect of Reaction Time on the Degree of Polymerization

Two sets of PPy/MWCNT samples with oxidant-to-monomer molar ratios (R_1) of 1 and 2.5 were prepared. The PPy contents of the fabricated samples were measured after 1, 5, and 24 hr to investigate the required reaction time to complete the polymerization process. The MWCNT-to-monomer mass ratio (R_2) was maintained at 1 for all samples. For an R_1 ratio of 1, the PPy contents in the fabricated samples were virtually unchanged (approximately 64.3 wt.%) when the polymerization time increased from 1 hr to 24 hr. Similarly, the PPy contents of the nanocomposites, prepared at the R_1 ratio of 2.5 and the polymerization time of 1 hr and 5 hr, were about the same (approximately 66.6 wt.%). In contrast, with the same R_1 ratio (i.e., 2.5), the PPy fraction slightly increased to 71.0 wt.% when the polymerization time increased to 24 hr. These results showed that the polymerization process of PPy was mostly accomplished in the first hour. However, in the remaining part of this study, all the PPy/MWCNT samples were fabricated with a polymerization time of 24 hr to ensure complete PPy polymerization.

3.3.2 Effect of Oxidant Concentration on the Structures and Properties of PPy/MWCNT Nanocomposites

Figure 3.2(a) through (e) illustrate the effects of oxidant concentration on the final MWCNT content, void fraction, and TE properties of PPy/MWCNT samples. Two series of samples were prepared with MWCNT-to-Py mass ratios of 0.1 and 1. The void contents of the nanocomposite samples, prepared with different oxidant-to monomer molar ratios (R_1), is shown in Figure 3.2(a). By increasing the oxidant concentration from 0.1 to 1, the volume percent of the voids within PPy/MWCNT samples significantly decreased as more PPy was produced and potentially exposed

within the porous structure of the entangled MWCNTs. Further increasing the oxidant concentration demonstrated less noticeable effect on the samples' void content, which means Py monomer had been mostly polymerized with R_1 ratio of 1. According to Figure 3.2(b), by increasing the R_1 ratio within the reaction system, the MWCNT content in the fabricated nanocomposites initially decreased and eventually became plateau when R_1 was raised beyond 2.5. This phenomenon indicated that setting R_1 to about 2.5 was sufficient to complete the polymerization process. Therefore, further addition of the oxidant had a negligible effect on polymerizing Py within the PPy/MWCNT samples. An optimum value of around 2 to 2.5 was also reported in the literature for the oxidant-to-monomer molar ratio to achieve 100% polymerization of Py monomer [122,125].

Figure 3.2(c) reveals that the electrical conductivity of the PPy/MWCNT samples with lower MWCNT loading (i.e., $R_2 = 0.1$) was significantly affected by the oxidant concentration while showed its maximum value at an R_1 ratio of 2.5. However, for the samples prepared with higher MWCNT loading (i.e., $R_2 = 1$), the effect of R_1 ratio on their electrical conductivity was less noticeable. Figure 3.2(d) indicates that the Seebeck coefficients of the nanocomposite samples had an inverse relation to their electrical conductivities. Such observation is consistent with the results reported in the literature [126,127].

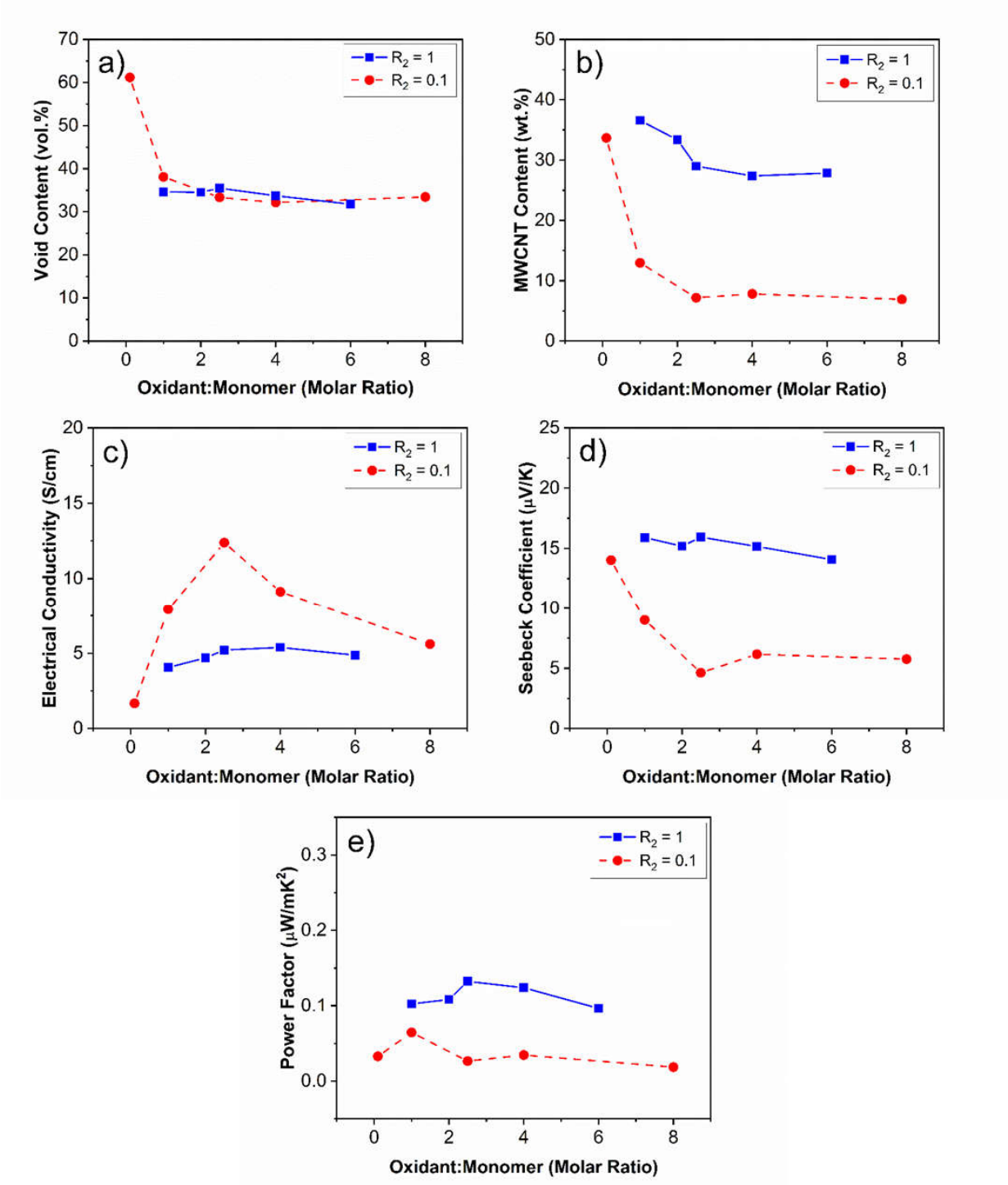

Figure 3.2 The effects of oxidant-to-monomer molar ratio on: (a) void fraction; (b) MWCNT content; (c) electrical conductivity; (d) Seebeck coefficient; and (e) power factor of PPy/MWCNT nanocomposite samples

Figure 3.2(e) illustrates the effect of oxidant-to-monomer molar ratio on the power factor of PPy/MWCNT samples. The results showed that increasing the R_1 ratio had a negligible influence on the TE performance of PPy/MWCNT nanocomposites; however, the samples with higher MWCNT loadings resulted in higher TE efficiencies. The effects of the processing parameters of PPy/MWCNT nanocomposites on their TE properties could be explained by considering the MWCNT content and the morphologies of the fabricated samples. A detailed discussion in this regard is provided in the following sections.

The SEM micrographs of PPy/MWCNT samples prepared with different oxidant-to-monomer molar ratios (i.e., 1, 2.5, and 8) are illustrated in Figure 3.3(a) through (f). The morphologies of the nanocomposite samples consisting of different amounts of PPy are demonstrated in Figure 3.3(a) through (c). A fibrous microstructure, which resembled the tubular shapes of MWCNTs, was observed for the samples prepared with an R_1 ratio of 1. However, when the R_1 ratio increased to 2.5 and 8, more continuous microstructures were observed due to the increased PPy content in the composite system. Figure 3.3(d) indicated that carbon nanotubes served as templates to direct the growth of PPy polymer chains along them, which was evidenced by the presence of a thin layer of PPy over MWCNTs. As it is shown in Figure 3.3(e), increasing the oxidant concentration in the Py/MWCNT reaction solution led to higher PPy contents (i.e., ~90 wt.% PPy with R_1 ratio of 2.5 versus ~65 wt.% PPy with R_1 ratio of 1). The pores among the entangled tubular PPy/MWCNT nanocomposites were filled up by additional PPy contents, leading to a more uniform and continuous microstructure. Further increasing the oxidant content showed a trivial effect on the morphology of PPy/MWCNT nanocomposites (Figure 3.3(f)). This observation supported the previous assumption that the R_1 ratio of 2.5 was sufficient to completely polymerize the monomers.

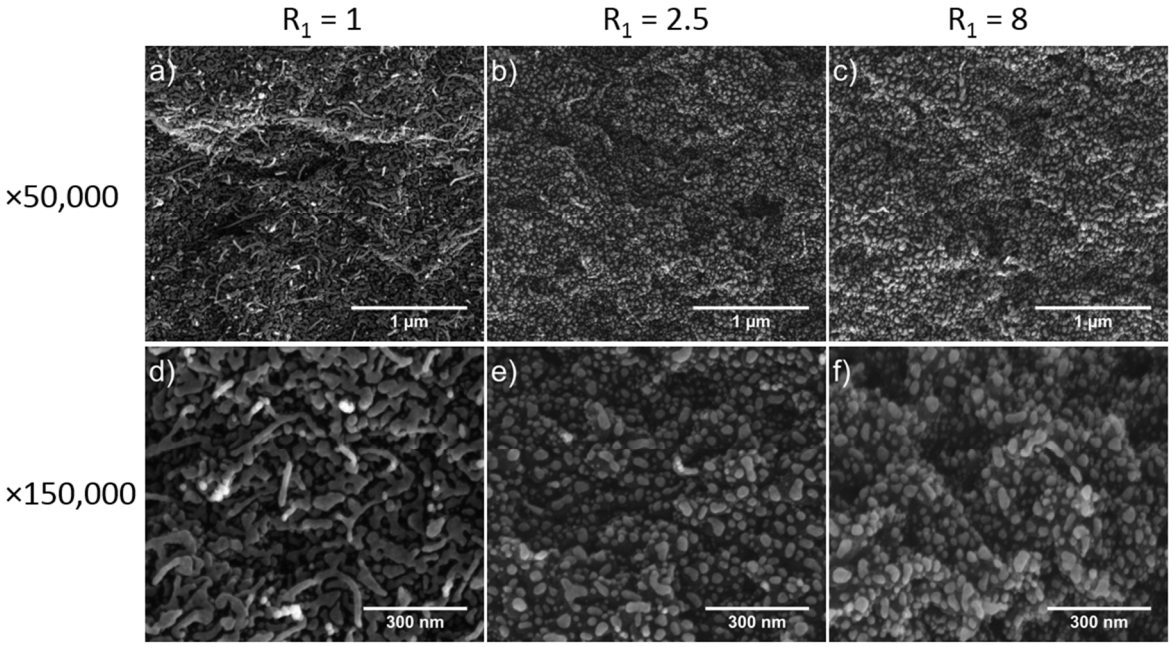

Figure 3.3 The SEM micrographs (with two different magnifications) of PPy/MWCNT nanocomposite samples prepared in water medium with R_2 ratio of 0.1 and containing different oxidant concentrations: (a) & (d) $R_1 = 1$; (b) & (e) $R_1 = 2.5$; and (c) & (f) $R_1 = 8$

3.3.3 Effects of MWCNT Content on the Structures and Properties of PPy/MWCNT Nanocomposites

The effects of MWCNT-to-Py mass ratio (R_2) on the final MWCNT concentration, void content, and TE properties of PPy/MWCNT samples are plotted in Figure 3.4(a) through (e). Two sets of samples were fabricated (i.e., samples prepared with and without the addition of methanol to the reaction solutions) to study the effect of methanol on the TE performance of PPy/MWCNT nanocomposite samples. According to Figure 3.4(a), increasing the R_2 ratio from 0.01 to 0.1 decreased the void content of the samples. At very low MWCNT loadings, the MWCNTs served as templates to grow PPy on their surfaces. Consequently, increasing the MWCNT content would help to produce a finely structured fibrous PPy/MWCNT morphology with better packing

efficiencies, which would provide lower void contents. The graphs also reveal that using methanol within the reaction medium created lower volume fractions of pores in the nanocomposite samples. This phenomenon indicated that methanol was more effective to produce a uniform distribution of PPy on top of the MWCNT networks and create a fine PPy/MWCNT microstructure. As shown in Figure 3.4(b), increasing the R_2 ratio would increase the MWCNT content in the fabricated nanocomposite, while its maximum MWCNT content remained constant at approximately 35 wt.%. This result indicated that at elevated R_2 ratios (i.e., $R_2 > 2$), the produced PPy matrix during the in-situ polymerization was not enough to perform as a binder phase among all MWCNTs. Therefore, the excess MWCNTs content was potentially washed off from the nanocomposite powders after completing the polymerization. Consequently, the final MWCNT content of PPy/MWCNT samples remained constant at approximately 35 wt.%.

According to Figure 3.4(c), the maximum measured electrical conductivity of the nanocomposite samples was at an R_2 ratio of 0.1, while the MWCNT contents of the samples were about 6-7 wt.%. Surprisingly, increasing the R_2 ratio above 0.1 resulted in a remarkable reduction in the electrical conductivity of the PPy/MWCNT nanocomposites. Similar behavior was observed in previous studies for the electrical conductivity of polymer/CNT composites by using a conducting type of polymer [42,128]. It is believed that a critical amount of PPy content was required to modify the MWCNT-MWCNT junctions and promote the formation of connected pathways for electron transferring through the polymer nanocomposite. By increasing the R_2 ratio above this critical level, less PPy polymer was exposed at the MWCNT-MWCNT intersections, which was insufficient to create a continuous path for electron transferring throughout the composite system. Therefore, the introduced electrical resistance at filler junctions suppressed the samples' electrical conductivities.

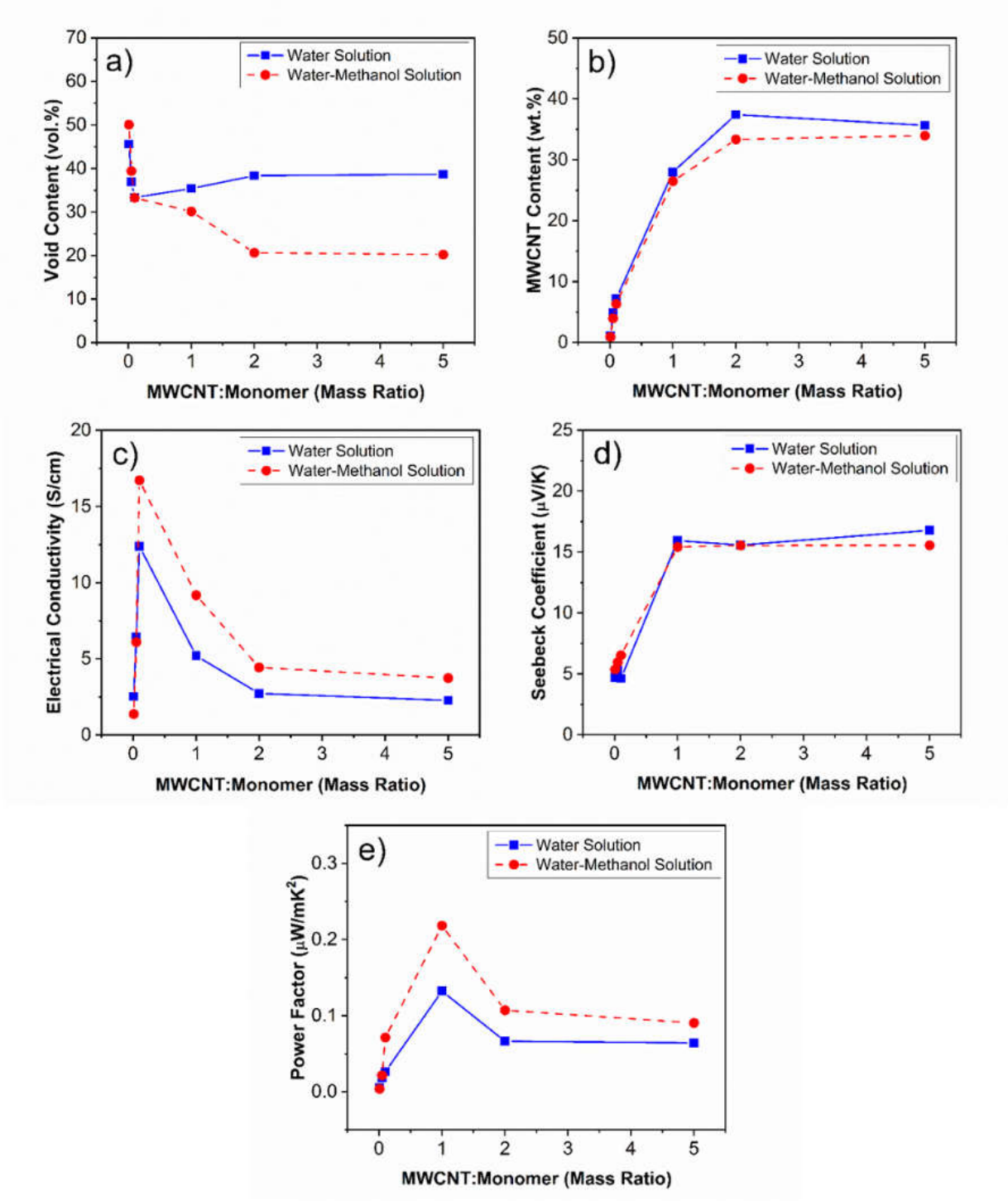

Figure 3.4 The effects of MWCNT-to-monomer mass ratio on: (a) void content; (b) MWCNT content; (c) electrical conductivity; (d) Seebeck coefficient; and (e) power factor of PPy/MWCNT nanocomposite samples

As shown in Figure 3.4(d), by increasing the MWCNT-to-Py mass ratio for the processing of the nanocomposite samples, the changes in Seebeck coefficients followed a similar trend to their MWCNT contents. For samples prepared by $R_2 \leq 0.1$, their Seebeck coefficients were approximately 6 μVK^{-1}. Increasing the R_2 ratio above 1 resulted in Seebeck coefficients within the range of 12-16 μVK^{-1}, which was similar to the values measured for pure MWCNT films. The MWCNT film was prepared by solution casting of the aqueous 1 wt.% MWCNT solution and drying at room temperature. The through-surface Seebeck coefficient of the MWCNT film was measured with the same method used for PPy/MWCNT composite samples. The observed results indicated that the Seebeck coefficient of PPy/MWCNT samples with MWCNT contents of higher than 30 wt.%, was mainly governed by the Seebeck effect of carbon nanotubes. Figure 3.4(e) plots the power factor of nanocomposite samples with different MWCNT contents. Experimental results revealed that an optimized level of filler loading within PPy nanocomposite samples is required to maximize their thermoelectric performances. The highest power factor was obtained for the samples with an R_2 ratio of 1, in which their MWCNT contents were around 30 wt.%.

Figure 3.4(c) through (e) also show the TE properties of the nanocomposite samples prepared by adding methanol to their reaction solution. Experimental results reveal that methanol helped to promote the electrical conductivity of PPy/MWCNT nanocomposites while had negligible effects on the nanocomposites' Seebeck coefficients. As a result, methanol could improve the overall power factor and thereby, the TE efficiency of PPy/MWCNT nanocomposite samples. As an example, the power factor of the samples prepared with R_2 ratios of 0.1 and 1 increased 2.6 and 1.6 times, respectively, after the addition of methanol in their polymerization process.

The SEM micrographs of the fabricated nanocomposite samples with different MWCNT loadings are shown in Figure 3.5(a) through (f). The SEM images with lower magnifications (i.e.,

Figure 3.5(a) through (c)) illustrate the morphology of the samples' cross-sections. With an R_2 ratio of 0.01, a rough surface morphology with porous structure was observed. By increasing the MWCNT loading of the samples, a more uniform structure was achieved with less porosity; however, further increasing the MWCNT content resulted in a fibrous structure. Figure 3.5(d) through (f) show that PPy/MWCNT samples, depending on their MWCNT contents, could demonstrate three different microstructures. The MWCNT-to-Py ratio of 0.01 created islands of polymer nanocomposite with poor packing efficiency and resulted in high levels of porosity.

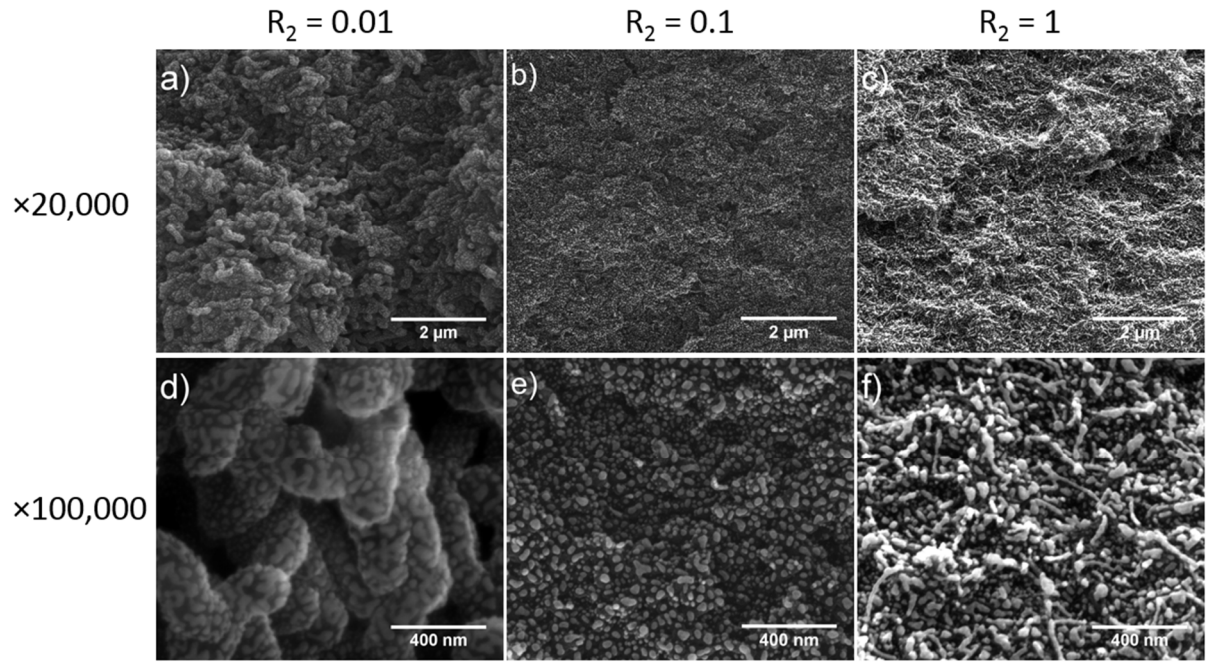

Figure 3.5 The SEM micrographs (with two different magnifications) of PPy/MWCNT nanocomposite samples prepared in water medium with R_1 ratio of 2.5 and loaded with different MWCNT contents: (a, d) $R_2 = 0.01$; (b, e) $R_2 = 0.1$; and (c, f) $R_2 = 1$

At an R_2 of 0.1, a finer polymer nanocomposite texture with lower porosity was observed. The PPy polymer was uniformly deposited on the network of MWCNTs and at their junctions that resulted in a continuous microstructure. Nanocomposite samples prepared with an R_2 ratio of 1

demonstrated a fibrous morphology because individual MWCNTs were lightly coated by PPy while the PPy content was not enough to create a continuous PPy/MWCNT microstructure.

Figure 3.6(a) through (d) compare the morphology of PPy/MWCNT nanocomposites prepared with and without the addition of methanol. The morphologies of the nanocomposite samples containing methanol in their reaction solutions revealed fine particles of PPy deposited on the surfaces of MWCNTs. In this case, PPy particles were mostly scattered along the MWCNT surfaces and at the MWCNT-MWCNT intersections rather than uniformly coating individual MWCNTs. Therefore, PPy polymer helped to create more connected MWCNT networks with fewer obstacles for electron transferring within the PPy/MWCNT material system.

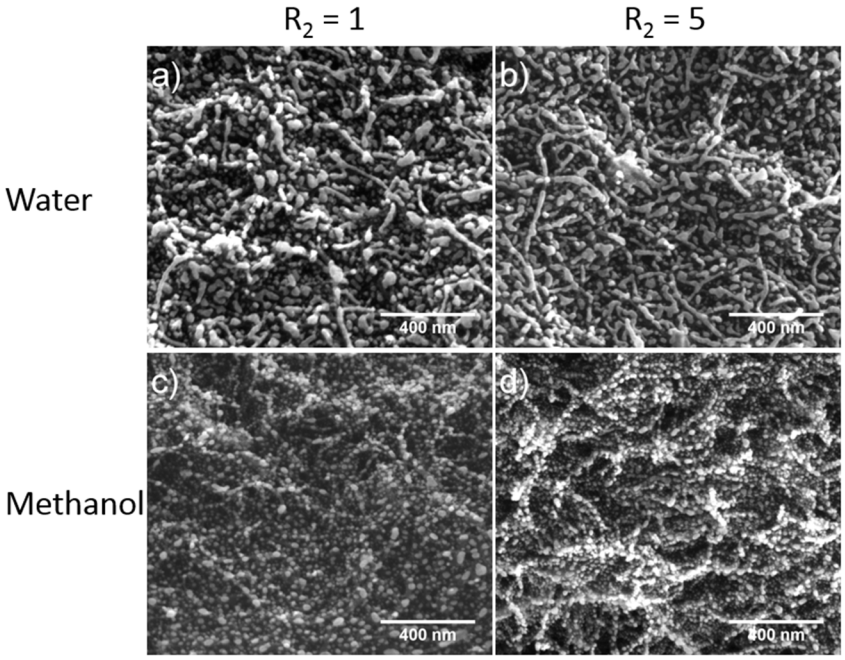

Figure 3.6 The SEM micrographs of PPy/MWCNT samples prepared with R_1 ratio of 2.5 by using: (a) water with $R_2 = 1$; (b) water with $R_2 = 5$; (c) methanol with $R_2 = 1$; and (d) methanol with $R_2 = 5$

3.3.4 Effects of Additives on the Structures and Properties of PPy/MWCNT Nanocomposites

According to literature, methanol, methyl orange (MO), and sodium dodecyl sulfate (SDS) are three additives that have been previously used as dopants to modify the microstructure and electrical conductivity of PPy [129–133]. These three additives were used in the current study, within the reaction systems during the polymerization of PPy, to explore their effects on the morphology and TE performance of the PPy/MWCNT nanocomposites. The MWCNT content, the void fraction, and the measured TE parameters of the fabricated samples with different reaction mediums are shown in Figure 3.7(a) and (b). All samples were prepared using R_1 and R_2 ratios of 2.5 and 1, respectively. Therefore, the MWCNT contents of the samples prepared using different additives were within the same range (i.e., 25 wt.% to 30 wt.%) as illustrated in Figure 3.7(a). The nanocomposite samples prepared by using methanol and water showed the lowest and highest void contents, respectively, compared with the other two samples (i.e., the ones prepared by using MO and SDS). These findings indicated that methanol was the best medium for creating a fine PPy/MWCNT microstructure with less porosity, which could help to promote their electron transport properties. Figure 3.7(b) shows that the Seebeck coefficients of the fabricated samples remained within the range of 13-16 μVK^{-1}, while all samples contained 25-30 wt.% of MWCNTs. The results indicated that the nanocomposite samples prepared by adding methanol demonstrated the best electrical conductivities and thereby the highest power factors. However, SDS and methyl orange provided a negligible effect on the TE performance of the fabricated nanocomposites. Therefore, methanol was the best additive, among the three being studied, to promote the TE efficiency of PPy/MWCNT nanocomposites.

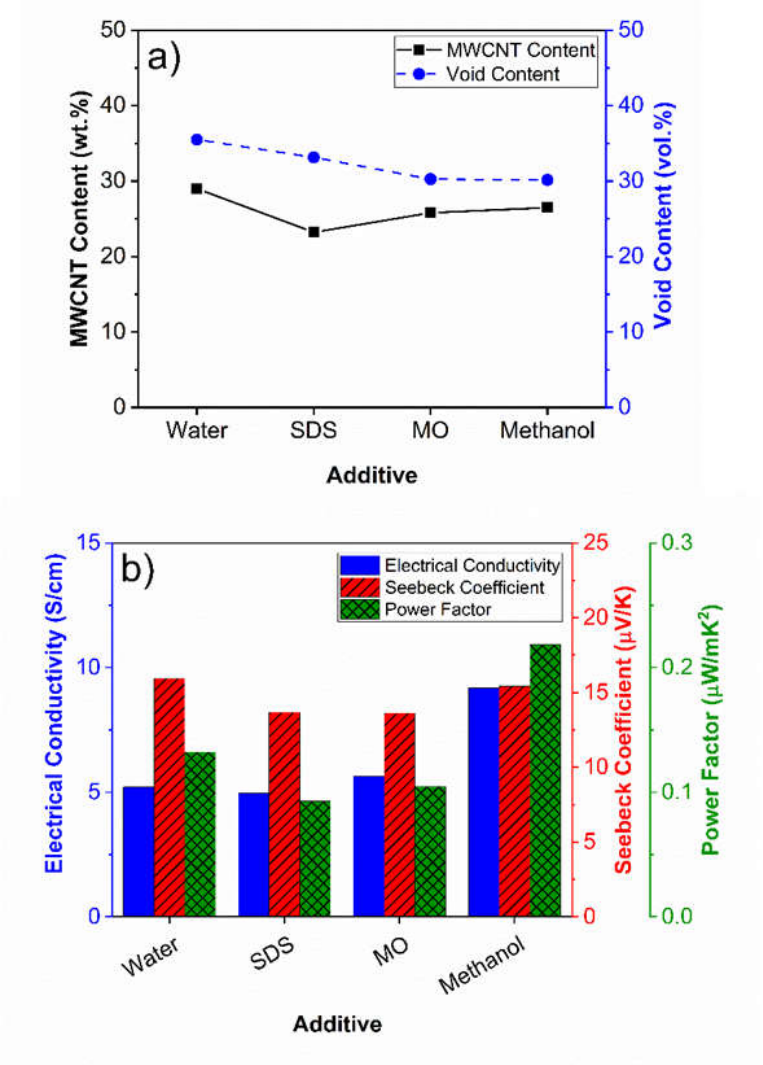

Figure 3.7 The effects of using different additives during the polymerization of PPy on: (a) MWCNT concentration and void content; and (b) TE properties of PPy/MWCNT nanocomposite samples (The R_1 and R_2 ratios were 2.5 and 1, respectively)

The microstructures of the PPy/MWCNT samples, fabricated by using different additives, are illustrated in Figure 3.8(a) through (h). The samples were prepared with R_1 and R_2 ratios of 2.5 and 1, respectively. The micrographs illustrate that methanol helped to create the most uniform nanocomposite structure with the lowest porosity when compared to the other two additives. These

findings reveal that the presence of pores in the nanocomposite samples could adversely affect their electrical conductivities by increasing the charge carriers' scattering within their structures.

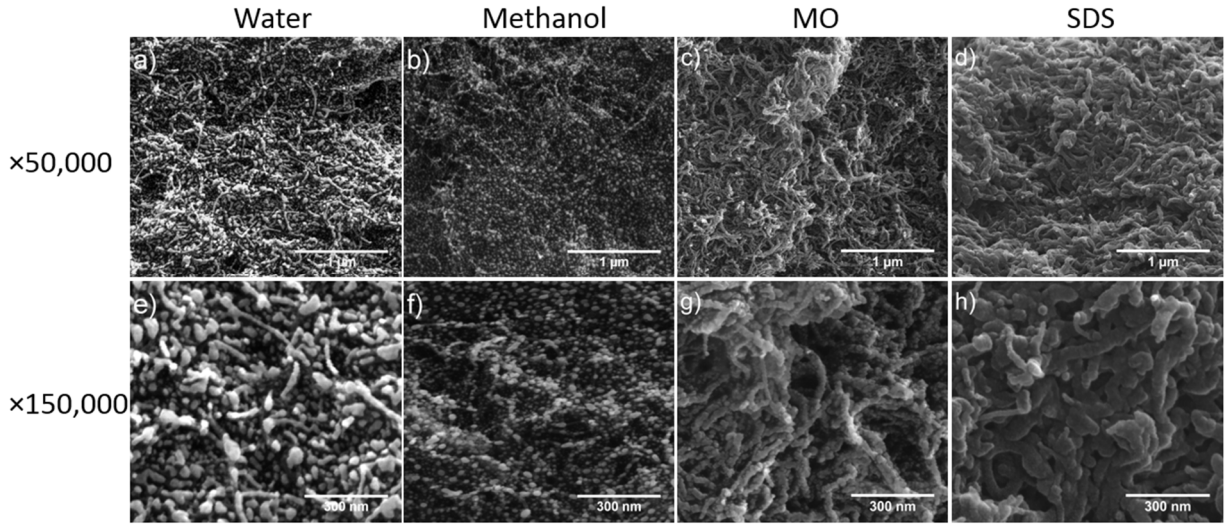

Figure 3.8 The SEM micrographs (with two different magnifications) of PPy/MWCNT nanocomposite samples prepared by using: (a) & (e) water; (b) & (f) methanol; (c) & (g) methyl orange (MO); and (d) & (h) and sodium dodecyl sulfate (SDS)

Previous studies reported that the electrical conductivity of PPy samples with tubular nanostructure is related to the nanotubes' diameters [134]. In this research, the microstructures of the samples, prepared with pure water or with the addition of MO and SDS, were in the form of nanofibers. The experimental results and the SEM micrographs indicated that the electrical conductivity of the fabricated samples has an inverse relation to the average diameters of their nanofibers. However, the Seebeck coefficients of PPy/MWCNT nanofibers were almost insensitive to their microstructures.

3.4 Conclusion

In this study, PPy/MWCNT nanocomposite samples were fabricated using in-situ polymerization method. The effects of different processing parameters such as polymerization time, oxidant concentration, MWCNT loading, and using additives within the reaction solution on the TE efficiencies of the PPy/MWCNT nanocomposites were thoroughly investigated. The optimal oxidant-to-monomer molar ratio was found to be around 2.5, which ensures complete polymerization of PPy using $FeCl_3$ as the oxidant. The MWCNT-to-Py mass ratio was identified as the most effective parameter on maximizing the electrical conductivity and TE power factor of PPy/MWCNT nanocomposites. Moreover, using methanol helped to promote the electrical conductivity and thereby the TE efficiency of the fabricated samples by modifying their morphologies. However, the effects of adding methyl orange and SDS during the polymerization process was negligible on tuning the TE properties of the samples. The results of this study provide a detailed insight about the potential of different processing parameters on controlling thermoelectric properties and the electrical conductivities of polymer nanocomposite materials containing conducting polymers and carbon nanotubes.

Chapter 4. Enhancement of Thermoelectric Conversion Efficiency of Polymer/Carbon Nanotube Nanocomposites through Foaming-Induced Microstructuring[2]

4.1 Introduction

This study aims to investigate the potential of using physical foaming as a novel strategy to enhance the TE conversion efficiency of nanocomposite materials. Multi-walled carbon nanotube/high density polyethylene (HDPE) nanocomposite foams were fabricated as a case example to explore the potential of the proposed method. The effects of different processing parameters on the thermal and electrical conductivity of the nanocomposite foams were studied in this phase of research.

This study revealed that an enhancement in the TE efficiency of the fabricated nanocomposite samples was achieved not only by promoting their electrical conductivity and Seebeck coefficient but also by simultaneously suppressing their thermal conductivity. The experimental results showed that introducing cellular structures in MWCNT/HDPE nanocomposites, loaded with 15 wt.% MWCNT, would enhance their *ZT* values by 600-fold. This great improvement was achieved through a significant reduction in their effective thermal conductivity, along with a simultaneous

[2] This chapter is based on reference [71]

improvement in their electrical conductivities and Seebeck coefficients. The findings have proven that foaming can serve as a novel technique to enhance the efficiency of various polymeric TE materials.

4.2 Experimental

4.2.1 Materials

Commercially available MWCNT/HDPE masterbatch (Nanocyl, Plasticyl HDPE1501) loaded with 15 wt.% of MWCNT was used as the base material to fabricate the nanocomposite foams. This material system was selected as a case study to demonstrate the effects of in-situ foaming on promoting the TE efficiency of polymer-based materials. The applied physical foaming agent was carbon dioxide (CO_2) (Linde Gas Inc., 99.8% purity). The physical properties of the masterbatch and its constituents (i.e., HDPE and MWCNT) are summarized in Table 4.1 to Table **4.3**.

Table 4.1 Physical properties of MWCNT/HDPE nanocomposite (Nanocyl, Plasticyl HDPE1501)

Property	**Value**	**Unit**
MWCNT loading	15	wt.%
Density	997	kgm^{-3}
Melting temperature	135	°C
Thermal conductivity	0.50-0.70	$Wm^{-1}K^{-1}$

Table 4.2 Physical properties of HDPE (Borealis, MG9641B)

Property	**Value**	**Unit**
Density	964	kgm^{-3}
Melting temperature	130-137	°C
Thermal conductivity	0.45-0.52	$Wm^{-1}K^{-1}$

Table 4.3 Physical properties of MWCNT (Nanocyl, NC7000^{TM})

Property	Value	Unit
Avg. diameter	9.5	nm
Avg. length	1.5	μm
Volume resistivity	10^{-5}-10^{-4}	Ωcm
Thermal conductivity	≥ 3000	$Wm^{-1}K^{-1}$
Surface area	250-300	m^2g^{-1}

4.2.2 Preparation of MWCNT/HDPE Nanocomposite Foams

A calculated amount of MWCNT/HDPE nanocomposite pellets was weighed and loaded into a circular disc mold of 115 mm in diameter and 500 μm in thickness. The pellets were compression molded by the following procedures:

Step 1. MWCNT/HDPE nanocomposite pellets were charged into the mold and loaded into a compression molding machine (Craver Press, 4386 CH) preset at 155 °C.

Step 2. The sample and the mold were equilibrated at 155 °C for 5 minutes to ensure complete melting of the nanocomposite.

Step 3. The sample and the mold were pressurized to and maintained at 4000 psi (at 155 °C) for 5 minutes to compression mold the materials into thin-disc samples.

Step 4. The samples were transferred to a cooling module with flowing water channels for solidification.

These nanocomposite samples were then cut into rectangular stripes of 4 cm by 2 cm before being physically foamed by carbon dioxide (CO_2). After that, the cut samples were placed into a batch foaming chamber and saturated with CO_2 at a designated pressure and temperature for a

specific time. Subsequently, a fast pressure drop and thereby thermodynamic instability were induced by rapidly releasing CO_2 from the foaming chamber. This pressure drop would result in the nucleation and expansion of bubbles in the nanocomposite matrices. Table 4.4 summarizes the ranges of key processing parameters studied in the foaming experiments.

Table 4.4 Investigated parameters in physical foaming experiments

Variable	Value	Unit
Saturation Pressure	1000 - 2000	psi
Saturation Temperature	130 - 145	°C
Saturation Time	15, 30, 60	min

4.2.3 Sample Characterization

The apparent densities of MWCNT/HDPE nanocomposite foams were determined in accordance with ASTM D792 [135]. After measuring their masses in air and water, the apparent density (ρ) and the volume expansion ratio (ϕ) can be determined by Equations (4-1) and (4-2), respectively:

$$\rho = \frac{m_{air}\rho_{water}}{m_{air} - m_{water}} \tag{4-1}$$

where ρ is the apparent density of samples, m_{air} and m_{water} are the samples' masses measured in air and water, respectively, and ρ_{water} is the density of water:

$$\phi = \frac{\rho_s}{\rho_f} \tag{4-2}$$

where ρ_s and ρ_f are the densities of solid and foam samples.

The phase and foam morphologies of MWCNT/HDPE nanocomposite foams were characterized by scanning electron microscopy (FEI Company Quanta 3D FEG). The cross-

sections of all samples were exposed by cryo-fracturing the samples under liquid nitrogen. The fractured surfaces were then sputter-coated with gold (Denton Vacuum, Desk V Sputter Coater). The cell-size and cell population density were obtained by analyzing the SEM micrographs of the foams. The cell population density (N_0) with respect to the unfoamed volume was determined by Equation (4-3):

$$N_0 = \left[\frac{nM^2}{A}\right]^{3/2} \times \phi \tag{4-3}$$

where n is the number of cells in the SEM micrograph, M is the magnification factor, and A is the area of the micrograph.

All three TE-related parameters of the samples were measured in the through-thickness direction of nanocomposite films in order to calculate their through-plane TE efficiencies. The effective thermal conductivity (k_{eff}) of MWCNT/HDPE nanocomposite and its foams were measured with a thermal conductivity analyzer (C-Therm Technologies Ltd., Tci Thermal Conductivity Analyzer) based on the modified transient plane source (MTPS) technique [136]. In this method, a small amount of heat is momentarily applied to the sample using a one-sided heat-reflectance sensor. By measuring the rate of voltage-change in the sensor, caused by the heating of the sample-sensor interface, the thermal conductivity of the sample can be calculated. The electrical conductivity of the samples was characterized based on the two-point probe technique using a multifunctional source meter (Keithley, 2450 Source Meter). A conductive silver-epoxy paste was applied to both sides of each sample as electrodes to introduce a current through the nanocomposite film. The Seebeck coefficients of the samples were measured using a custom-made unit. By applying a temperature difference (ΔT) across the sample's thickness within the range of

2 ºC to 8 ºC, the generated voltage (ΔV) was recorded by the source meter. The Seebeck coefficient was calculated from the slope of the ΔV versus ΔT plot. The electrical conductivity and the Seebeck coefficient were simultaneously characterized at the same point of contact on the samples to minimize measurement inconsistency. The effects of foaming on the melting temperature and crystallinity of the MWCNT/HDPE nanocomposites were analyzed using differential scanning calorimetry (DSC) (TA Instruments, Q20). The DSC test was performed by heating the samples from 60 °C to 170 °C at a rate of 10 °Cmin^{-1}.

4.3 Results and Discussion

4.3.1 Effects of Foaming Conditions on Volume Expansion Ratios

Figure 4.1(a) through (c) illustrate the effects of different foaming conditions (i.e., saturation time, saturation pressure, and saturation temperature) on the volume expansion ratio of MWCNT/HDPE nanocomposite foams. The saturation time, saturation temperature, and saturation pressure of the base case were set to be 30 minutes, 135 °C, and 1000 psi, respectively. To examine the effect of each foaming parameter on the volume expansion ratio of the foamed samples, the other two parameters remained constant at the values corresponded to the base case. The average values and the standard deviation of all data points were obtained from measurements of three samples.

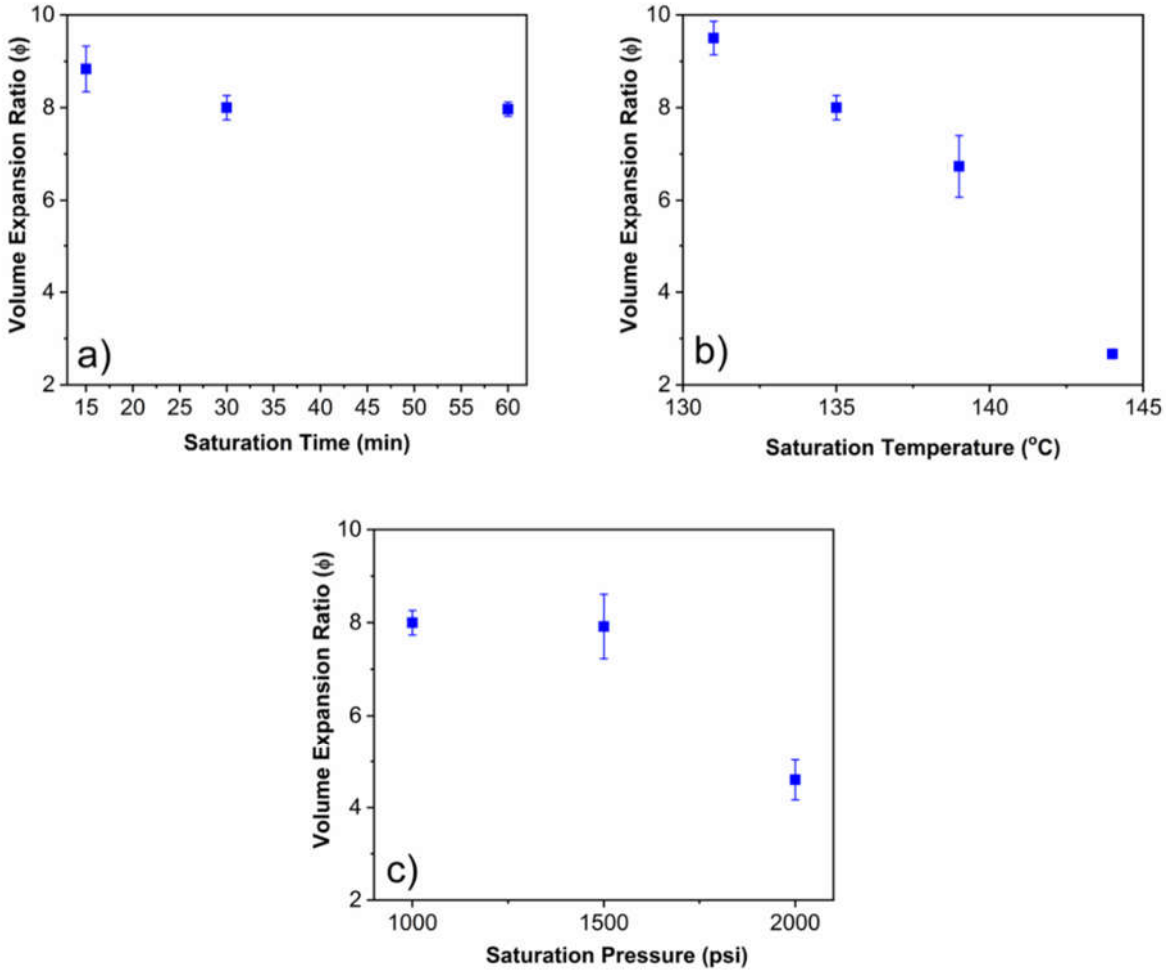

Figure 4.1 Effects of foaming conditions on the volume expansion ratios of MWCNT/HDPE foams: (a) saturation time; (b) saturation temperature; and (c) saturation pressure

Experimental results reveal that saturation time had a negligible effect on the volume expansion of the nanocomposite foams. This observation indirectly suggests that 15 minutes or more would be sufficient to saturate the MWCNT/HDPE specimens. Therefore, the saturation time for all remaining foaming experiments was fixed at 30 minutes to ensure full saturation of the samples. Unlike the saturation time, both the saturation temperature and saturation pressure had significant effects on the volume expansion ratios of MWCNT/HDPE foams. The trends show that

the volume expansion ratios of the nanocomposite foams decreased as these two parameters increased. The processing-to-structure relationship in the physical foaming of MWCNT/HDPE nanocomposites would be discussed in the next section by evaluating the average cell-size and the cell population density of different foam samples.

4.3.2 Effects of Foaming Conditions on Foam Morphologies

The cell morphologies of MWCNT/HDPE foams, fabricated at different saturation temperatures or different saturation pressures, were evaluated in terms of their average cell-sizes, cell-size distributions, and cell population densities. The results were illustrated in Figure 4.2(a) and (b). It can be observed that increasing the saturation temperature would suppress the cell nucleation without significantly affecting the average cell-size of the foam samples. As the saturation temperature increased, the solubility of CO_2 in HDPE decreased. The reduced CO_2 contents in the HDPE matrices led to lower nucleating power and thereby a gradual reduction in the nanocomposite foam's cell population density. As a result, the nanocomposite foams' volume expansion ratios decreased with increasing their saturation temperatures.

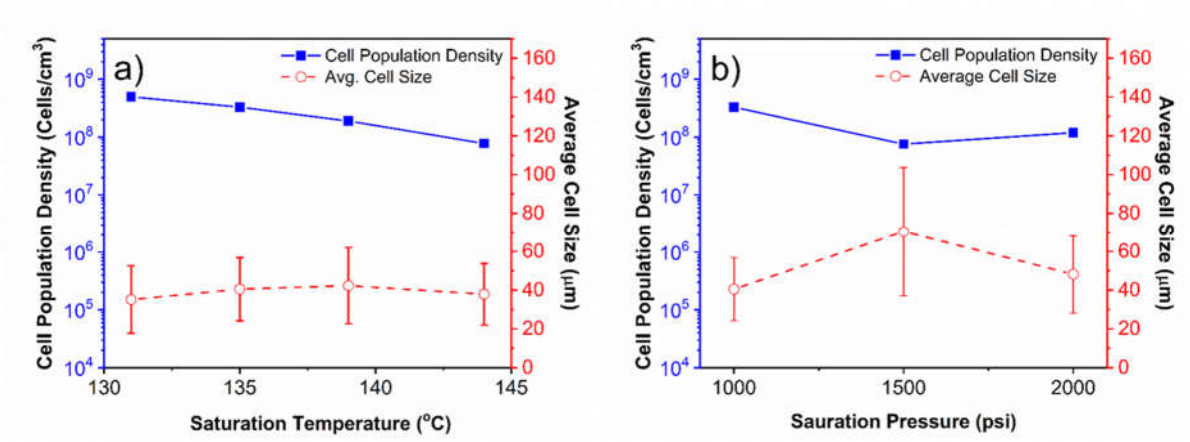

Figure 4.2 Effects of foaming conditions on the cell morphologies of MWCNT/HDPE foams: (a) saturation temperature; and (b) saturation pressure

Surprisingly, it was observed that the cell population density was decreased by increasing the saturation pressure from 1000 psi to 1500 psi or 2000 psi. In contrast, the average cell-size had an opposite relationship with the saturation pressure. It was due to the coupled effects of higher cell nucleating power and promoted cell coalescence at elevated saturation pressures. Higher saturation pressure would result in more dissolved CO_2 within the polymer matrix, which was expected to promote the cell nucleation as well as the volume expansion ratio. However, when the saturation pressure was too high, the plasticizing effect, caused by the dissolved CO_2, became more pronounced [103]. This effect led to a severe cell coalescence, which suppressed the cell population density while simultaneously increased the cell-sizes and their size distribution. The excessive gas loss caused by the cell-wall rupture contributed to the reduction in the volume expansion ratio, as the saturation pressure further increased to 2000 psi. Overall, the processing-to-structure relationships of the fabricated MWCNT/HDPE foams could be revealed by examining their microstructures. Figure 4.3 through Figure 4.6, show the SEM micrographs as well as the cell-size distributions of the MWCNT/HDPE foams prepared at different processing conditions.

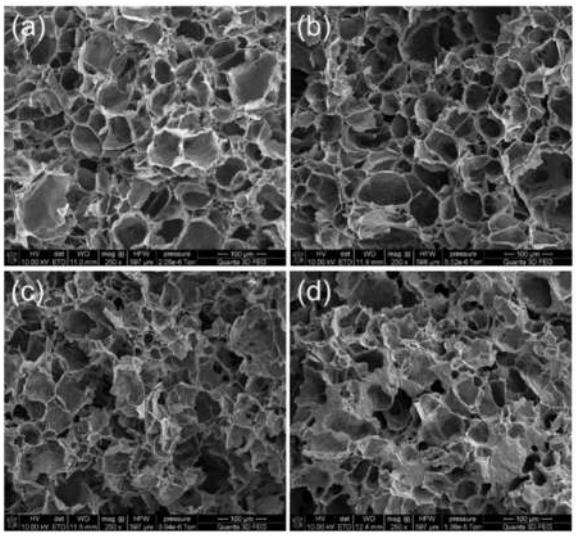

Figure 4.3 SEM micrographs of MWCNT/HDPE foams fabricated at different saturation temperatures: (a) 131 °C; (b) 135 °C; (c) 139 °C; and (d) 144 °C

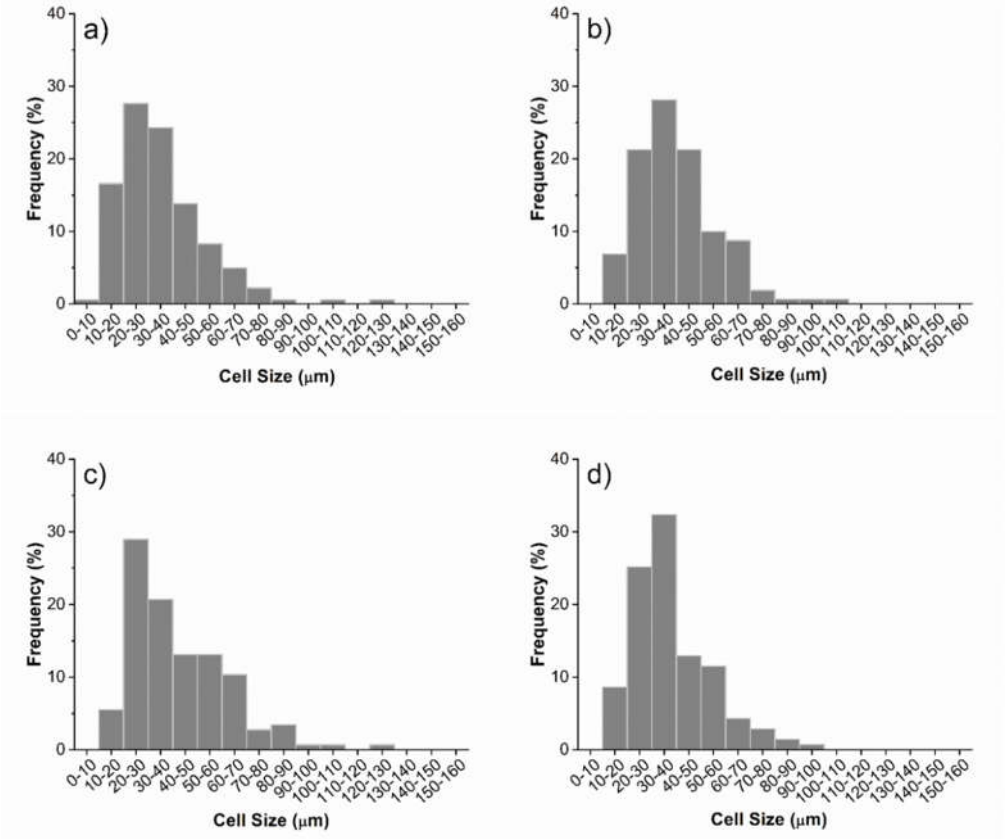

Figure 4.4 Cell-size distributions of MWCNT/HDPE foams fabricated at different saturation temperatures: (a) 131 °C; (b) 135 °C; (c) 139 °C; and (d) 144 °C

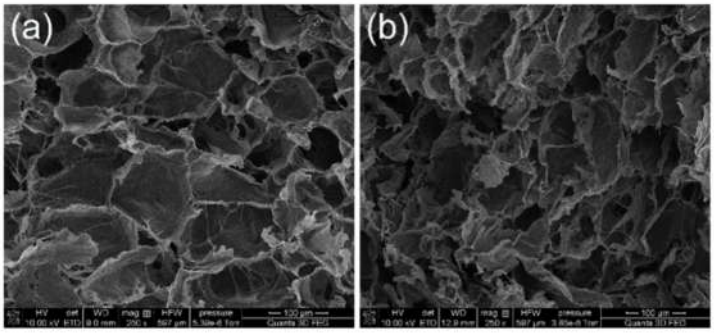

Figure 4.5 SEM micrographs of MWCNT/HDPE foams fabricated at different saturation pressures: (a) 1500 psi; and (b) 2000 psi

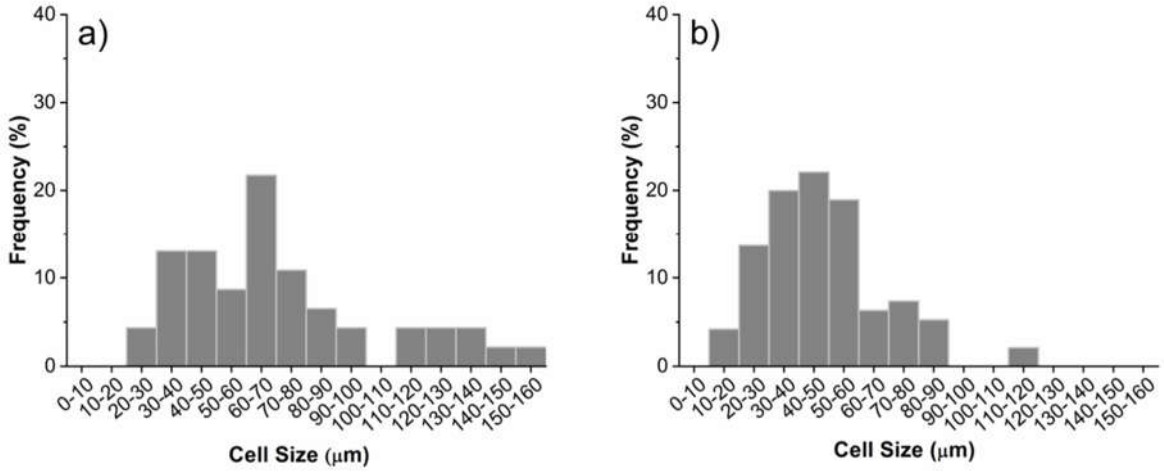

Figure 4.6 Cell-size distributions of MWCNT/HDPE foams fabricated at different saturation pressures: (a) 1500 psi; and (b) 2000 psi

4.3.3 Effects of Foaming on HPDE Crystallization

The results of the previous section revealed that the nanocomposites foamed at 1000 psi yielded more uniform cellular morphologies. Therefore, the effects of foaming on crystallization of the HDPE matrix in MWCNT/HDPE samples were explored with varying the saturation temperature while maintaining the saturation pressure at 1000 psi. Figure 4.7 illustrates the thermograms obtained from MWCNT/HDPE nanocomposites and their foams, prepared at different saturation temperatures and at a saturation pressure of 1000 psi. The average degrees of crystallinity of all the foamed samples were compared with that of their solid nanocomposite. The degree of crystallinity was determined by Equation (4-4) considering the enthalpy of fusion for a 100% crystalline HDPE sample as 293.6 Jg^{-1} [137].

$$\chi = \frac{\Delta H}{H_c V_p} \tag{4-4}$$

where χ is the degree of crystallinity; ΔH is the enthalpy of fusion of the sample; H_c is the enthalpy of fusion of a 100% crystalline HDPE sample, and V_p is the weight fraction of polymer in the nanocomposite specimen.

The DSC thermographs indicate that foaming induces a negligible effect on the melting temperature of the nanocomposite. The degrees of crystallinity of all foamed samples, in contrast, were higher than the unfoamed samples. It was found that CO_2 foaming had led to an average increase in the degree of crystallinity from 66.1% to 73.1%, with a standard deviation of 3.1% among nanocomposite foams prepared at different temperatures. This deviation was caused by the plasticization effect of the dissolved CO_2 in the polymer matrices as well as the strain-assisted crystal nucleation during the foam expansion [138].

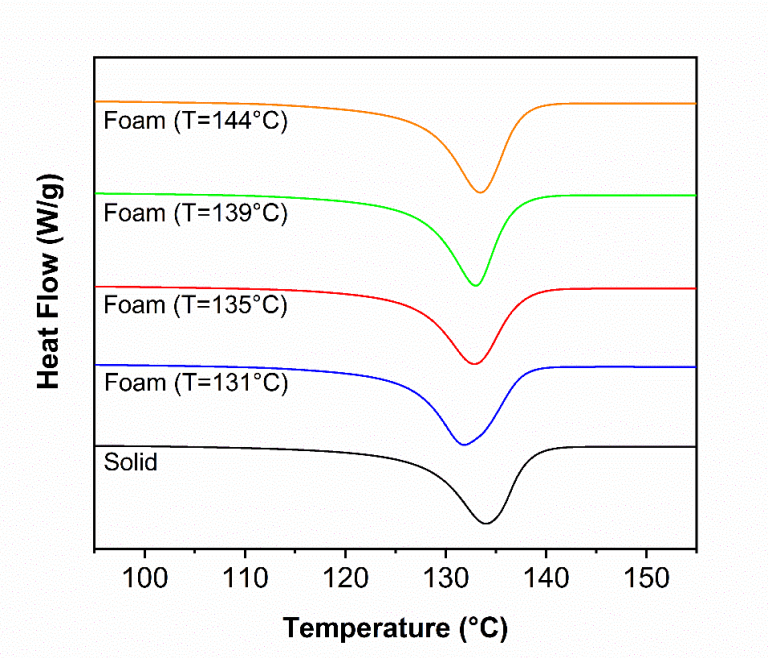

Figure 4.7 DSC thermograms of MWCNT/HDPE nanocomposite and their foams prepared at different saturation temperatures (saturation pressure = 1000 psi)

4.3.4 Effects of Foaming Conditions on the Effective Thermal Conductivity of MWCNT/HDPE Nanocomposite Foams

Figure 4.8(a) and (b), plot the effects of foaming conditions on the effective thermal conductivity of MWCNT/HDPE nanocomposite foams. Experimental results reveal that reducing either the saturation temperature or the saturation pressure helped to suppress the nanocomposite foam's effective thermal conductivity. This observation can be explained by the higher volume expansion ratio of nanocomposite foams achieved under these conditions. High volume expansion ratio led to more insulating voids in the matrices. Moreover, it would also enhance the number of boundaries throughout the matrices, and thereby hindered the movement of phonons as heat carriers through the bulk of material [139]. As illustrated in the SEM micrographs in Figure 4.5, higher saturation pressure would result in more cell coalescence. The high degree of cell openings would be detrimental to the thermal insulation of the nanocomposite foams and thereby increased their effective thermal conductivity. The results indicate that the effective thermal conductivity of nanocomposite foams is one order of magnitude lower than the nanocomposite samples before foaming. In particular, an average thermal conductivity of 0.06 $Wm^{-1}K^{-1}$ for nanocomposite foams was obtained versus 0.61 $Wm^{-1}K^{-1}$ for the solid nanocomposites. In other words, while the addition of MWCNT to HDPE would increase its thermal conductivity by about twofold, the incorporation of cellular structures in nanocomposite matrices considerably suppressed their effective thermal conductivity [140,141].

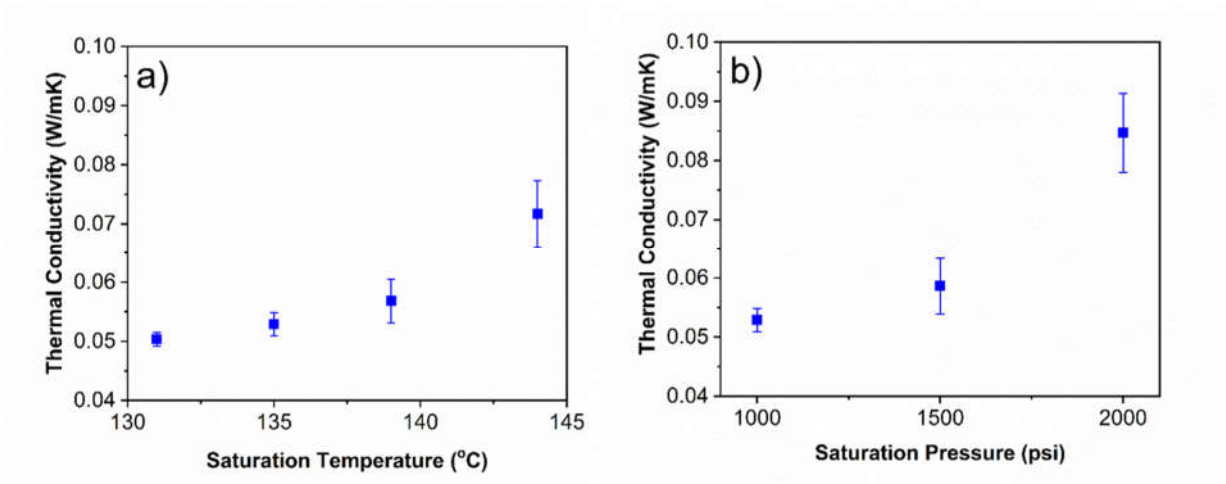

Figure 4.8 Effects of foaming conditions on the effective thermal conductivity of MWCNT/HDPE nanocomposite foams: (a) saturation temperature; and (b) saturation pressure

4.3.5 Effects of Foaming Conditions on the Electrical Conductivity of MWCNT/HDPE Nanocomposite Foams

The effects of foaming conditions on the through-thickness electrical conductivity of the MWCNT/HDPE nanocomposite foams are shown in Figure 4.9(a) and (b). The experimental measurements show that MWCNT/HDPE nanocomposite foams provided higher electrical conductivities than their solid counterparts. In particular, the average electrical conductivity of the foamed samples was up to five times higher than that of the solid nanocomposite specimens (i.e., 1.0×10^{-1} Scm^{-1} vs. 1.9×10^{-2} Scm^{-1}). During the compression molding process to prepare the nanocomposite specimens, some degrees of MWCNT alignment along the in-plane direction would have been caused by the flow of polymer melt. In the nanocomposite foam specimens, these partially aligned MWCNTs were reoriented and led to more connected paths across the thickness direction. This phenomenon could be attributed to the growth of the nucleated cells during the foaming process. Moreover, the foaming-induced biaxial stress field around the cell-walls would

generate a local flow of polymer melt tangential to the cell-walls. This stress would lead to the stretching of the cell-walls that increased their lateral dimension and reduced their thickness. Overall, these effects resulted in localization and enhanced alignment of fillers along the cell-walls [142]. As a result, the nanocomposite foams would contain more electrically conductive paths in the through-plane direction of the samples. This observation was consistent with those made by Ameli *et al.* and Motlagh *et al.* [143,144]. The results also indicated that reducing either the saturation temperature or the saturation pressure decreased the foam's electrical conductivity. This phenomenon could be related to the fact that excessive volume expansion beyond an optimal level would be detrimental to the filler-to-filler interactions because of the breakage of the conductive network.

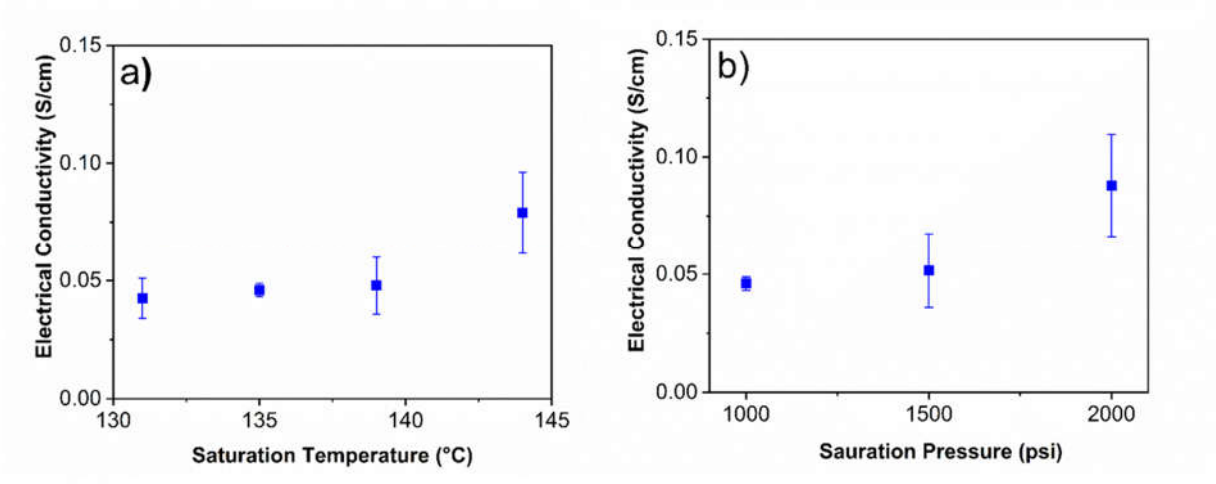

Figure 4.9 Effects of foaming conditions on the electrical conductivity of MWCNT/HDPE nanocomposite foams: (a) saturation temperature; and (b) saturation pressure

Figure 4.10 shows the SEM images of MWCNT's dispersion in polymer matrices for foamed and unfoamed nanocomposites. By introducing cellular structures in polymer nanocomposites, MWCNTs were localized around the bubbles while being aligned along the cell-walls. Eventually,

MWCNT created a series of conductive networks throughout the insulative polymer matrices, which helped to increase the overall electrical conductivity of the nanocomposite foams.

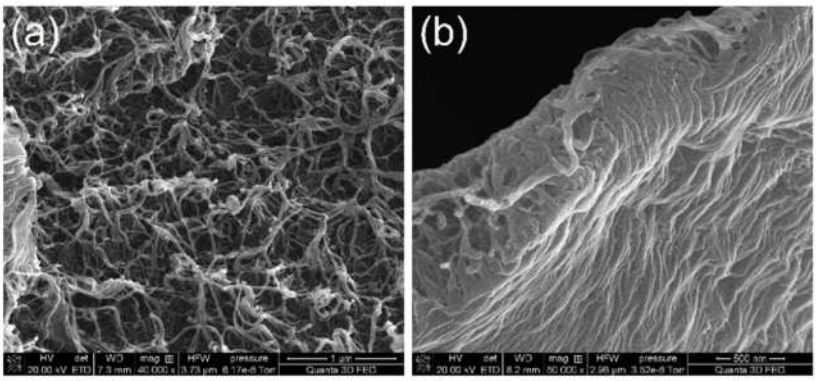

Figure 4.10 Distribution of carbon nanotubes in polymer matrix for (a) solid; and (b) foam samples

4.3.6 Effect of Foaming on Seebeck Coefficient of MWCNT/HDPE Nanocomposites

In order to study the effect of foaming on the Seebeck coefficients of MWCNT/HDPE nanocomposites, measurements were conducted on both solid and foamed samples. Measuring the Seebeck coefficients in the through-thickness direction of the solid MWCNT/HDPE nanocomposite samples was challenging. The small thickness of the samples together with their moderate effective thermal conductivity resulted in a very small temperature difference across them. To circumvent this challenge, several layers of solid samples were pressed together to conduct the measurement. For verification purpose, measurements were also made to nanocomposite samples with larger thicknesses (i.e., 1.5 mm to 3.0 mm). The through-plane Seebeck coefficients of both thin and thick solid nanocomposite samples were consistent with an average value of 1.56 μVK^{-1} and a standard deviation of 0.25. More importantly, the experimental results also reveal that foaming could result in more than three-fold increase in the Seebeck

coefficients of the MWCNT/HDPE nanocomposites. The measured Seebeck coefficient of the MWCNT/HDPE foams had an average value of 5.28 μVK^{-1} with a standard deviation of 0.35. The foaming-induced localization and partial alignment of MWCNTs along the cell-walls would result in the formation of highly interconnected MWCNT networks within the HDPE matrix. It is speculated that reorientation of MWCNTs induced by the foam expansion might alter the HDPE/MWCNT interfacial barrier by introducing more junctions among the MWCNTs. The filtration of the charge carriers with low energy levels at these filler junctions, could contribute to the moderate increase in the Seebeck coefficient of the foamed samples. This outcome is similar to the observation made by Zhang *et al.* in a PEDOT hybrid system [145]. However, further investigation in future work will be needed to elucidate the underlying mechanism behind this trend. Moreover, the Seebeck coefficients of the nanocomposite foams were virtually independent to the saturation temperature and pressure used in the foaming process.

4.3.7 Effect of Physical Foaming on the Thermoelectric Conversion Efficiency of MWCNT/HDPE Nanocomposite Foams

Figure 4.11 compares the average values for the TE parameters of the MWCNT/HDPE nanocomposite foams, with those of solid MWCNT/HDPE nanocomposites loaded with 15 wt.% MWCNT. While previous sections showed varying foaming conditions could influence the nanocomposite foam's TE properties, all foams demonstrated a drastic decrease in their effective thermal conductivities (i.e., one order of magnitude) and a moderate increase in their electrical conductivities and Seebeck coefficients (i.e., about five and three times respectively) compared with solid MWCNT/HDPE nanocomposites. Previous studies on TE materials demonstrated that promoting the electrical conductivity usually result in increasing in the thermal conductivity and suppressing the Seebeck coefficient, which adversely affects the TE figure of merit of the material.

Therefore, the experimental results obtained in this work reveal that foaming is a useful technique to favorably decouple these three interrelated properties of nanocomposites in an attempt to promote their TE energy conversion efficiency. As discussed earlier, simultaneously promoting the TE material's electrical conductivity and Seebeck coefficient, and suppressing its thermal conductivity would be beneficial in increasing its *ZT* value. Overall, MWCNT/HDPE nanocomposite foams demonstrated a 600-fold increase, on average, in their TE efficiencies (*ZT*) over the solid nanocomposites. The results of this study suggest that foaming would significantly increase the polymeric TE material's *ZT* value and provide a feasible route to improve their TE conversion efficiency to a practical level. Currently, the best CNT/polymer TE composites have a *ZT* value of approximately 0.02, which is still much lower than the TE efficiency of semiconducting materials (i.e., $ZT \approx 1$). While HDPE/MWCNT nanocomposites were used in this work as a case study to demonstrate the effects of physical foaming on different TE-related parameters and thereby the TE efficiency of nanocomposites, this technique can easily be adopted in a wide spectrum of polymer nanocomposite material systems to enhance their TE efficiencies. Therefore, the significant increase in the TE efficiency, demonstrated in this study, represents a remarkable advancement in the development of polymeric TE materials.

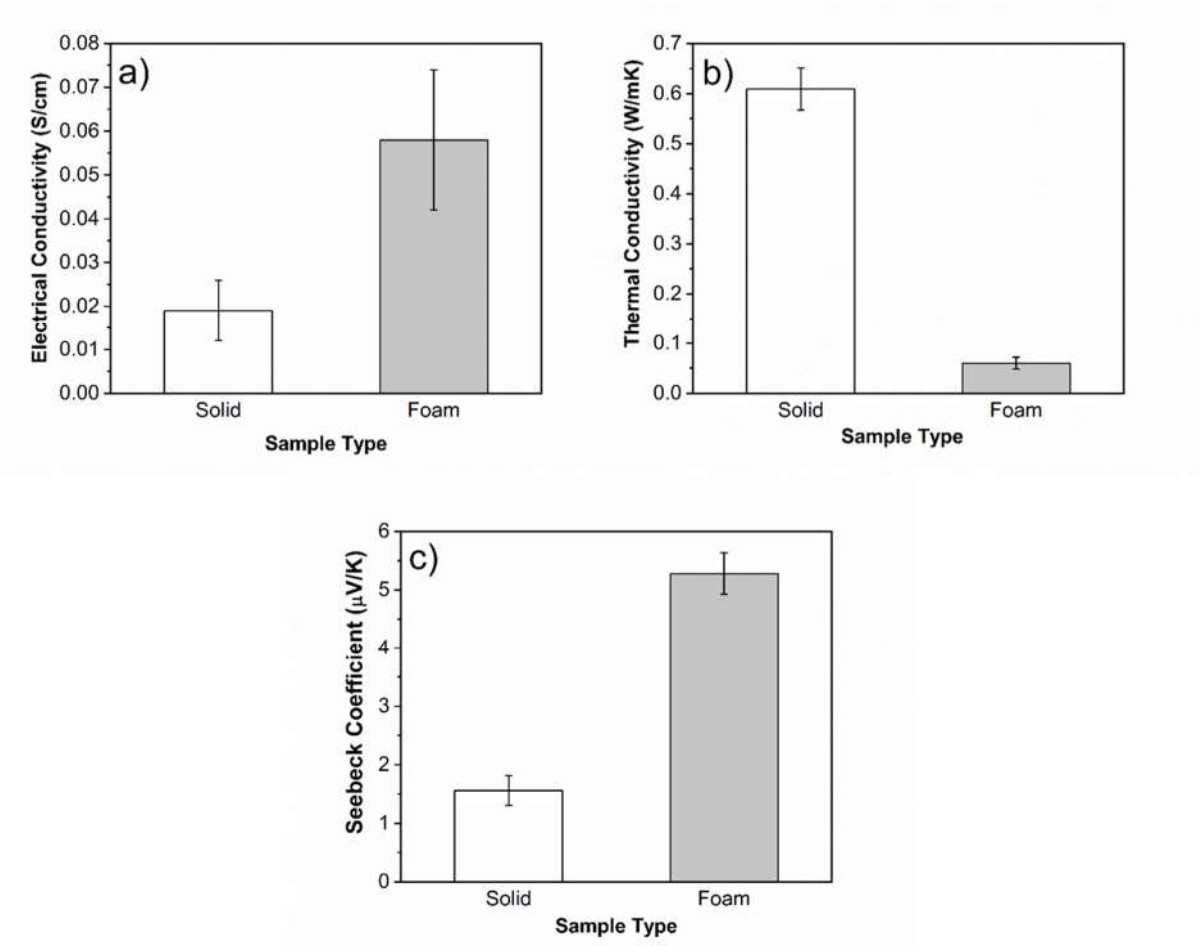

Figure 4.11 Comparison of MWCNT/HDPE nanocomposites and their foams in terms of: (a) electrical conductivity; (b) effective thermal conductivity; and (c) Seebeck coefficient

4.4 Conclusion

Physical foaming was utilized in this research as a processing technique to improve the TE efficiency of polymer-based materials. The MWCNT/HDPE nanocomposite foams were fabricated by physical foaming, using CO_2 as the foaming agent. The effects of different foaming conditions (i.e., foaming temperature, foaming pressure, and saturation time) on the thermal and electrical conductivity as well as on the Seebeck coefficient of the nanocomposite samples were investigated. While the saturation time had a negligible effect on cell structure and physical

properties of the nanocomposite foams, the saturation pressure and saturation temperature showed pronounced effects on expansion ratio and TE properties of the foamed samples.

Experimental results revealed that introducing cellular structures in nanocomposites significantly suppressed their effective thermal conductivity by about one order of magnitude. Moreover, the nanocomposite's through-thickness electrical conductivity and Seebeck coefficient were also improved about three and five times, respectively, after foaming. Consequently, the *ZT* value of MWCNT/HDPE nanocomposites enhanced more than two orders of magnitude (about 600 times), which would lead to a promising improvement in the energy conversion efficiency of these materials. This study suggests foaming as a novel strategy to effectively promote the TE efficiency of polymer nanocomposites. This makes them viable for energy harvesting from waste heat sources, especially at low-temperature gradients. Extending this processing strategy in future studies to prepare TE polymer-blend nanocomposites, consisting of conductive polymers, is believed to provide a new venue for fabricating highly efficient polymeric TE material systems.

Chapter 5. Fabricating Freeze-Dried Poly(vinyl alcohol)/Polypyrrole/Graphene Nanoplatelets Foams with Enhanced Thermoelectric Efficiencies

5.1 Introduction

The previous phase of our studies demonstrated that introducing microcellular foam structure within polymer nanocomposite materials could significantly improve their thermoelectric efficiency [71]. Using physical foaming method to create a closed-cell foam structure within the polymer matrix, yielded simultaneous improvement in all three TE parameters of high-density polyethylene (HDPE)/MWCNT nanocomposites and thereby enhanced their *ZT* values by about 600 times.

In this research, Poly(vinyl alcohol) (PVA)/Polypyrrole nanocomposite foam samples were fabricated, with enhanced TE efficiencies, using freeze-drying and vapor-phase oxidative polymerization techniques. An aqueous solution of PVA/iron(III) chloride was firstly prepared and freeze-dried in order to create a foam sample with high porosity and open-cellular structure. The PVA/oxidant foam samples were then exposed to the pyrrole monomer vapor at room temperature to start the polymerization process of PPy. Graphene nanoplatelets were also incorporated within the polymer matrix to promote the electrical conductivity and Seebeck coefficient of the samples.

The effects of oxidant concentration and GnP content, as the most important processing parameters on TE efficiencies of the nanocomposite samples, were investigated in this research.

The experimental results revealed that incorporating the conducting polymer effectively enhanced the electrical conductivity of PVA samples, while their measured conductivity values were orders of magnitude higher than the reported results for PVA/CNT nanocomposites. Addition of GnPs, on the other hand, resulted in promoting the Seebeck coefficients of the fabricated samples. Moreover, introducing foam structures helped to simultaneously suppress the thermal conductivity of the nanocomposite foams. Consequently, the thermoelectric efficiency of the material system significantly enhanced due to the partial decoupling of its three TE parameters.

5.2 Experimental

5.2.1 Fabrication of PVA Foam Samples

Poly(vinyl alcohol) (PVA, 99% hydrolyzed, Sigma-Aldrich) powders were firstly dissolved in D.I. water at 80 °C for 2 hours. The iron(III) chloride ($FeCl_3$, reagent grade 97%, Sigma-Aldrich) powders were then added to the prepared PVA solution and stirred for 5 minutes at room temperature to fully dissolve the oxidant and achieve a uniform PVA/oxidant solution. Three PVA concentrations (i.e., 2, 5, and 10 wt.%) were used to fabricate foam samples with different porosities and various foam structures. The oxidant concentrations of the prepared solutions were also set at 20 and 40 wt.% to study its effect on the TE properties of the fabricated samples. To fabricate foam samples with graphene fillers, the graphene platelets (GnP, Grade 2, CheapTubes) were also added into the polymer/oxidant solution. The solution was sonicated with a sonicator probe for 10 minutes to effectively disperse the GnP fillers within the PVA polymer matrix. The nanocomposite samples were prepared with 5 and 10 wt.% GnP loading.

For the freeze-drying process, the aqueous solution was first frozen at -40 °C for 10 hr, then put into a freeze-drying machine (Harvest Right freeze dryer). The polymeric foams were achieved after drying the samples for 36 hr in the freeze-dryer. The PPy polymerization process for the foam samples was performed while exposing the PVA foams to the pyrrole vapor in a sealed container at room temperature. The polymerization process was very slow. This process can be recognized by the color changing of the samples. To ensure achieving a complete vapor-phase polymerization, the samples were kept inside the containers for three days.

5.2.2 Characterization

The electrical conductivity of each foam sampl was measured at room temperature using the four-point method. The samples' Seebeck coefficients were measured using a Seebeck coefficient analyzer, which was a custom set-up in our lab (M^3Lab). The generated voltage (V_{TE}) in the samples, resulted from an applied temperature gradient ($\Delta T \approx$ 2-4 K), was recorded using a source meter. The samples' Seebeck coefficients were calculated from the slope of V_{TE} versus ΔT graph. The thermal conductivity of the nanocomposite samples was measured by a thermal conductivity analyzer (C-Therm Technologies Ltd., TCi Thermal Conductivity Analyzer). The foam and phase morphologies were characterized by exploring the cross-sections of the samples using a scanning electron microscopy (FEI Company Quanta 3D FEG).

5.3 Results and Discussion

5.3.1 Morphology and Microstructure of Freeze-Dried Foams

The cell structures of the fabricated foam samples (without adding GnP) were shown in Figure 5.1. The SEM micrographs compare the foam samples prepared using two different PVA concentrations (i.e., 2 and 10 wt.% PVA) at two magnification levels. The micrographs reveal that

the foam samples had high levels of porosity with lots of interconnections among their cells, which imply open-cellular structures. By increasing the PVA concentration, the porosities of the polymer foams decreased due to the increased amount of solid phase within the bulk of foam samples.

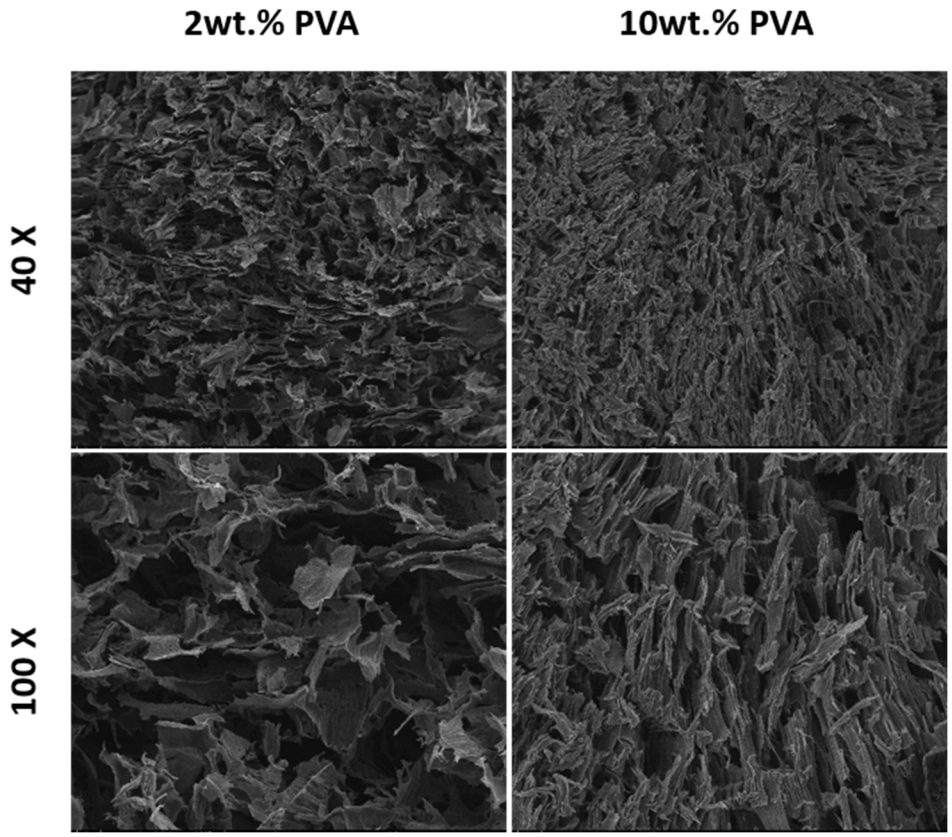

Figure 5.1 SEM micrographs of the freeze-dried PVA foams prepared with 2 and 10 wt.% of PVA at two different magnifications

Figure 5.2 illustrates the effects of GnP addition on the foam morphologies of the fabricated PVA samples with 2 wt.% PVA concentration. The SEM graphs show that by loading the polymeric foams with 10 wt.% GnP, the shapes of the cells changed into a layered structure due to the 2D structures of the graphene nanoplatelets. However, the open-cell structures of the foams was retained.

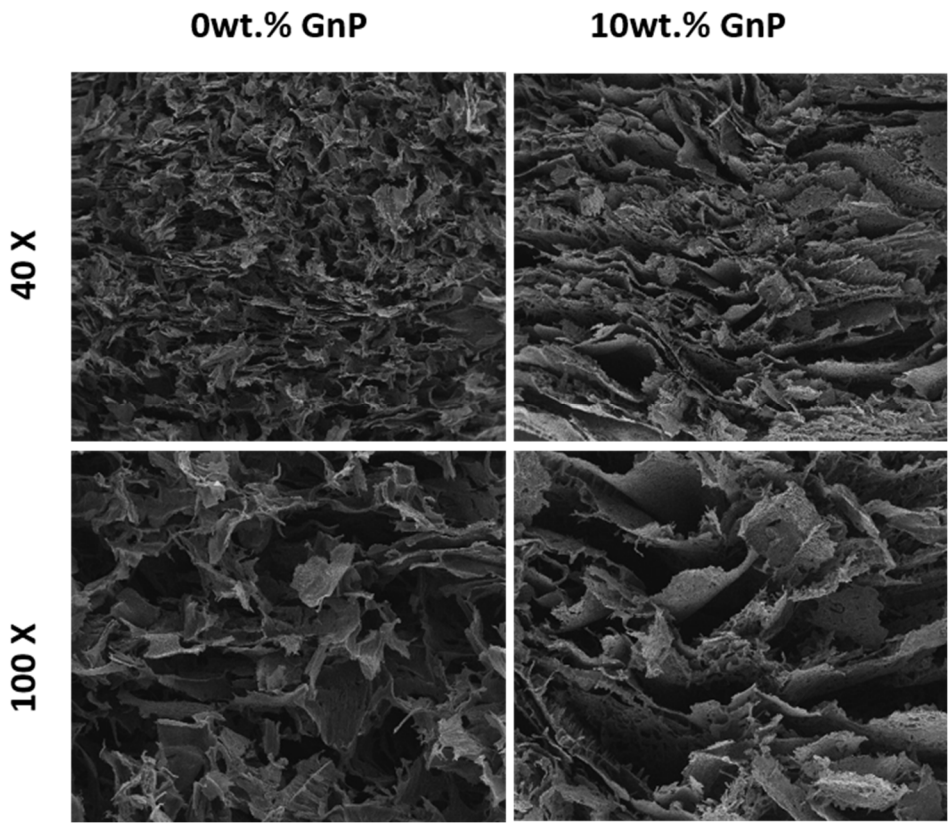

Figure 5.2 SEM micrographs of the freeze-dried PVA foams prepared with 2 wt.% PVA, and loaded with 0 and 10 wt.% GnP, at two different magnifications

The surface morphologies of the foam samples, before and after the creation of PPy within their structures, are displayed in Figure 5.3. The SEM micrographs reveal that after PPy polymerization throughout the porous structure of the PVA foams, a completely different phase morphology was achieved due to the growth of PPy polymer chains on the cell walls of the foam samples.

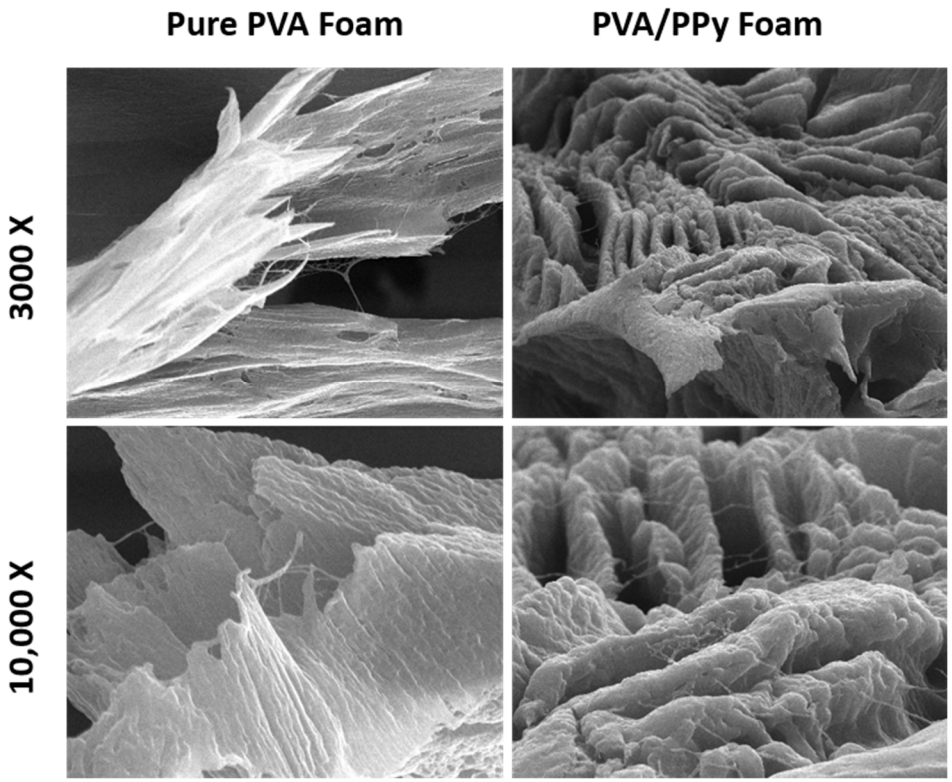

Figure 5.3 Surface morphology of the freeze-dried PVA foams prepared with 2 wt.% PVA and 20 wt.% oxidant, before and after the creation of PPy polymer, at two different magnifications

The fibrous structure of PPy polymer, formed within the PVA foams, is shown in Figure 5.4. Due to the growth of PPy polymer throughout the porous structures of the PVA foam templates, a network of conducting PPy fibers was generated throughout the foams' cellular structures. This PPy network would provide an efficient electron transferring through the insulating PVA matrix. The effect of increasing the oxidant concentration from 20 wt.% to 40 wt.%, on the cell-wall structure of PVA foams is illustrated in Figure 5.5. The SEM pictures show that increasing the oxidant resulted in creating lots of pores and ruptures of the cell-walls after polymerization of PPy. Increasing the oxidant concentration in the polymer solution led to higher PPy contents after the vapor phase polymerization of PVA foams. The unidirectional growing of PPy polymer chains,

embedded within the PVA matrix, could be the potential reason for creating the cell-wall ruptures and holes.

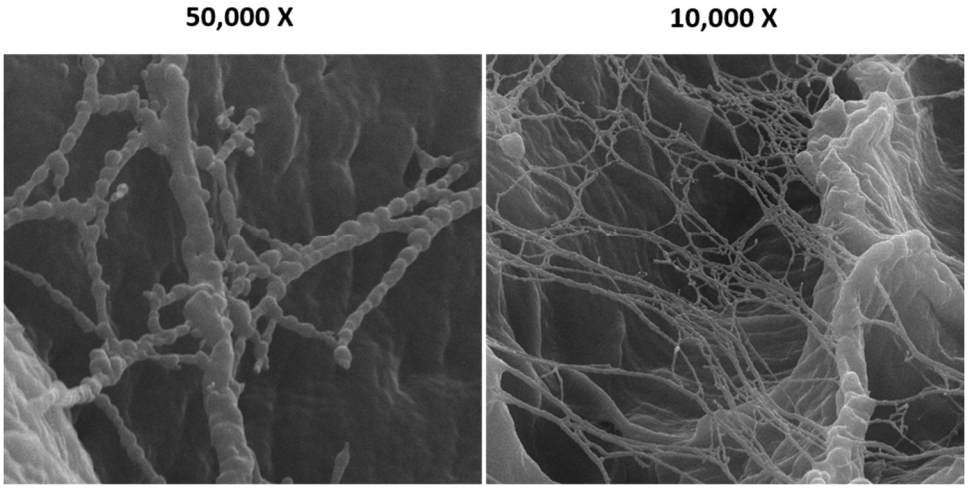

Figure 5.4 Creation of PPy networks after exposing the PVA foams to the monomer vapor

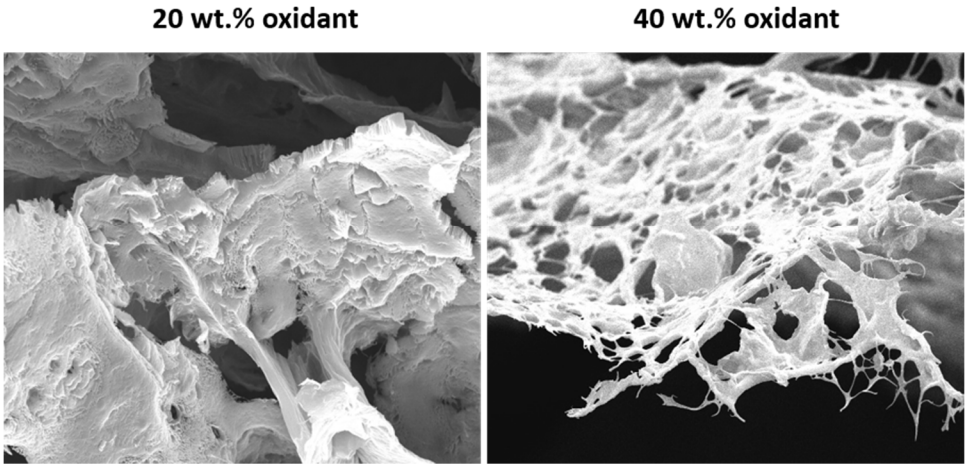

Figure 5.5 Comparing the cell-wall structures of the PVA foams prepared with 20 wt.% and 40 wt.% oxidant concentrations

5.3.2 Thermal Conductivity of the Thermoelectric Foams

The thermal conductivity of PVA/PPy nanocomposite foams containing different amount of GnP loadings is plotted in Figure 5.6. The conductivity results are measured for the foam samples

prepared with 2 wt.% and 5 wt.% of PVA and containing 20 wt.% of oxidant. The experimental results show that by increasing the GnP loading from 0 to 10 wt.%, the thermal conductivity of the samples slightly increased. However, all the samples provided extremely low thermal conductivity values (i.e., $k < 0.04$ $Wm^{-1}K^{-1}$) because of their high porosities, which were achieved from the utilized freeze-drying fabrication technique. The results also indicated that the thermal conductivities of the samples prepared with 2 wt.% PVA were inferior to those prepared with 5 wt.% PVA. Higher PVA concentration results in larger solid volume in the fabricated foams. Consequently, more heat conduction through the solid part of the samples contributed to the promotion of their thermal conductivities.

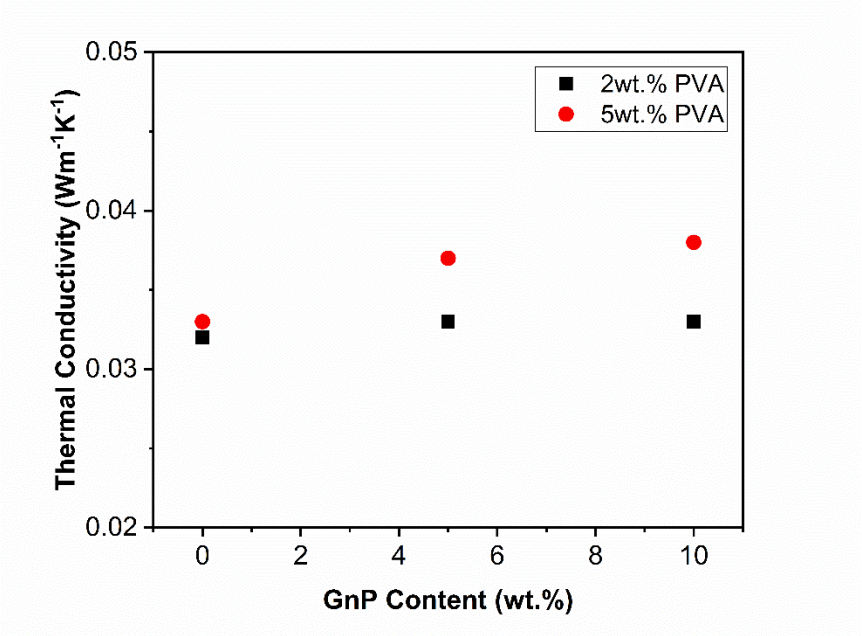

Figure 5.6 Thermal conductivity of PVA/PPy foams prepared with different PVA and GnP concentrations

5.3.3 Electrical Conductivity of the Thermoelectric Foams

The electrical conductivity of the fabricated PVA/PPy nanocomposite foams is plotted in Figure 5.7. The results show that adding 5 wt.% GnP particles significantly promoted the electrical

conductivity (i.e., around one order of magnitude) of the samples prepared with 2 wt.% of PVA. However, further increasing the GnP loading provided a negligible effect in this regard. The 2D structure of the graphene nanoparticles, their extremely high aspect ratios (~ 100-1000), and the strong Van der Waals interaction between these nanosheets made it very difficult to uniformly disperse them within the polymer solution, especially at elevated loading levels. Therefore, at 10 wt.% GnP loading, more stacking of the nanosheets would prevent their efficient distribution throughout the polymer matrix and thereby adversely affected the electrical conductivity of the samples.

Figure 5.7 also demonstrates that the foam samples prepared with 5 wt.% of PVA provided slightly lower electrical conductivity values while incorporating GnPs showed a negligible effect on promoting their electrical conductivities. Lower PVA concentration (i.e., 2 wt.% versus 5 wt.%) results in less solid content and more porosities within the nanocomposites foams, which is detrimental for the electron transferring throughout the material system. As a result, the electrical conductivity of the PVA/PPy foams with 5 wt.% PVA and 0 wt.% GnP was noticeably higher than those fabricated with 2 wt.% PVA. On the other hand, once GnPs are added to the polymer matrices, more PVA concentration promotes the chances of entirely wrapping the graphene sheets within the insulating polymer. This phenomenon would create electron blocking at the fillers' intersections and suppressed the electron transferring throughout their networks. Consequently, loading GnPs to the foam samples prepared with 5 wt.% PVA showed a negligible impact on their electrical conductivities.

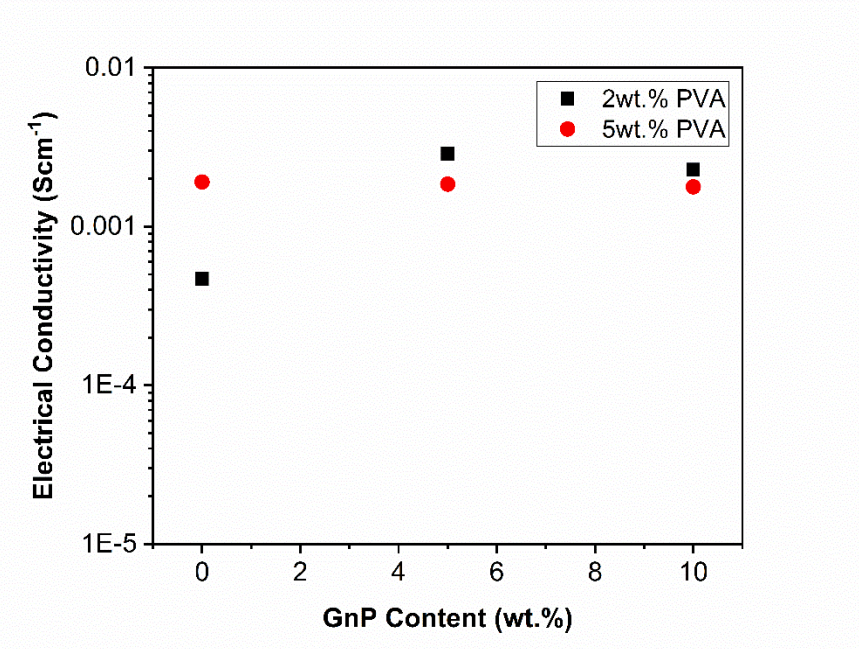

Figure 5.7 Electrical conductivity of PVA/PPy foams prepared with different PVA and GnP concentrations

5.3.4 Seebeck Coefficient of the Thermoelectric Foams

The relation of the Seebeck coefficients of the PVA/PPy nanocomposite foams to their GnP contents is depicted in Figure 5.8. The results showed that by increasing the GnP loading, the Seebeck coefficient of the samples also increased because of the intrinsic properties of the added fillers. Moreover, the PVA/PPy foams with 2 wt.% PVA provided higher Seebeck values compared with the 5 wt.% PVA samples. This phenomenon is due to more charge carrier mobilities throughout the filler networks, which came from more efficient interaction of the fillers within the nanocomposite foams. Thinner polymer interphases at GnP junctions in 2 wt.% PVA samples facilitated the electron mobilities.

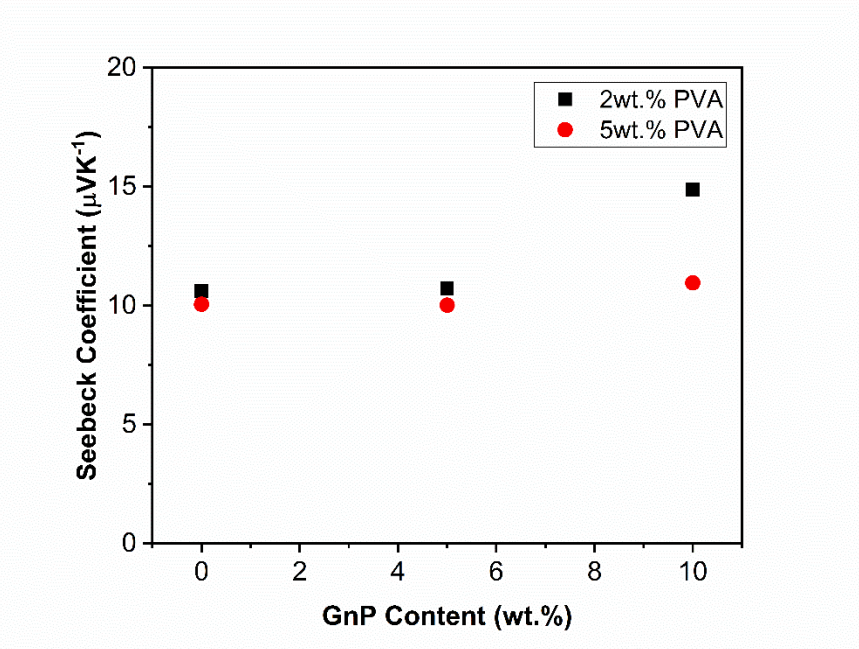

Figure 5.8 Seebeck coefficient of PVA/PPy foams prepared with different PVA and GnP concentrations

5.3.5 Effects of Oxidant Concentration on TE Properties of the Thermoelectric Foams

The effects of increasing the oxidant concentration on the electrical conductivity and the Seebeck coefficient of PVA/PPy nanocomposite foams are illustrated in Figure 5.9 and Figure 5.10, respectively. Surprisingly, experimental results revealed that higher oxidant concentration adversely affected both TE parameters of the samples. By increasing the oxidant content of the polymer foams from 20 to 40 wt.%, their electrical conductivities decreased around one order of magnitude, while their Seebeck coefficients also suppressed up to around 50%. This could be due to the increased number of pores and ruptures in cell-walls of the foams at higher oxidant levels (Figure 5.5), which caused more charge carrier blocking or scattering within the bulk of material.

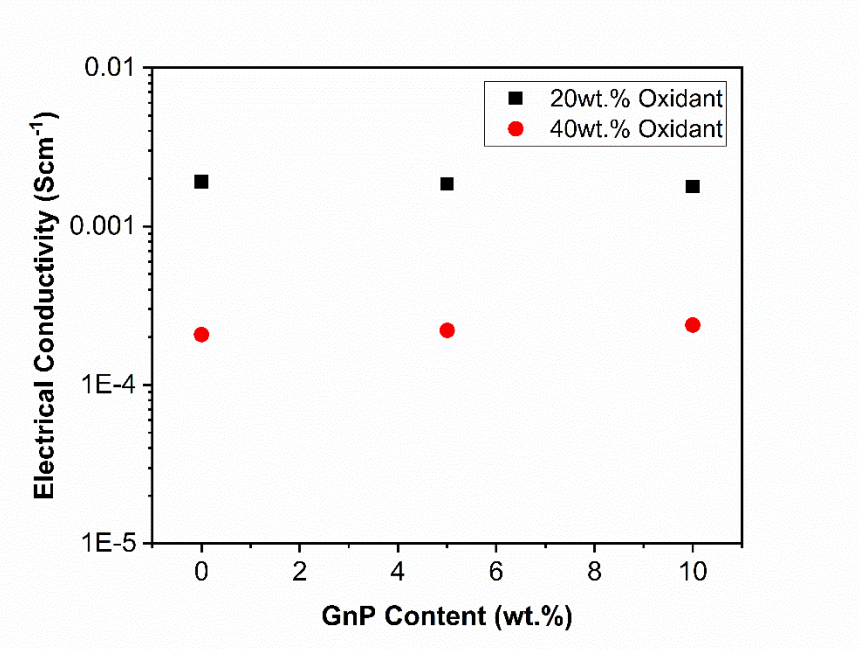

Figure 5.9 Effects of oxidant concentration on the electrical conductivity of PVA/PPy foams prepared with different PVA and GnP concentrations

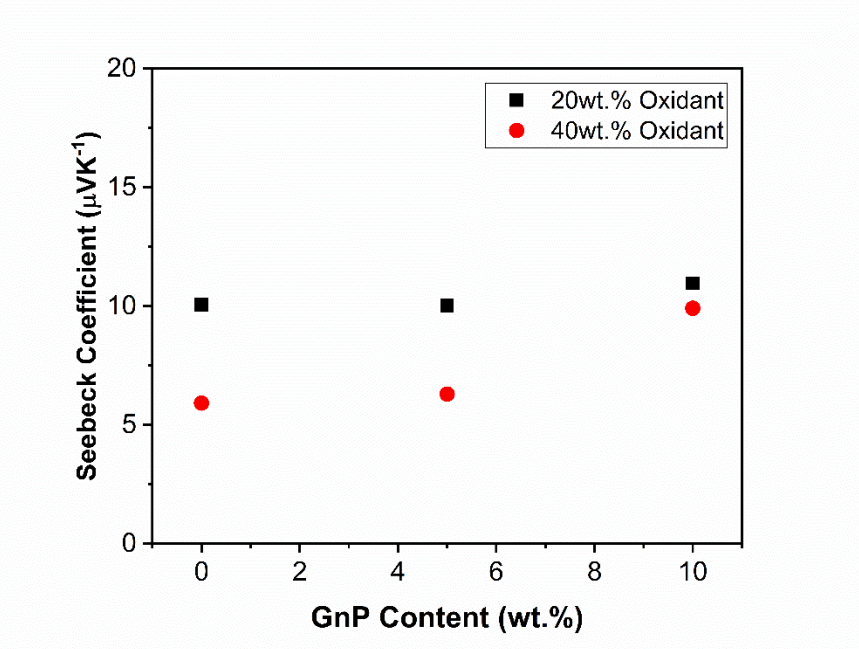

Figure 5.10 Effects of oxidant concentration on the Seebeck coefficient of PVA/PPy foams prepared with different PVA and GnP concentrations

5.3.6 Energy Conversion Efficiency of the Thermoelectric Foams

The calculated power factors (*PF*) and *ZT* values of the nanocomposite foams are plotted in Figure 5.11. The results are shown for the samples prepared with 2 wt.% and 5 wt.% PVA concentrations and containing different GnP amounts. For the samples prepared with 2 wt.% PVA, both TE parameters increased about one order of magnitude by adding GnP fillers to their matrices. However, the TE efficiencies of the nanocomposite foams fabricated using 5 wt.% PVA were almost unchanged after the addition of carbon nanoparticles. This result was expected as GnP loading showed a negligible effect on promoting the electrical conductivity or Seebeck coefficient of these samples. Overall, maximum *PF* and *ZT* values of 5.04×10^{-5} $\mu Wm^{-1}K^{-2}$ and 4.58×10^{-7}, respectively, were achieved for PVA/PPy foams prepared with 2 wt.% PVA and loaded with 10 wt.% GnP.

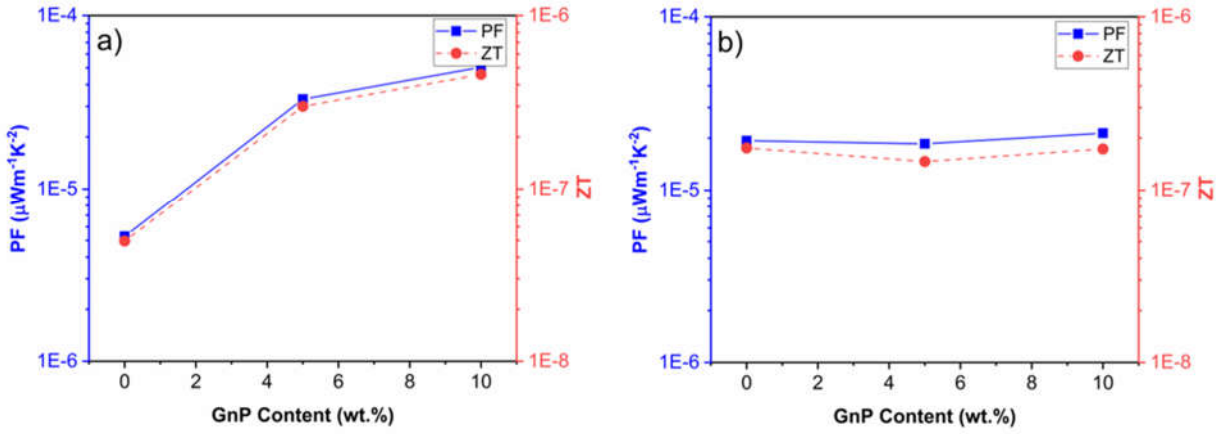

Figure 5.11 Effects of GnP contents on the power factor (*PF*) and *ZT* value of the PVA/PPy foams prepared with: (a) 2 wt.% PVA; and (b) 5 wt.% PVA

5.4 Results Comparison

A summary of the highest achieved values for the TE properties of the PVA/PPy foams is shown in Table 5.1. The results of the current study are compared with some reported values for solid composite samples (without porous structures) in the literature. The results indicated that the maximum electrical conductivity of the fabricated PVA/PPy nanocomposite foams (with and without GnPs) was more than one order of magnitude higher than the reported values for PVA/CNT nanocomposites with 20 to 40 wt.% filler loadings. These results were also comparable with the reported electrical conductivity value for a PVA-PPy nanocomposite.

Introducing a porous structure within a material system adversely affects the material's electrical transport properties due to the electron scattering effects. Therefore, the increased electrical properties of the nanocomposite foam samples due to the fabrication method in this research are promising. Moreover, the highest *ZT* value of the fabricated foam samples was two orders of magnitude higher than the reported results for a PVA/GnP nanocomposite containing 40 wt.% of nanofillers. This significant enhancement in the TE efficiency of the PVA/PPy foam samples was the result of foaming effects on suppressing their thermal conductivities without compromising their charge carrier transport properties (i.e., σ and S). These findings indicated that foaming is an effective technique to simultaneously promote the TE parameters of polymer nanocomposite materials and thereby enhance their TE efficiencies.

Table 5.1 Comparison of the thermoelectric properties of the fabricated PVA/PPy foam samples with the reported results for similar polymer nanocomposites in the literature

Material	**Fabrication Method**	**Electrical Conductivity (Scm^{-1})**	**Seebeck (μVK^{-1})**	***PF***	***ZT***	**Ref.**
PVA-MWCNT (20 wt.%)	Solution casting	1.3×10^{-5}	-	-	-	[146]
PVA-CNT (40 wt.%)	Wet spinning	$<10^{-4}$	-	-	-	[147]
PVOH/CNT (20 wt.%)	Solution casting	$<10^{-3}$	-	-	-	[148]
PVA-PPy	Solution casting & Chemical oxidative polymerization	2.16×10^{-3} (@ 303 K)	-	-	-	[149]
PVA-PPy	Freeze drying & Vapor phase polymerization	1.91×10^{-3}	10.06	1.93×10^{-5}	1.75×10^{-7}	This study
PVA/GnP (40 wt.%)	Solution casting	0.22	23.1	1.17×10^{-2}	4.47×10^{-9}	[150]
PVA-PPy-GnP (10wt.%)	Freeze drying & Vapor phase polymerization	2.28×10^{-3}	14.87	5.04×10^{-5}	4.58×10^{-7}	This study

5.5 Conclusion

A simple processing strategy was proposed in this study to fabricate organic TE materials with low density, high flexibility, and enhanced TE efficiency. The fabricated nanocomposite foams demonstrated ultra-low thermal conductivities even after being loaded with conducting fillers (i.e.,

GnPs and PPy). The proposed processing method helped to partially decouple the three TE parameters (i.e., electrical conductivity, thermal conductivity, and Seebeck coefficient) of the material and simultaneously tune their properties to promote their TE efficiencies. The experimental results revealed that optimized levels of PVA and oxidant concentrations are required to achieve the best TE efficiency of the fabricated samples. By replacing the utilized conducting materials in this research with their counterparts, which possess more promising TE properties (like SWCNTs, PEDOT:PSS, and PANI) higher TE efficiencies would be achieved with this fabrication method. The proposed processing technique can be utilized to design organic nanocomposite materials with enhanced TE efficiencies for industrial applications.

Chapter 6. Fabrication of Open-Cell Thermoelectric Polymer Nanocomposites by Template-Assisted Multi-Walled Carbon Nanotubes Coating[3]

6.1 Introduction

In this study, open-cellular PVDF foams were fabricated and coated with MWCNTs to create a polymer nanocomposite material system with high TE efficiency. Using open-cellular polymer foams as templates helped to effectively localize carbon nanotubes within the polymer and create a continuous three-dimensional (3D) network of conductive fillers throughout the insulating matrix. The achieved highly interconnected MWCNT network would enhance polymer nanocomposites' electrical conductivity while the super porous structure would help to retain the ultra-low thermal conductivity of the polymeric template. The effects of different foam morphologies on the TE properties of the PVDF/MWCNT nanocomposites were also investigated in this study.

The present study has proven that the proposed approach can serve as a potential technique to fabricate polymer-based TE materials using conventional non-conducting polymers. Furthermore, by incorporating conducting PPy polymer within the PVDF/MWCNT nanocomposite foams, the

[3] This chapter is based on reference [157]

changes in the TE properties of the resultant material system was also explored in this research. Using an in-situ polymerization method, MWCNT fillers were wrapped with PPy to enhance the Seebeck coefficient of the polymer nanocomposite through carrier filtering effects at CNT-polymer interfaces [69]. Finally, the TE parameters of both PVDF/MWCNT and PVDF/MWCNT/PPy nanocomposite foams were compared in this chapter. An optimum *ZT* value of 1.4×10^{-5} was achieved for PVDF/MWCNT nanocomposite foams with 24.9 wt.% MWCNT loading. In the current work, PVDF polymer matrix and MWCNT/PPy conducting fillers were selected as a case study to demonstrate the effects of the recommended fabrication process on development of polymeric materials with high TE efficiencies. This study presents a new route to effectively decouple the TE properties of polymeric materials and promote their TE efficiencies.

6.2 Experimental

6.2.1 Fabrication of Open-Cell Organic Thermoelectric Foams

PVDF (KAYNAR 740, ARKEMA) powders were dry-blended with sieved sodium chloride (NaCl) powders. PVDF-NaCl mixtures were prepared using different salt sizes (i.e., 106 – 250 μm, 250 – 500 μm, and >500 μm) and different salt contents (i.e., 85 wt.%, 90 wt.%, and 95 wt.%) to fabricate PVDF foams with various cell morphologies. The PVDF-NaCl mixtures, loaded with NaCl, were molded by a compression molding machine (Craver Press, 4386 CH) at 185 °C and 4000 psi into disc samples of 20 mm in diameters and 2 mm in thicknesses. The open-cell PVDF templates were achieved after leaching out NaCl from the PVDF matrices by immersing the samples into water at room temperature (23 °C) for 72 hours, while water was changed regularly to avoid saturation of NaCl. The open-cell PVDF templates were then dried in an oven at 50 °C for 24 hours. A low drying temperature was selected to prevent any potential phase transformation

or change in the crystal structure of the polymer matrix because of the heat treatment. The masses of dried samples were weighed to confirm the complete leaching of NaCl from the PVDF matrices. The fabricated PVDF open-cell templates were immersed into an aqueous solution of 1.0 wt.% MWCNT for multiple cycles and subsequently dried in an oven at 50 °C for 24 hours. A commercially available MWCNT solution (AQUACYL AQ0102, Nanocyl), which contains an anionic surfactant to provide stability and uniform dispersion of nanofillers within the solution, was used in this study. In each MWCNT coating cycle, the submerged templates and the MWCNT solution were sonicated using a sonicator probe (Q700, QSonica) to facilitate the penetration of carbon nanofillers throughout the porous template and create a uniform MWCNT coating on the cell-walls of PVDF foams. The sample masses were weighted before and after each cycle to determine the MWCNT loading in the open-cell PVDF-MWCNT nanocomposite foams.

The PVDF-PPy-MWCNT nanocomposite foams were prepared by similar procedures used for fabricating the PVDF-MWCNT samples, except the additional steps for the in-situ polymerization of PPy. The PVDF open-cell templates were immersed into a solution of MWCNT and pyrrole (Py) monomers (reagent grade, 98%, Sigma Aldrich) in deionized (DI) water. The MWCNT-to-Py mass ratio was set at 2 for the experiments. The solution was sonicated for three minutes to facilitate the proper coating of templates by MWCNT and Py. An aqueous solution of $FeCl_3$ was used as an oxidant and its dropwise addition into the Py-MWCNT solution would initiate the in-situ polymerization of PPy. The $FeCl_3$-to-Py molar ratio was set at 2.5, which is close to the optimized value reported in the literature to achieve PPy powders with high electrical conductivity [91,98]. The solution temperature retained at 0 to 5 °C in an iced bath, while the entire solution was vigorously stirred for 5 hours to complete the polymerization process. The PVDF-PPy-

MWCNT open-cell nanocomposite foams were washed multiple times, using DI water and ethanol, to remove any impurities. The samples were then dried in an oven at 50 °C for 48 hours.

6.2.2 Characterization

The electrical conductivity of the samples was measured at room temperature by using a two-probe setup equipped with a source meter unit (SMU, Keithley, 2450 Source Meter). A conductive silver-epoxy paste was applied to both sides of each sample as an electrode to impose electric voltage across the sample's thickness for the measurements. The samples' Seebeck coefficients were measured using a Seebeck coefficient analyzer equipped with a pair of temperature-regulated heating and cooling blocks as well as two T-type thermocouples. Preset temperature differences (ΔT), ranging from 2 K to 4 K, were applied across the opposite surfaces of each sample. The generated voltage (V_{TE}) from the thermoelectric effect was measured by the SMU. The Seebeck coefficient was calculated by the slope of the V_{TE} versus ΔT graph. The electrical conductivity and the Seebeck coefficient were measured simultaneously at the same points of contact on each sample to ensure measurement consistency. The effective thermal conductivity was measured by using a thermal conductivity analyzer (C-Therm Technologies Ltd., TCi Thermal Conductivity Analyzer), which was based on the modified transient plane source (MTPS) technique. In this method, a small amount of heat is applied on the sample's surface using a sensor coil. By measuring the rate of voltage-change in the sensor, caused by heating of the sample-sensor interface, the effective thermal conductivity of the sample was calculated. The foam and phase morphologies were characterized using scanning electron microscopy (FEI Company Quanta 3D FEG). The cross-sections of all samples were exposed by cryo-fracturing the samples under liquid nitrogen. The fractured surfaces were then sputter-coated with gold (Denton Vacuum, Desk V Sputter Coater). The open-cell content of each foam sample was analyzed by a pycnometer

(Ultrapyc 1200e). Using the gas-displacement method, the total volume of the solid part and the closed-cell part of the foam samples was firstly measured (V_P) by employing the ideal gas law. The volume percentage of open cells (O_C) is then calculated by considering the geometric volume of open-cell foams (V_G):

$$O_C = \frac{V_G - V_P}{V_G} \tag{6-1}$$

6.3 Results and Discussion

6.3.1 Fabrication and Morphology of Organic Thermoelectric Foams

The PVDF thermoelectric foams were fabricated by open-cell template-assisted MWCNT coating. The effects of NaCl content and size on the open-cell morphology of the nanocomposite foams were studied. The effects of cell morphology on the development of 3D MWCNT networks were also investigated. As-fabricated PVDF nanocomposite foams covered with MWCNTs maintained the sponge-like structures of their open-cell templates. They had extremely low densities (around 210 $mgcm^{-3}$) and high porosities. The SEM micrograph, as shown in Figure 6.1(a) and (b), reveal that the 3D MWCNT network uniformly adhered on all the cell-walls and created a continuous mat-like surface morphology, which resembled MWCNT structures.

The formation of continuous layers of MWCNT on both sides of a cell-wall, within the PVDF foam template, is shown in Figure 6.2. It must be noted that a high level of porosity creates lots of ruptures on the cell-walls, which provides openings and pathways for the MWCNT solution to penetrate the templates' cores. The development of a uniform and highly interconnected 3D MWCNT network is crucial to promote the electrical conductivity of the organic TE materials.

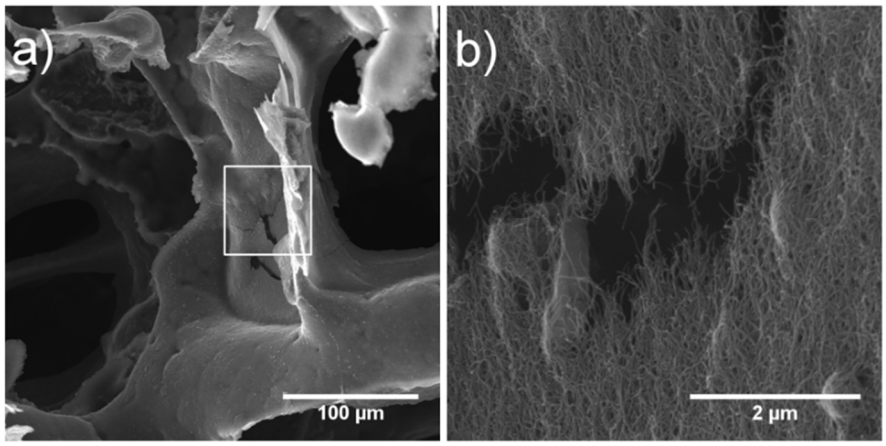

Figure 6.1 SEM micrographs of a PVDF open-cell foam coated with 3D MWCNT network (NaCl content and size were 90 wt.% and 250-500 µm, respectively for the fabricated foams): (a) low magnification image showing the cell-wall of a PVDF foam; and (b) high magnification image demonstrating the surface morphology of the cell-wall coated with MWCNTs

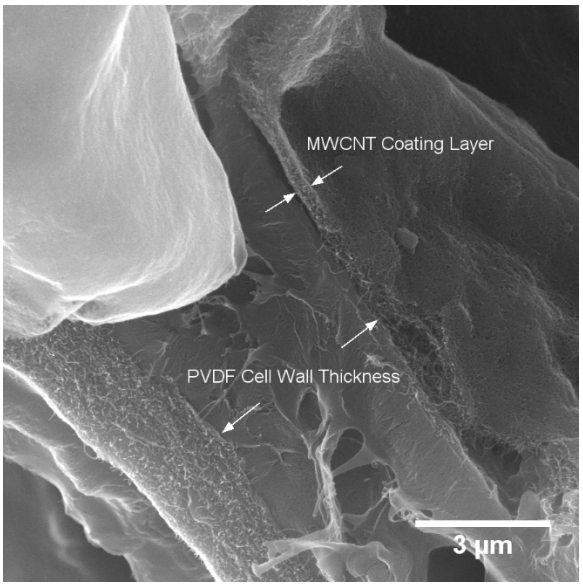

Figure 6.2 An SEM micrograph from the cell-wall of a PVDF foam, representing thin layers of MWCNT coated on both sides of the cell-wall

Figure 6.3(a) through (c) illustrate the morphologies of the PVDF-MWCNT open-cell foams, fabricated by the particulate leaching method, using 90 wt.% of NaCl with three different size ranges of the salt particles: (i) 106 – 250 μm; (ii) 250 – 500 μm; and (iii) >500 μm. The individual cells resembled the cubic NaCl crystals which were uniformly distributed throughout the PVDF matrices before being removed during the salt leaching process. As expected, using larger NaCl particles yielded open-cell foams with larger cell-sizes and lower cell population densities. It can be observed that holes and cell ruptures were omnipresent on virtually all cell-walls, ensuring a continuous flow path for the MWCNT solution to penetrate throughout the entire template in the solution immersion step.

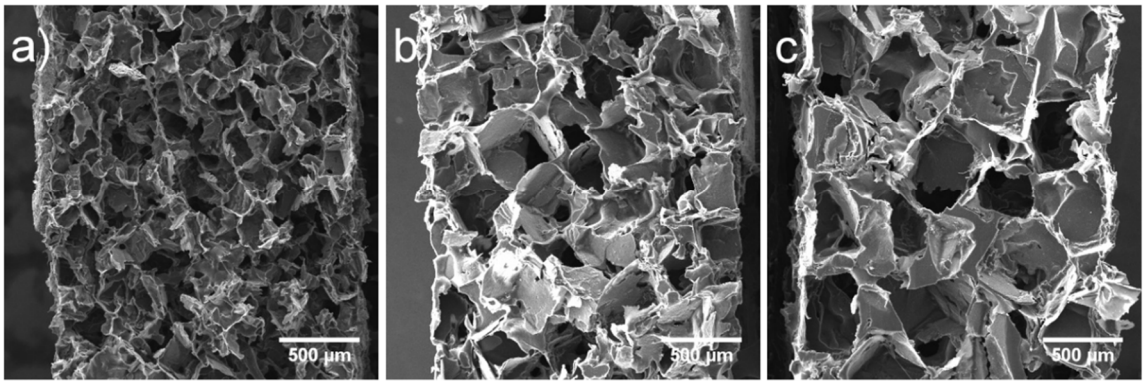

Figure 6.3 SEM micrographs of open-cell PVDF-MWCNT foams prepared by 90 wt.% of NaCl particles (before salt leaching) with different cell-sizes: (a) 106 – 250 μm; (b) 250 – 500 μm; and (c) >500 μm

The NaCl content and size are two governing factors that affect the open-cell morphology of the PVDF templates. Figure 6.4 illustrates the effects of these two parameters on the open-cell contents of the PVDF foams before and after MWCNT coating. The experimental results revealed that the open-cell contents of PVDF foams increased with the NaCl loadings; however, the NaCl

particle size had negligible effect on their open-cell contents. It is believed that the high NaCl loadings (i.e., ≥85 wt.%) were sufficient to achieve close-packing of NaCl particles throughout the PVDF matrices, and thereby ensured high levels of openness and interconnections among adjacent cells after all the salt particles had been leached out. Furthermore, the MWCNT coating slightly reduced the templates' open-cell contents as the resultant 3D MWCNT networks would cover some small openings on the cell-walls. Nevertheless, the open-cell contents of all the PVDF foams remained very high (i.e., ≥87 vol%) after MWCNT coating.

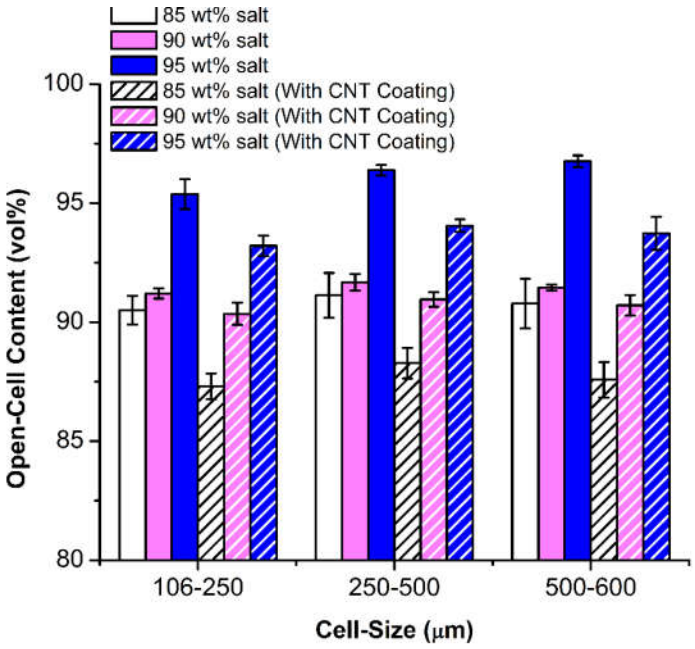

Figure 6.4 Effects of the cell-size and the salt-content (before salt leaching) on open-cell content of PVDF foams

Figure 6.5 illustrates the effects of both salt-content and cell-size on final MWCNT loading of the PVDF foams. Increasing both parameters resulted in higher MWCNT coating on the polymeric porous template; however, the effect of salt content had been more pronounced. Increasing the salt content promoted the volume percent of voids inside the foam samples, which provided larger surface area to absorb carbon nanotubes. Larger salt size, on the other hand, would result in larger

cell-openings because of the lower packing efficiency of larger salt particles. This led to a slight increase in the open-cell content, as shown in Figure 6.4, and provided readily accessible pathways for MWCNT solution throughout the polymer foam during the coating process.

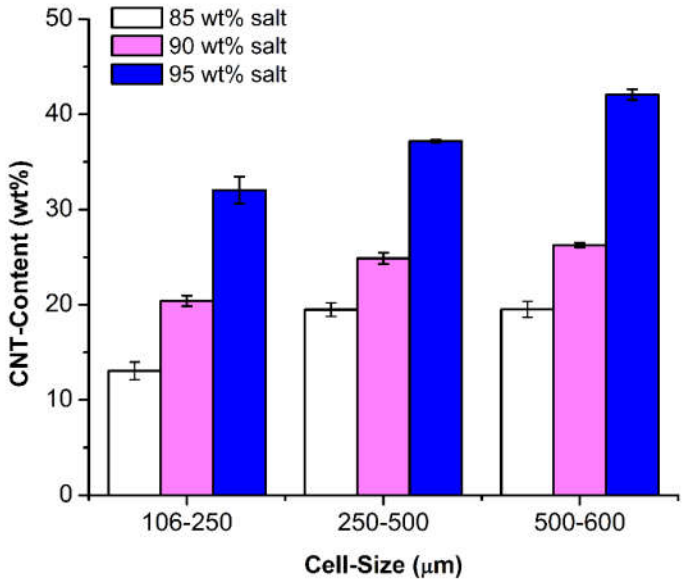

Figure 6.5 Effects of the cell-size and the salt-content (before salt leaching) on MWCNT absorption into PVDF foams

6.3.2 Effective Thermal Conductivity of Organic Thermoelectric Foams

The effective thermal conductivity of PVDF foams and their nanocomposites, prepared by using different salt-contents and different cell-sizes, are demonstrated in Figure 6.6. The experimental results revealed that by increasing the salt-content, the effective thermal conductivity of the polymer foams decreased. Higher salt-contents created foam samples with elevated amount of void fraction. This helped to further reduce their effective thermal conductivity due to the trapped air in voids, as well as because of the increased phonon scattering within their porous structures. The cell-size, however, had negligible effect on the effective thermal conductivity of

PVDF foams. It is believed that the investigated cell-size range in this study was too small to clearly show the effect of this parameter on the effective thermal conductivity of polymer foams. According to Figure 6.6, the effective thermal conductivity of PVDF foam templates increased after coating with MWCNT; however, it remained very low (i.e., ≤0.056 $W \cdot m^{-1} \cdot K^{-1}$) even after 40 wt.% MWCNT coating.

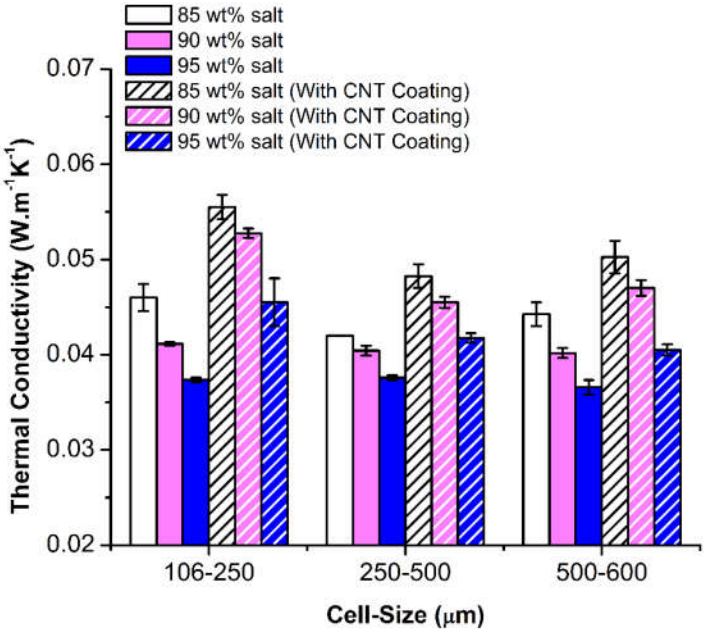

Figure 6.6 Effects of the cell-size and the salt-content (before salt leaching) on effective thermal conductivity of PVDF foams before and after the CNT coating

6.3.3 Electrical Conductivity of Organic Thermoelectric Foams

The electrical conductivity of PVDF-MWCNT samples with different cell-sizes and different salt-contents are shown in Figure 6.7. The achieved electrical conductivity values in this study was higher than the values reported in the literature (i.e., 10^{-2} Scm^{-1} for PVDF/MWCNT nanocomposite with 20 wt.% filler loading) by more than one order of magnitude [151]. The electrical conductivity

of the nanocomposite samples with different foam morphologies was directly related to their MWCNT content (as illustrated in Figure 6.5 and Figure 6.7).

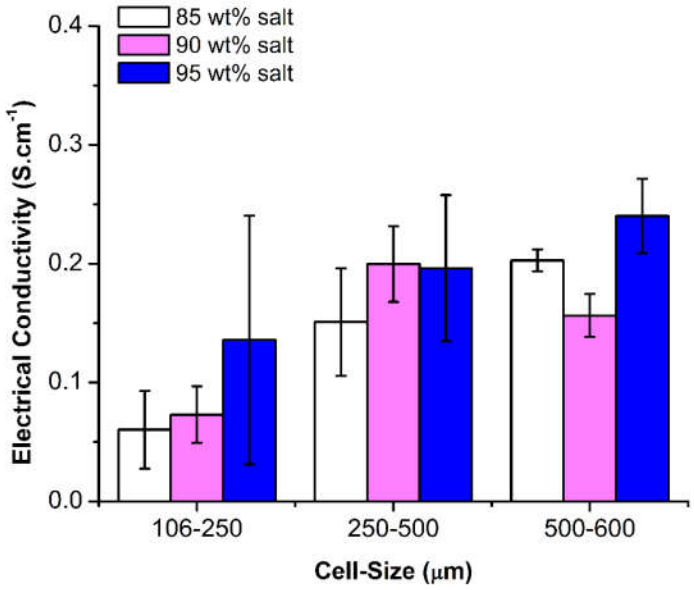

Figure 6.7 Effects of the cell-size and the salt-content (before salt leaching) on electrical conductivity of PVDF-MWCNT foams

By increasing both the cell-size and the salt-content used to fabricate PVDF foams, the resultant nanocomposites' electrical conductivities were also enhanced because of the higher amount of MWCNT absorption during the solution coating process. The error bars of the conductivity graph indicated that the foam templates fabricated by using 95 wt.% NaCl, showed less consistent measurements. This might be due to a lower uniformity in MWCNT coating because of their flimsy cellular structure. Moreover, considering the electrical conductivity data and the MWCNT contents of all PVDF-MWCNT samples, the PVDF foams prepared with 90 wt.% salt-content and salt-size of 250-500 μm demonstrated the best performance serving as a template to efficiently create 3D conductive networks after CNT coating.

6.3.4 Seebeck Coefficient and TE Efficiency of Organic Thermoelectric Foams

The Seebeck coefficient of the PVDF-MWCNT nanocomposite foams with different cellular morphologies is presented in Figure 6.8. The cell-morphology of the polymeric templates demonstrated a negligible effect on the Seebeck coefficient of PVDF-MWCNT nanocomposites. The measured Seebeck coefficients of all PVDF-MWCNT nanocomposite foams, regardless of their MWCNT loadings, were between 9 and 10 μVK^{-1}; however, their electrical conductivities increased from 0.06 Scm^{-1} to 0.24 Scm^{-1} as the MWCNT loading increased. This trend is in contrast with bulk semiconducting materials in which the Seebeck coefficient usually decreases as their electrical conductivity increases [15,152,153]. The potential to promote the PVDF-MWCNT nanocomposite foam's electrical conductivity without compromising its Seebeck coefficient would be beneficial to optimize the overall TE property of such polymeric material system.

The effects of salt-content and cell-size of PVDF foams on the *ZT* value of their resultant PVDF-MWCNT nanocomposites is shown in Figure 6.9. By increasing the cell-size range from 106-250 μm to 250-500 μm, the *ZT* value significantly improved. This improvement was more noticeable for foam samples fabricated using lower NaCl contents. As the effective thermal conductivity and the Seebeck coefficients of all samples were maintained at the same levels, the nanocomposite foams' *ZT* values were mostly governed by their electrical conductivities, and thereby by their 3D MWCNT networks.

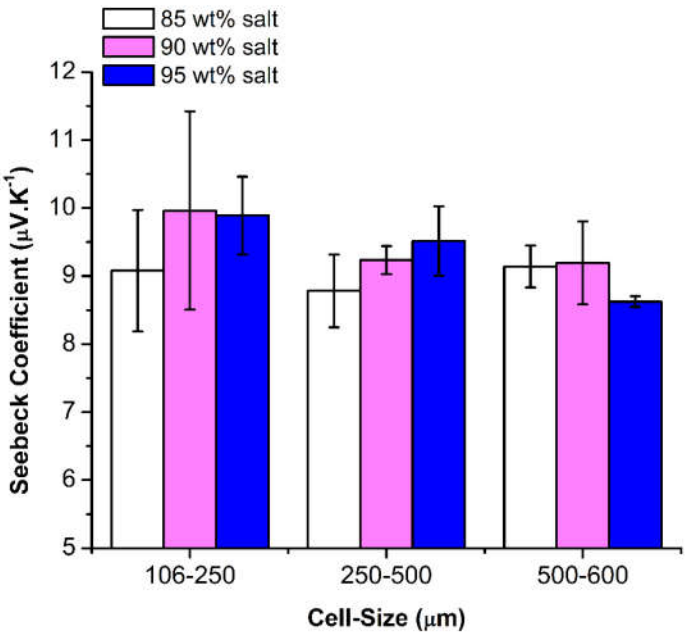

Figure 6.8 Effects of the cell-size and the salt-content (before salt leaching) on Seebeck coefficient of PVDF-MWCNT foams

The reduction in the *ZT* value indicated that the polymer foams prepared by using salt-size of <250 μm and salt-content of <90 wt.% yielded a fewer number of 3D conductive paths as a result of less interconnections in their cellular structures. Less porosity was another reason which caused poor absorption of MWCNTs into their porous structure that suppressed their electrical conductivity. The foam samples prepared with high salt-content (i.e., >90 wt.%) and large cell-sizes (i.e., >500 μm), on the other hand, demonstrated a negligible improvement in their *ZT* values even with higher MWCNT absorption; these samples were also too fragile because of their high porosity and elevated amount of cell ruptures. The results of TE parameters for the PVDF-MWCNT samples with different foam morphologies indicated that polymer foams with 90 wt.% salt-content and the cell-size of 250-500 μm served as best templates for fabricating PVDF-MWCNT nanocomposites for TE applications.

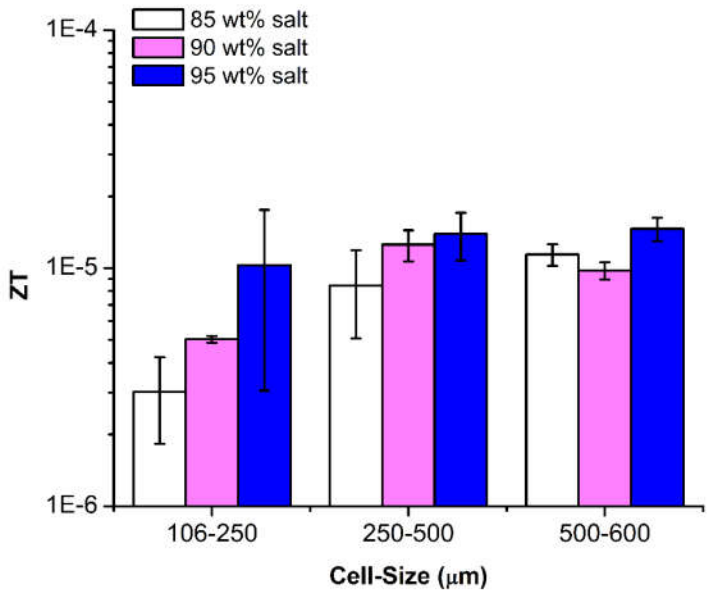

Figure 6.9 Effects of the cell-size and the salt-content (before salt leaching) on *ZT* value of PVDF-MWCNT foams

6.3.5 Effect of MWCNT-Content on TE Properties of Organic Thermoelectric Foams

To investigate the effects of MWCNT-content on the thermoelectric properties of PVDF-MWCNT nanocomposite samples, the salt-content and the salt-size used to fabricate the polymer foam templates were retained constant at 90 wt.% and 250–500 μm, respectively, as a standard foam preparation condition. Figure 6.10 and Figure 6.11 plot the relationships between MWCNT loadings and the TE properties (i.e., electrical conductivity, thermal conductivity, Seebeck coefficient, and *ZT* value) of the PVDF-MWCNT foams. By increasing the MWCNT-content of the polymer foams from 12 wt.% to 29 wt.%, their electrical conductivity improved by more than 8 times without a significant increase in their effective thermal conductivity (i.e., only 20% increase).

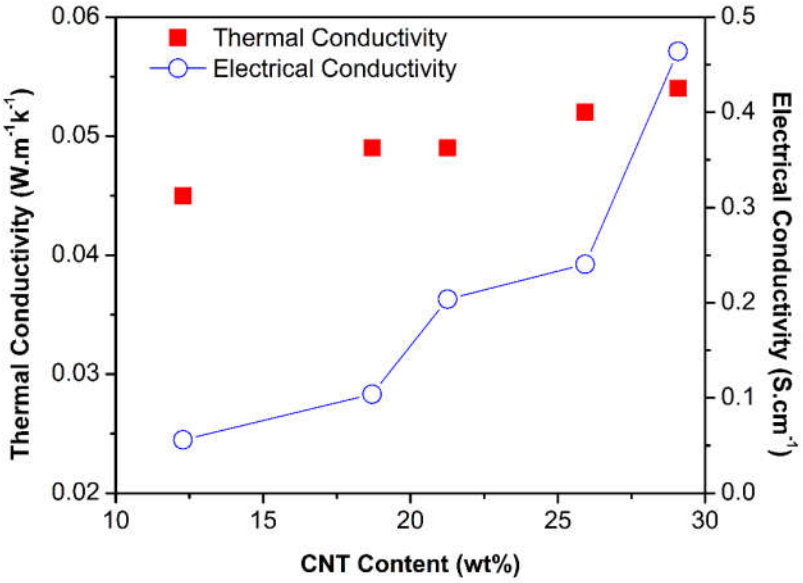

Figure 6.10 The CNT-content effect on the thermal and electrical conductivity of PVDF-MWCNT foams

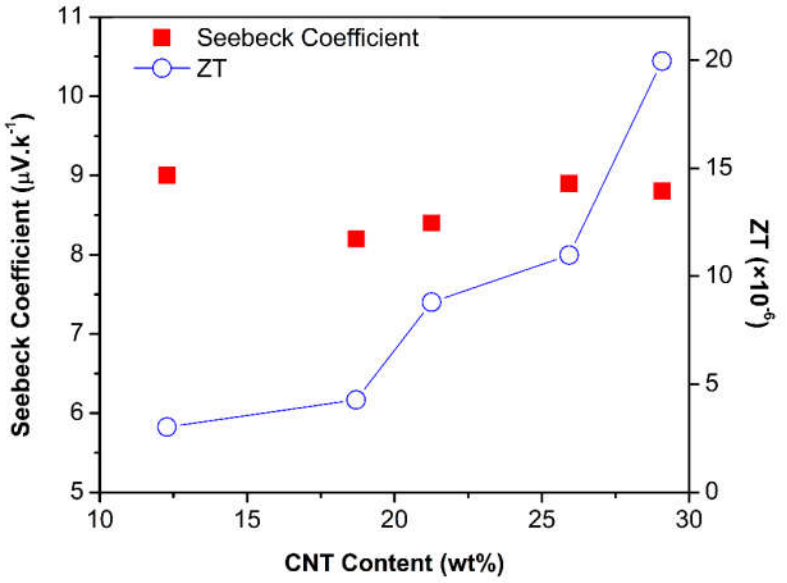

Figure 6.11 The CNT-content effect on the Seebeck coefficient and *ZT* value of PVDF-MWCNT foams

The results indicated that the open-cell PVDF foam templates had a dominant contribution on suppressing the effective thermal conductivity of the final nanocomposite samples. The Seebeck coefficient of the polymer nanocomposites remained insensitive to their MWCNT-content and demonstrated a negligible relation to their electrical conductivity values. Consequently, the TE figure of merit of the nanocomposite foams showed nearly 7-folded improvement after increasing their MWCNT-content from 12 wt.% to 29 wt.%. The experimental results revealed that the proposed fabrication method effectively decoupled the TE parameters of polymer-based TE materials, which provided an easier processing route to optimize their *ZT* values.

6.3.6 Effect of In-situ Polymerization of PPy on TE Properties of Organic Thermoelectric Foams

The thermoelectric properties of PVDF-PPy-MWCNT nanocomposite foams are summarized in Table 6.1 while their results are compared with PVDF-MWCNT samples incorporating similar amount of filler-content. PVDF foam templates with similar cell structures (i.e., cell-size of 250-500 μm and the salt-content of 90 wt.%) were used to fabricate both types of nanocomposite samples. The results revealed that the effective thermal conductivity of all samples remained in the same range of that of PVDF foams (i.e., about 0.045 $Wm^{-1}K^{-1}$). The addition of conductive fillers (i.e., MWCNTs and PPy) had negligible effect on the effective thermal conductivity of the polymer foams. The electrical conductivity of the nanocomposite foams containing PPy was lower than the measured values for PVDF-MWCNT samples.

Table 6.1 Thermoelectric properties of PVDF-MWCNT foam samples with and without PPy

Sample	Coating wt.%	Thermal Conductivity ($Wm^{-1}K^{-1}$)	Electrical Conductivity (Scm^{-1})	Seebeck Coefficient (μVK^{-1})	*ZT*
PVDF–MWCNT	24.9	0.045	0.199	10.1	1.4E-5
PVDF-PPy-MWCNT	26.6	0.044	0.055	19.8	1.5E-5

Figure 6.12 demonstrated an SEM micrograph of a PVDF foam template coated with PPy-MWCNT. The surface morphology of the PPy-MWCNT coated sample is similar to the uniform fibrous morphology of PVDF templates coated with pure MWCNTs (Figure 6.1(b)). This observation indicated that an in-situ polymerization of PPy resulted in coating of individual MWCNTs with a thin layer of PPy polymer, which provided lower electrical conductivities than pure MWCNTs. This phenomenon increased the electrical resistance at the CNT-CNT junctions and adversely affected the overall electrical conductivity of the nanocomposite samples. The measured Seebeck coefficient of the PVDF-PPy-MWCNT samples, on the other hand, was two times higher than that of the PVDF-MWCNT nanocomposites. This can be attributed to the energy filtering effect at the introduced MWCNT-PPy interfaces in MWCNT-MWCNT junctions that prohibited transferring of charge carriers with lower energy, thereby increased mean carrier energy level [154–156]. Consequently, the *ZT* value of PVDF-MWCNT nanocomposite foams remained around the same range after addition of the conducting polymer.

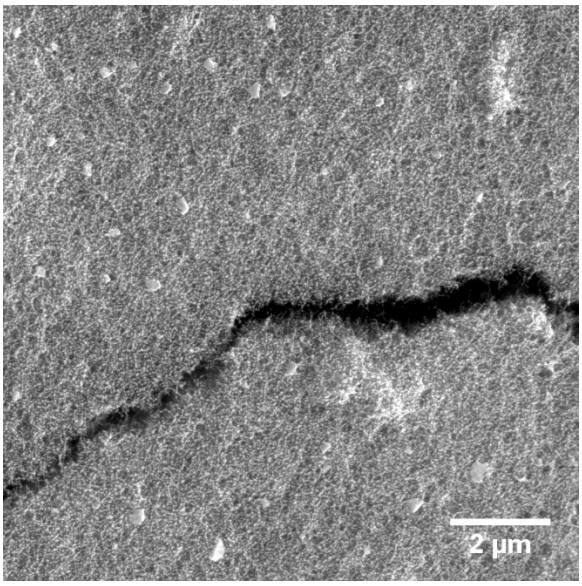

Figure 6.12 An SEM picture of a PVDF foam template coated with PPy-MWCNT

Using other types of conducting polymers with higher intrinsic electrical conductivities (such as poly(3,4-ethylenedioxythiophene) polystyrene sulfonate (PEDOT:PSS) or PANI) could result in further improvement in the *ZT* value of the final material system. The results showed that while the introduction of MWCNT-PPy interfaces would effectively promote the material system's Seebeck coefficient, the undesired decrease in the electrical conductivity prohibited further improvement in its TE efficiency. Therefore, a maximum *ZT* value for PVDF-PPy-MWCNT nanocomposite foams should be achieved by optimizing their power factor.

The results of this study showed that polymer foams with open-cell structure can be utilized as a template to effectively create a 3D network of conductive fillers within polymer matrices. Fabricating a polymer nanocomposite with the proposed method helped to simultaneously achieve high electrical conductivity and ultra-low thermal conductivity values. Moreover, coating the PVDF templates with a combination of conducting polymers and carbon nanotubes was an effective strategy to promote the material system's Seebeck coefficient. Consequently, the

suggested processing strategies provide potential routes to independently tune the polymer nanocomposites' TE parameters in attempt to maximize their *ZT* values.

6.4 Conclusion

This study suggested a new route to develop polymer nanocomposite materials with enhanced TE energy conversion efficiencies. The introduced technique also helped to separately tune the thermoelectric parameters (i.e., electrical conductivity, effective thermal conductivity, and Seebeck coefficient) of polymer nanocomposites. Salt leaching technique was utilized to fabricate open-cell polymer foams with ultra-low thermal conductivity. Open-cell polymer foams were used as templates to assist the formation of 3D conductive multi-walled carbon nanotubes networks throughout the polymer matrix. Both salt size and salt content, used in the particulate leaching process, were found to be important factors governing the morphology of porous templates and thereby the amount of MWCNT uptake. Therefore, these two parameters critically influenced the nanocomposite foam's electrical conductivity. Furthermore, the in-situ polymerization of polypyrrole during the MWCNT coating within the open-cell matrix helped to promote the Seebeck coefficient of the nanocomposite material by creating multiple CNT-polymer junctions, which act as barriers for low-energy charge carriers. The addition of PPy, however, suppressed the electrical conductivity of the nanocomposite foams which adversely affected their TE efficiency. The optimum achieved *ZT* value was about 1.4×10^{-5} for PVDF/MWCNT nanocomposite foams with 24.9 wt.% MWCNT loading. The proposed method provides an opportunity to favorably tune the thermal and electrical conductivity of polymer nanocomposites and promote their TE efficiency. In the long run, this research can open a window to develop polymeric TE materials with high energy conversion efficiencies for green energy harvesting.

Chapter 7. Thermoelectric Nanocomposite Foams using Non-Conducting Polymers with Hybrid 1D and 2D Nanofillers[4]

7.1 Introduction

A facile processing strategy to fabricate thermoelectric polymer nanocomposite foams with non-conducting polymers and carbon fillers is reported in this study, while the hybridization effects of conducting nanoparticles on the TE performances of the fabricated samples were investigated. Multilayered networks of graphene nanoplatelets and multi-walled carbon nanotubes are deposited on macroporous polyvinylidene fluoride foam templates using layer-by-layer (LBL) assembly technique. The open cellular structures of the foam templates provide a platform to form segregated 3D networks consisting of one-dimensional (1D) and two-dimensional (2D) carbon nanoparticles. Hybrid nanostructures of GnP and MWCNT networks synergistically enhance the material system's electrical conductivity. Furthermore, the polymer foam substrates possess high porosity to provide ultra-low thermal conductivity without compromising the electrical conductivity of the TE nanocomposites. With an extremely low GnP loading (i.e., ~1.5 vol.%), the macroporous PVDF nanocomposites exhibit a thermoelectric figure-of-merit of ~10^{-3}. To the best of our knowledge, this *ZT* value is the highest value reported for organic TE materials using non-conducting polymers and MWCNT/GnP nanofillers. The proposed technique represents an industrially viable approach to fabricate organic TE materials with enhanced energy conversion

[4] This chapter is based on reference [72]

efficiencies. Current study demonstrates the potential to develop light-weight, low-cost, and flexible TE materials for green energy generation.

7.2 Materials and Methods

7.2.1 Fabrication of Macroporous PVDF Templates

Polyvinylidene fluoride (PVDF, Kynar 740, Arkema) was used to fabricate polymeric foam templates by salt-leaching method. A typical thermoplastic polymer was selected in this study due to its ease of processing, good mechanical strength and flexibility to serve as a template for fabricating TE polymer nanocomposite samples. PVDF powders were dry-blended with sodium chloride (NaCl) salt with particle sizes ranged from 250 μm to 500 μm. PVDF-NaCl samples were made by hot-pressing the mixture at 185 °C and 4000 psi into disc-shaped molds of 20 mm in diameters and 2 mm in thicknesses. PVDF-NaCl composite samples were immersed in a water bath at room temperature (i.e., 23 °C) for 72 hours to leach out the salt content and produce macroporous PVDF foam templates with open-cellular structures. The fabricated PVDF foams were dried in an oven at 70 °C for 12 hours and weighed to ensure complete removal of their salt contents. A high percentage of salt particles within the PVDF-NaCl mixtures was crucial in this fabrication technique to allow the complete removal of all NaCl and achieve open cellular foam structures. The effects of different foam structures on the thermal conductivities and filler adsorption abilities of PVDF templates were investigated in the previous phase of our research [157]. In this study, the PVDF foam templates were fabricated using 90 wt.% of NaCl to achieve high porosity with excessive specific surface areas. This type of morphology made the foams ideal templates for absorbing carbon nanoparticles in a way that they form continuous filler networks.

7.2.2 Multilayer Deposition of GnP-MWCNT Network

The nanocomposite samples were prepared by layer-by-layer (LBL) deposition of conducting nanofillers on the cell-walls of as-fabricated polymeric foam templates, prepared by the salt leaching method. Multi-walled carbon nanotubes (MWCNT, 1.0 wt.% aqueous dispersed, AQ0101, Nanocyl) and graphene nanoplatelets (GnP, Grade 2, CheapTubes) were used as conducting nanoparticles to fabricate polymer nanocomposite samples. As-fabricated PVDF foams were repeatedly immersed into aqueous solutions of carbon nanofillers following by drying in an oven at 70 °C for 12 hours to coat multiple layers of nanoparticles over their porous structures. Each coating cycle was performed by sonicating the templates in the filler solutions for two minutes using an ultrasonic probe (Q700, QSonica). This would facilitate the penetration of nanoparticles throughout the pores of PVDF templates and create a uniform coating of nanoparticles on their cell walls.

An aqueous solution of GnPs was prepared using sodium dodecyl sulfate (SDS, Sigma-Aldrich) as surfactant, with GnP:SDS mass ratio of 1, to ensure a stable dispersion of GnP. Solutions of MWCNT-GnP mixtures with MWCNT:GnP mass ratios of 1 and 0.1 were also prepared to fabricate nanocomposite samples filled with hybrid GnP-MWCNT fillers. The solutions were sonicated for 10 minutes to ensure uniform dispersion of nanoparticles. The total filler content of all the solutions were gradually increased after each coating cycle from 0.1 wt.% to 1 wt.% in order to achieve a desired coating level and ensure proper attachment of fillers onto the cell walls. The adsorption of MWCNTs and GnPs onto the interior surfaces of the interconnected pores within the PVDF foams, would yield a multilayered and continuous network of conductive nanoparticles throughout them. The experimental results revealed that fewer coating cycles would be needed to achieve a desired filler loading level while using MWCNTs compared

with GnPs or hybrid fillers. This phenomenon is because of the unidirectional shape of MWCNTs and their wavy structure, which provide better entanglement during their multilayered stacking within polymeric foam templates.

7.2.3 Sample Characterization

Scanning electron microscopy (FEI Company, Quanta 3D FEG) was used to analyze the surface morphologies and microstructures of the nanocomposite foams. The cross-sections of nanocomposite foams were exposed by cryo-fracturing the samples under liquid nitrogen. The fractured surfaces were sputter-coated by gold using a sputter-coating machine (Denton Vacuum, Desk V Sputter Coater). The electrical conductivities of the nanocomposite foams were measured by four-point method using a multifunctional source meter (Keithley, SMU 2450) and a collinear four-point probe (SP4 probe head) installed on a probing fixture (Signatone probe S-302-4). A constant electric current was induced on the surfaces of all the fabricate nanocomposite samples, while the measured voltage was recorded to calculate the resistance value. A very small current level (i.e., 1 mA) was selected to avoid joule heating within the samples which could cause measurement error. Using ASTM F84-02 standard, the sample's surface electrical conductivity was converted into their bulk conductivity value by using the size and thickness correction factors for each sample. The thermal conductivities of the nanocomposite foams were measured based on the modified transient plane source (MTPS) method using a thermal conductivity analyzer (C-Therm Technologies Ltd., TCi Thermal Conductivity Analyzer). The Seebeck coefficient was measured using a custom-made unit. By applying a temperature difference (ΔT) across the sample's surface, within the range of 2 ºC to 4 ºC, the generated voltage (V_{TE}) was recorded by a source meter. The Seebeck coefficient was calculated from the slope of the V_{TE} versus ΔT plot. All

the thermoelectric parameters of the fabricated samples were measured at room temperature (i.e., 300 K) to provide consistent and comparable results.

7.3 Results and Discussion

7.3.1 Open-Cellular Morphologies of Macroporous PVDF Templates

Figure 7.1 illustrates the SEM micrographs of the PVDF foams, before and after coating with carbon nanoparticles, at different magnifications. The open-cellular foam morphologies revealed the high levels of porosity and interconnectivity of pores throughout the polymeric templates. The SEM micrographs also indicated that after depositing multilayered structure of carbon nanofillers, the open-cellular structures of the foam templates remained nearly intact.

7.3.2 Phase Morphology of Macroporous PVDF Templates and their Nanocomposites

The phase morphologies of the nanocomposite foams are demonstrated in SEM micrographs with higher magnifications in Figure 7.1. The micrographs revealed uniform coating of conductive fillers on the interior pore surfaces of the PVDF foams, while carbon nanoparticles were interconnected and evenly adhered to the cell walls. This uniform coating was achieved as filler solutions were able to penetrate throughout the entire volume of the templates due to their open-cellular structures and high porosities. Figure 7.1(f) illustrates that the PVDF-MWCNT nanocomposite sample contained a continuous fibrous layer of MWCNT which was thoroughly covering the cell walls of the PVDF foam. As shown in Figure 7.1(o), the PVDF-GnP nanocomposite sample demonstrated a different surface morphology caused by the stacked layers of GnPs deposited on top of the PVDF template.

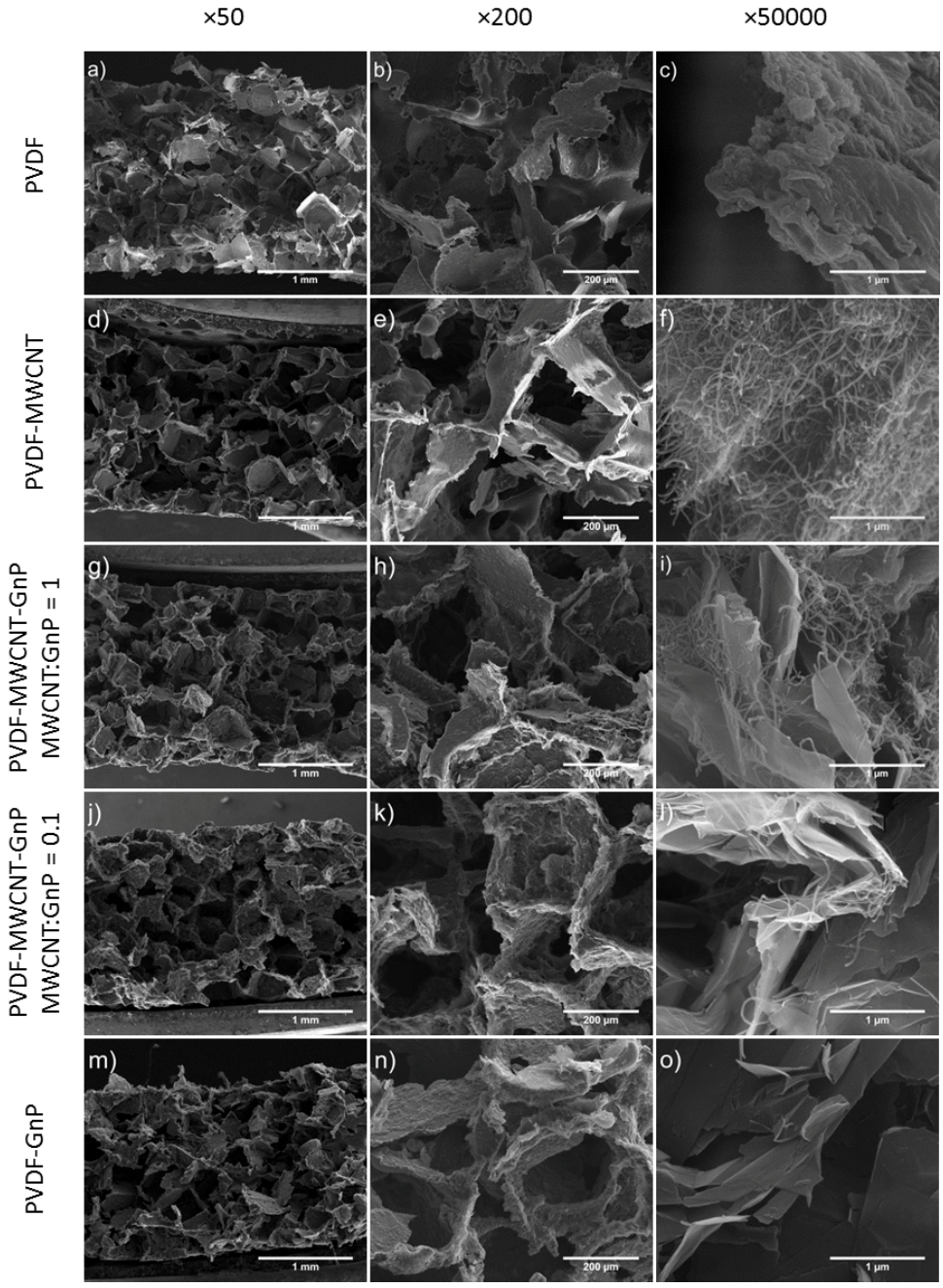

Figure 7.1 SEM micrographs that illustrate the foam and phase morphologies of: (a-c) PVDF foams; (d-f) PVDF-MWCNT nanocomposites; (g-i) PVDF-MWCNT-GnP nanocomposites with MWCNT:GnP ratio of 1; (j-l) PVDF-MWCNT-GnP nanocomposites with MWCNT:GnP ratio of 0.1; and (m-o) PVDF-GnP nanocomposites at three different magnifications

Figure 7.1(i) and (l) show the interactions between MWCNTs and GnPs within the PVDF nanocomposites containing hybrid nanoparticles with MWCNT:GnP ratios of 0.1 and 1, respectively. In PVDF-MWCNT-GnP nanocomposite samples with MWCNT:GnP ratio of 1, MWCNTs were widespread all over the samples due to their high aspect ratios compared with GnPs. Consequently, MWCNTs were covering most of the surface areas of GnPs while MWCNT agglomerations were observed on templates' surfaces. In PVDF-MWCNT-GnP nanocomposites with MWCNT:GnP ratio of 0.1, on the other hand, MWCNTs were scattered on GnPs' surfaces while bridging along the surfaces and the gaps of adjacent graphene nanoplatelets. Therefore, hybridization of 1D and 2D nanoparticles with low 1D:2D filler ratio created more connected pathways for electron transferring throughout the polymer matrix.

7.3.3 Electrical Conductivity of Macroporous PVDF Nanocomposites

The current-voltage graph for the PVDF nanocomposite samples containing different nanofillers is plotted in Figure 7.2. As a case study, the samples loaded with about 1.4 wt.% of carbon fillers were selected to investigate their conductivity behavior by changing the induced electric current. All samples showed a linear current-voltage characteristic, which represented their ohmic behavior within the applied current range. The electrical conductivities of the samples could be calculated from the slop of their *I-V* graphs.

Figure 7.3(a) plots the electrical conductivity of the polymer nanocomposites, containing different carbon nanoparticles, as a function of the volume percentage of nanoparticles within PVDF templates. The weight percent of nanofillers loaded on PVDF foams were obtained by measuring the weight of samples before and after each coating cycle. The volume fraction (vol.%) of carbon fillers within PVDF templates were calculated using their wt.% and taking into account the total volume of voids and the solid part of foams. The densities of MWCNTs and GnPs were

considered to be 1.75 g cm^{-3} (for NC7000 type of MWCNTs) and 2.2 g cm^{-3} (a typical reported value for GnPs in literature), respectively [158,159].

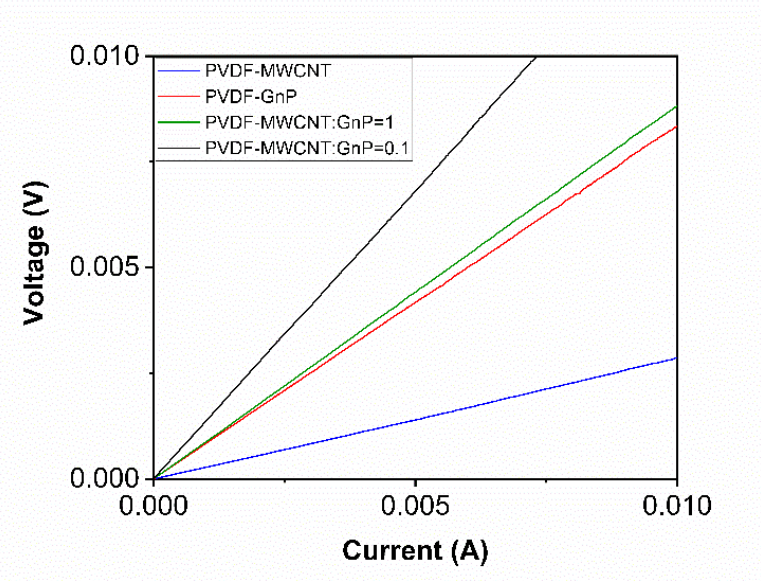

Figure 7.2 The current-voltage graph of PVDF nanocomposite samples loaded with about 1.4 wt.% of different carbon nanofillers

By increasing the filler loadings of the nanocomposite samples, their electrical conductivities showed an initial sharp increase following by a gradual improvement at higher filler loadings. This behavior indicated that a percolated network of conducting nanoparticles had established. The percolation behavior for the electrical conductivity typically follows a power law relationship as expressed in Equation (7-1):

$$\sigma \propto (\emptyset - \emptyset_c)^t \tag{7-1}$$

where σ is the electrical conductivity, ϕ is the filler content, ϕ_c is the percolation threshold, and t is a critical exponent reflecting the dimensionality of the composite system [160].

The log(σ) versus log(ϕ-ϕ_c) plot for the experimental measurements of all nanocomposite samples, as shown in the inset of Figure 7.3(a), demonstrated a linear trend representing the

percolation behaviors. According to Table 7.1, the nanocomposite foams containing only MWCNTs had the lowest percolation threshold, which was consistent with the reported experimental results in the literature [161,162]. The higher aspect ratios of MWCNTs increased their chances of creating conducting networks within the polymeric matrix at low filler contents. The results also revealed that the calculated percolation thresholds of the polymeric foams containing hybrid nanofillers were at least 50% lower than their values for PVDF-GnP samples. At low filler loadings, MWCNTs helped to bridge among scattered GnP fillers, and thereby facilitated the formation of percolated pathways for electron transferring throughout the PVDF foam templates.

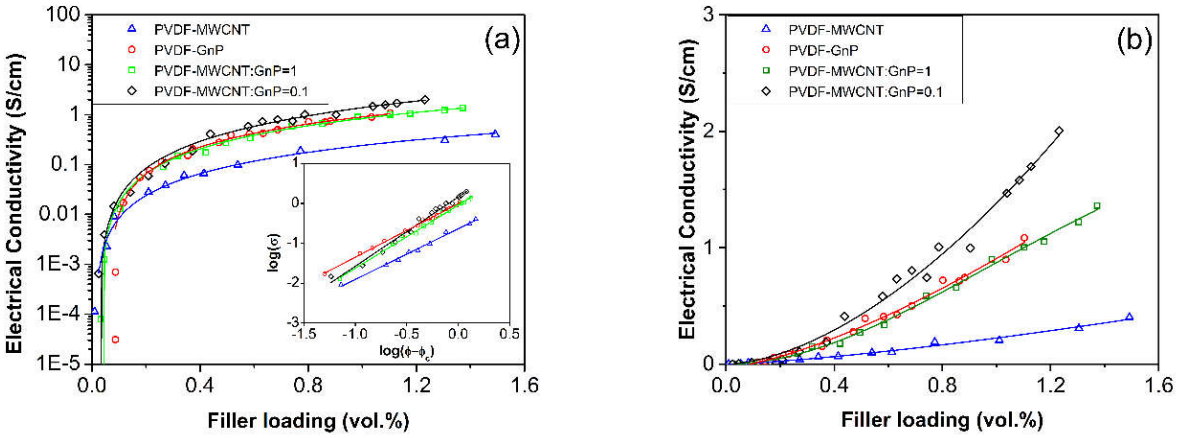

Figure 7.3 The electrical conductivities of PVDF nanocomposite samples as a function of filler loadings: (a) a logarithmic plot showing the percolation behaviors of σ with increasing filler loadings; and (b) a linear plot demonstrating differences in σ values of PVDF nanocomposites

As illustrated in Figure 7.3(a), increasing the nanofiller loadings above 0.1 vol.%, significantly enhanced the electrical conductivity of the nanocomposite foams containing GnPs and surpassed that of PVDF-MWCNT samples. Figure 7.3(b) plots the electrical conductivity of the fabricated samples in linear scale to clearly demonstrate the changes in their σ values by increasing their filler

contents. With 1.0 vol.% filler loading, the electrical conductivity of the PVDF-GnP samples were 3.5 times higher than that of the PVDF-MWCNT nanocomposites. This observation indicated that GnPs provided more efficient electron transferring pathways within the polymer matrix. Similar results were reported in literature comparing the electrical conductivity of polymer nanocomposites prepared with GnPs, MWCNTs or a mixture of them [163,164]. This behavior could be attributed to the 2D structures of graphene platelets, which provided high electron mobility and strong filler interactions [165]. It should be noted that the overall electrical conductivity of the nanocomposite samples was much lower than the measured values for pure MWCNT and GnP samples (i.e., 30 S/cm for MWCNT film prepared by solution casting, and 74 S/cm for GnP solid sample prepared by cold pressing) due to the electrical contact resistance at the introduced filler interfaces.

Table 7.1 The percolation thresholds and the critical exponents of PVDF nanocomposite foams coated with different types of carbon nanoparticles

Sample	**PVDF-MWCNT**	**PVDF-MWCNT-GnP MWCNT:GnP=1**	**PVDF-MWCNT-GnP MWCNT:GnP=0.1**	**PVDF-GnP**
Percolation Threshold (ϕ_c)	0.009	0.032	0.024	0.065
Critical Exponent (t)	1.40	1.45	1.63	1.36

The experimental results also revealed that the hybrid nanocomposite foams with MWCNT:GnP ratio of 0.1 showed the highest electrical conductivity values among all the nanocomposite samples. Omnipresence of MWCNTs among GnPs helped to bridge the adjacent platelets and thereby promoted the formation of interconnected networks throughout the insulating PVDF matrix. Therefore, simultaneously utilizing the high intrinsic electrical conductivity of GnPs

and the low percolation threshold of MWCNTs, resulted in promoting the nanocomposite's electrical conductivity. However, with a MWCNT:GnP ratio of 1, MWCNTs were presented all over the foam's cell-walls and created more agglomerated domains on GnPs' surfaces. Consequently, the MWCNT fillers with their inferior electrical conductivities adversely affected the electron transferring among the GnP networks.

7.3.4 Thermal Conductivities of Macroporous PVDF Nanocomposites

The effect of filler contents on the thermal conductivities (k) of the nanocomposite foams is depicted in Figure 7.4. As expected, the thermal conductivity of the open-cellular PVDF templates without nanoparticle coating was extremely low (i.e., ~0.04 $Wm^{-1}K^{-1}$) because of their high porosity.

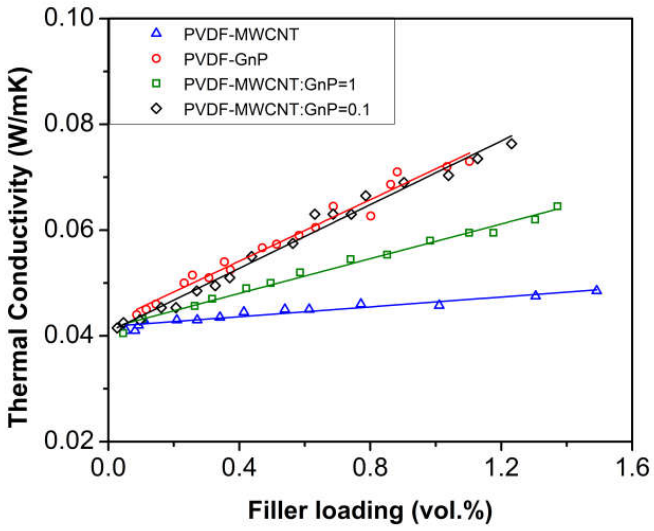

Figure 7.4 Thermal conductivities of PVDF nanocomposites as a function of filler loadings

The experimental results indicated that the deposition of MWCNTs on PVDF templates had negligible effects on their thermal conductivity, while PVDF foams containing GnPs showed a slight increase in their k. GnPs have reportedly better thermal transport properties compared with

MWCNTs because of their unique 2D atomic structures [166–168]. Nevertheless, the overall thermal conductivities of all PVDF nanocomposites remained very low (i.e., $k < 0.08$ $Wm^{-1}K^{-1}$) despite the adsorption of up to 15 wt.% nanoparticles. The increased phonon scattering due to the introduced interfacial thermal resistance at filler-filler junctions along with the high porosity of the PVDF templates, helped to retain the extra-low thermal conductivities of the nanocomposite foams [169]. Consequently, the measured thermal conductivities of the PVDF nanocomposites were significantly lower than the typical values reported for polymer nanocomposites containing carbon fillers (i.e., ~0.5-1 $Wm^{-1}K^{-1}$) [53].

7.3.5 Seebeck Coefficient of Macroporous PVDF Nanocomposites

The effects of filler-type and filler concentration on the Seebeck coefficients (S) of the fabricated nanocomposite foams are illustrated in Figure 7.5. All nanocomposite samples had positive Seebeck values indicating a p-type thermoelectric behavior. MWCNT and GnP have reportedly shown p-type thermoelectric behavior because of their oxygen-doping during exposure to the air. Surprisingly, the experimental results revealed that the Seebeck coefficients of the nanocomposite foams were significantly higher than the measured values for pure conducting fillers (i.e., $S < 8$ μVK^{-1} for MWCNT film prepared by solution casting, and $S < 11$ μVK^{-1} for GnP solid sample prepared by cold pressing). This phenomenon could be attributed to the energy filtering effect aroused from charge carrier scattering at the significantly large number of filler junctions throughout the pore surfaces of the open-cellular templates [22,170].

The maximum Seebeck coefficients for the PVDF nanocomposites were achieved once their filler loadings had reached their percolation thresholds. By increasing the filler loadings of the nanocomposite foams, their Seebeck coefficients initially dropped and thereafter remained around the same range. The reduction in their Seebeck coefficients was expected as higher filler loadings

led to enhanced electrical conductivities and there is usually a trade-off between σ and S in TE materials. It should be noted that the decrease in the Seebeck coefficients of all the nanocomposite foams was negligible compared to the increase in their electrical conductivities (i.e., $\Delta S < 30\%$ vs. $\Delta\sigma > 10^3$ times). The increased interfacial interaction between the conducting nanoparticles, as a result of the layer-by-layer coating process, helped to retain the high Seebeck coefficients of the nanocomposite samples while enhanced their electrical conductivities.

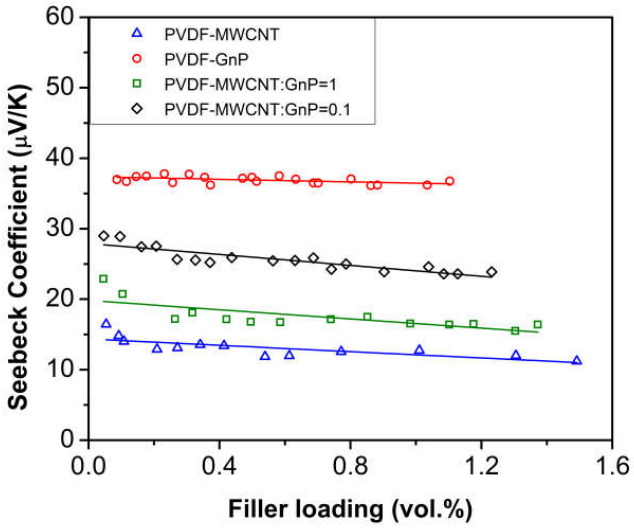

Figure 7.5 Seebeck coefficients of PVDF nanocomposites foams as a function of filler loadings

The PVDF-GnP foams demonstrated the highest Seebeck values among all the nanocomposite samples (i.e., ~37 μV K^{-1}) and their Seebeck coefficients were three times higher than those of PVDF-MWCNT samples. The experimental results for the nanocomposite samples loaded with hybrid fillers also showed that a lower MWCNT:GnP ratio was more favorable to achieve high Seebeck coefficients. These evidences indicated that GnPs have better Seebeck properties than MWCNTs.

7.3.6 TE Figure-of-Merit of Macroporous PVDF Nanocomposites

The measured *ZT* values of the fabricated nanocomposite samples are displayed in Figure 7.6. By increasing the filler contents of the polymeric foams, their TE efficiencies significantly improved showing a percolation behavior. At high filler loadings, the PVDF-GnP nanocomposite samples demonstrated the highest *ZT* values among all fabricated nanocomposites due to their high Seebeck coefficients. Despite the highest measured electrical conductivities, the *ZT* values of PVDF foams containing hybrid nanofillers with MWCNT:GnP ratio of 0.1 were slightly lower than those of PVDF-GnP samples because of their lower Seebeck coefficients. At low loadings (i.e., < 0.1 vol.%), however, PVDF-GnP nanocomposites showed the lowest TE efficiencies because of their low electrical conductivities. It is worth to mention that among the three TE parameters (i.e., σ, S, and k) of the fabricated samples, the changes in their electrical conductivities during nanoparticle deposition were more noticeable. Therefore, σ was the decisive parameter for designing the nanocomposite foam sample with highest *ZT* value.

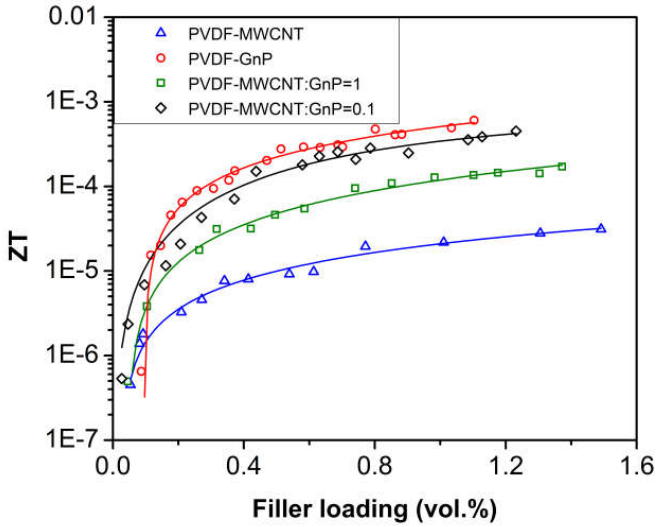

Figure 7.6 TE efficiencies of PVDF nanocomposite foams as a function of filler loadings

The results of this study suggested that GnP was the more promising candidate than MWCNT for fabricating TE polymer nanocomposites. The observations indicated that the TE efficiencies of the nanocomposite samples containing hybrid fillers could potentially be maximized by optimizing the MWCNT:GnP mass ratio and utilizing the interactions between 1D and 2D conducting nanoparticles. Figure 7.7 shows a schematic diagram, illustrating the synergistic effects of the hybridization of 1D and 2D nanoparticles. The Loose packing of the hybrid MWCNT-GnP fillers can facilitate the electron transferring through their 3D networks without compromising the Seebeck coefficients due to the carrier filtering effect at the filler-filler interfaces. Moreover, this 3D filler network can suppress the thermal conductivity via phonon scattering at the introduced multiple filler junctions.

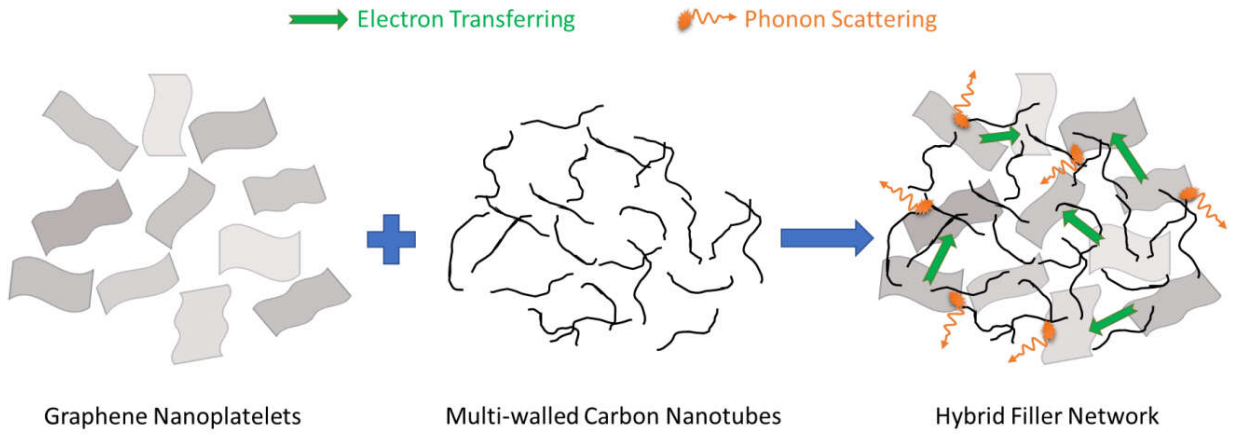

Figure 7.7 The synergistic effects of 1D and 2D conducting nanoparticles on electron and phonon transferring through their 3D networks

This study proposed the utilization of polymer foam templates as a new fabrication strategy to partially decouple the TE properties of polymer nanocomposite materials and promote their TE efficiencies. A maximum *ZT* value approaching 10^{-3} was achieved by PVDF nanocomposites containing extremely low loadings (i.e., < 1.5 vol.%) of carbon nanoparticles. This value is among

the highest *ZT* values reported in literature for organic TE materials using conventional non-conducting polymers. It is believed that by using the suggested fabrication technique and utilizing conducting fillers with better σ and *S* properties (e.g., SWCNTs or semiconducting fillers), further increase in *ZT* values could undoubtedly be achieved for polymeric TE materials.

7.4 Conclusion

A new technique has been developed in current study to fabricate lightweight organic materials with high TE efficiencies. Polymeric foams with open-cellular structures were employed as templates to create segregated networks of conducting nanofillers within the insulating polymer matrices. The resultant composite material system demonstrated low percolation thresholds and high electrical conductivities, without compromising the ultra-low thermal conductivities of the PVDF foam templates. The synergistic effects of 1D and 2D carbon nanoparticles in promoting the TE properties of polymer nanocomposites containing hybrid fillers was also investigated in this research. The experimental results revealed that by controlling the MWCNT:GnP mass ratio, incorporated in polymeric matrices, it was possible to tune their electrical conductivities, Seebeck coefficients, and percolation thresholds. The proposed processing method has proven to be a facile and effective approach to simultaneously improve the electrical conductivities, enhance the Seebeck coefficients, and suppress the thermal conductivities of polymer nanocomposites. Overall, it helps to promote the TE efficiency of polymer nanocomposites without the uses of conducting polymers that have poor processability. The suggested fabrication method is simple and scalable for processing flexible TE nanocomposites, which increases the potential of their industrial applications.

Chapter 8. Conclusion

8.1 Summary of Contributions

Thermoelectric generators can be utilized to harvest green energy by recycling waste heat generated from various sources and converting it into electrical energy. Organic or polymer-based thermoelectric materials have recently received a significant research interest due to their many advantages over conventional semiconducting TE materials. The poor energy conversion efficiency of polymeric TE materials, as their main drawback, should be significantly improved to make them industrially applicable. Most of the previous studies have focused on developing conjugated polymers as organic materials for TE applications. Because of the delocalized electrons in their backbones, conducting polymers usually provide high Seebeck coefficients and good electrical conductivities. However, their complex processing techniques and instability in air has limited their widespread application.

This study aimed at developing novel processing techniques to fabricate fully organic TE materials by mostly using non-conducting polymers as the matrix, with minimal loading of conducting fillers such as carbon nanoparticles or conjugated polymers. This objective ensures simultaneously achieving good mechanical properties, simple and replicable fabrication process, low manufacturing cost, stable physical properties, and enhanced TE efficiency of the material system. Achieving this objective requires to overcome a critical challenge which is separately tuning and optimization of the highly interrelated TE parameters of the material.

In the first part of this study, nanocomposite samples were characterized by using PPy as a conducting type of polymer with MWCNTs as conducting carbon nanoparticles. The effects of

different processing parameters (i.e., the oxidant:monomer molar ratio, the MWCNT:monomer mass ratio, and the secondary solution additive) on the TE parameters and microstructures of the fabricated samples were also investigated in this chapter. The optimized processing parameters were explored to achieve the maximum TE efficiency of the material. The samples prepared by using water-methanol as their solution medium, with oxidant:monomer molar ratio of 2.5, and MWCNT:monomer mass ratio of 1 provided the highest TE performance. The experimental results proved that there is an inverse correlation between the electrical conductivity and the Seebeck coefficient of the samples which prohibited increasing their TE efficiencies higher than a certain level.

Considering the complexities of the synthesizing of conducting polymers, conventional non-conducting polymers were suggested in the next phase of this research for fabricating organic TE materials. Polymer foaming was utilized to develop HDPE/MWCNT polymer nanocomposite samples with super-low thermal conductivities. Supercritical carbon dioxide foaming was used, as an in-situ foaming technique, to create bubbles within polymeric matrices and fabricate nanocomposite foams with closed-cell structures. The in-situ foaming of the polymer nanocomposite samples resulted in decoupling their TE parameters and simultaneously tuning these properties of the materials. The thermal conductivity of nanocomposite foams was decreased up to one order of magnitude by introducing an insulating cell structure within the polymer matrix. The electrical conductivity of nanocomposite foams increased about three times while their Seebeck coefficients were promoted by five times of the original values from unfoamed samples. Consequently, the *ZT* value of the polymer nanocomposites significantly increased (i.e., about 600 times) after the foaming process.

In the third phase of this research, freeze-drying method was used to fabricate polymer nanocomposite foams with enhanced TE properties. By incorporating a conducting polymer (i.e., PPy) in combination with GnP carbon nanoparticles within PVA polymer matrices, the electron transport properties of the insulative samples were improved. Therefore, polymer foam samples with high electrical conductivities and increased Seebeck coefficients were achieved. The experimental results showed that the electrical conductivities of the fabricated samples were significantly higher than the reported values for PVA nanocomposites containing carbon fillers. The proposed processing method was simple and replicable to be easily adopted in industries for the fabrication of lightweight and flexible thermoelectric modules. The overall *ZT* values of the foam samples were still very low, indicating that the PVA matrix was entirely wrapping the conducting fillers and probably blocking their intersections from transferring the charge carriers through the filler networks.

Salt-leaching method was introduced in the next chapter of this dissertation to prepare polymeric samples with high porosities and open-cellular structures. The fabricated open-cellular PVDF foams were then used as templates and coated with conducting nanoparticles (i.e., MWCNTs). Utilization of the foam templates helped to create 3D networks of conducting nanofillers within polymer matrices. As a result, the nanocomposite samples demonstrated low percolation thresholds and high electrical conductivities, along with ultra-low thermal conductivities. These material properties are desirable to achieve high TE efficiencies. The effects of incorporating a conducting polymer (i.e., PPy) within conventional thermoplastic polymers were also investigated in this study and has proven to be substantial in enhancing the TE efficiency of organic materials. The nanocomposite foams provided a maximum *ZT* value of 1.4×10^{-5} with

24.9 wt.% MWCNT loading. This value was up to two orders of magnitude higher than the achieved value from the previous phases of this study.

In the last part of this dissertation, polymer nanocomposite material systems containing hybrid fillers were synthesized and their TE properties were characterized. The effects of using a combination of one-dimensional and two-dimensional conducting fillers on charge carrier transportation of the polymer nanocomposites were investigated in this research. The experiments revealed that the hybridization of 1D and 2D carbon nanoparticles will help to promote the TE properties of polymer nanocomposites due to the synergistic effects of the nanoparticles in charge carrier transportations. In this chapter, the effects of using GnPs as conducting fillers in promoting the TE properties of the nanocomposite foams also were studied while compared with the results for MWCNT-loaded samples. A maximum *ZT* value of ~10^{-3} was measured for the nanocomposite foams prepared with extremely low filler loadings (i.e., ~1.5 vol.%). To the best of our knowledge, this value is the highest reported *ZT* value for organic thermoelectric materials prepared with non-conducting polymers and carbon nanofillers.

The maximum achieved thermoelectric properties of the fabricated nanocomposite samples from different phases of this study are summarized in Table 8.1. The measured densities and filler loadings of the polymer nanocomposite samples are also reported in this table. The uncertainty values of the measured TE parameters were calculated using the general error propagation rule considering the error limits of the testing instruments:

$$R = f(x, y, \dots) \;\rightarrow\; \delta R = \sqrt{(\frac{\partial R}{\partial x}\delta x)^2 + (\frac{\partial R}{\partial y}\delta y)^2 + \cdots} \qquad (8\text{-}1)$$

Table 8.1 Summary of maximum achieved TE properties, densities and filler contents of the fabricated nanocomposite samples in this study

Sample	Density (gr/cm^3)	K (W/mK)	σ (S/cm)	S (μV/K)	ZT ($\times 10^{-3}$)
PVA-PPy/GnP *(10 wt.%)*	0.04	0.035±0.002	0.002±(2e-8)	14.9±0.11	0.0004±(1e-5)
HDPE/MWCNT *(15 wt.%)*	0.1	0.06±0.003	0.1±(1e-5)	5.3±0.04	0.0014±(7e-5)
PVDF/MWCNT *(21 wt.%)*	0.2	0.048±0.0024	0.48±(5e-6)	13±0.09	0.052±0.0026
PPy/MWCNT *(35 wt.%)*	1	0.55±0.0275	13.5±0.0016	14.1±0.10	0.15±0.0076
PVDF/MWCNT-GnP *(22 wt.%)*	0.2	0.08±0.004	3.79±0.0004	23.6±0.18	0.79±0.0413
PVDF/GnP *(22 wt.%)*	0.2	0.077±0.0038	1.75±0.0002	36.1±0.27	0.89±0.0464

The results show a dramatic improvement in the TE efficiency of the fabricated samples during different phases of study. It should be noted that the PVDF-GnP nanocomposite foams demonstrated the highest *ZT* value among all samples. While the figure of merit of these nanocomposite foams surpassed the measured values from the PPy-MWCNT nanocomposites without foaming, the densities and the filler loadings of these foam samples were much lower than

the PPy-MWCNT samples. These findings indicated that much lower conducting fillers were required to fabricate organic materials with high TE efficiencies as a result of foaming technique.

This study suggested a new processing route to develop polymer materials with enhanced TE energy conversion efficiencies. The proposed method has proven as an effective approach to partially decouple and tune the three TE properties of polymer nanocomposites, which resulted in promoting their TE performance. The suggested fabrication method has the potential for industrial scale application due to its ease of processing and repeatability. In the long run, this research can open a new route to develop polymer-based TE materials for green energy harvesting which can contribute on preserving the environment and resolving the global warming issue.

8.2 Future Outlooks

The research and studies on organic thermoelectric materials are still in its early stages. Despite the significant improvements within the last decade, the TE performance of polymer-based materials requires further enhancement to achieve the desired value (i.e., $ZT > 1$) for their widespread application in industries. To achieve this objective, the structure-to-properties relationships of these materials should be thoroughly investigated in molecular levels and in microstructures. Moreover, the measurement techniques and test methods for evaluating TE properties of materials require further improvement to provide more reliable and replicable results. In this regard, some worldwide standards should be defined for characterization of TE properties of materials which will be utilized by all researchers to report comparable results.

The results of this study revealed that partial decoupling of the TE properties (i.e., electrical conductivity, thermal conductivity, and Seebeck coefficient) of nanocomposite materials is possible through foaming methods. This achievement enlightens new routes to simultaneously

promote these TE parameters and thereby effectively enhance the TE performance of the material. The proposed foaming techniques in this dissertation potentially can be utilized to promote the TE efficiency of not only polymer composites, but also other families of TE materials. Various types of fillers such as metallic or semiconducting particles can also be used in limited amounts to promote the electron transportation properties of polymer matrices without significantly affecting their favorable mechanical properties.

Most of previous studies on thermoelectric area have experimentally explored the TE properties of different materials and designed various material systems for TE applications. Along with the experimental research, more computational studies and numerical simulations are required to provide a detailed insight into these material properties. These studies are necessary to assist in material selection while designing highly efficient TE material systems. Computational studies can also suggest the optimized levels of material combinations to maximize the TE efficiency of thermoelectric composites.

Most of current studies are focused on developing p-type TE materials, while a limited number of studies have been devoted to designing n-type TE materials due to their instable properties in ambient conditions. To fabricate thermoelectric generators with highest efficiencies, both p-type and n-type TE materials should be designed with similar ranges of ZT values. The ultimate purpose of this research is to make organic thermoelectric generators with high energy conversion efficiencies as a renewable source of energy. In this context, inventing new techniques for fabricating polymeric TEGs with improved efficiencies, high flexibilities, and light weights is required to prove the potential of organic TE materials for industrial applications in energy generation. Due to multiple advantages of polymers compared with many other families of materials, TE polymer nanocomposites have a great potential to achieve widespread applications,

even with low TE efficiencies, as portable thermoelectric generators in remote areas. They can also be used in clothing industries or wearables devices to capture the heat from human bodies and provide power for small electronic modules.

References

[1] Fitriani, R. Ovik, B. D. Long, M. C. Barma, M. Riaz, M. F. M. Sabri, S. M. Said, and R.Saidur, "A review on nanostructures of high-temperature thermoelectric materials for waste heat recovery," Renew. Sustain. Energy Rev., vol. 64, pp. 635–659, Oct. 2016.

[2] Y. Du, J. Xu, B. Paul, and P. Eklund, "Flexible thermoelectric materials and devices," Appl. Mater. Today, vol. 12, pp. 366–388, Sep. 2018.

[3] L. E. Bell, "Cooling, Heating, Generating Power, and Recovering Waste Heat with Thermoelectric Systems," Science, vol. 321, no. 5895, pp. 1457–1461, Sep. 2008.

[4] A. W. Van Herwaarden and P. M. Sarro, "Thermal sensors based on the seebeck effect," Sensors and Actuators, vol. 10, no. 3–4, pp. 321–346, Nov. 1986.

[5] M. H. Elsheikh, D. A. Shnawah, M. F. Mohd Sabri, S. B. Mohd Said, M. H. Hassan, M. B. A. Bashir, and M. Mohamad, "A review on thermoelectric renewable energy: Principle parameters that affect their performance," Renew. Sustain. Energy Rev., vol. 30, no. 2014, pp. 337–355, Feb. 2014.

[6] N. Zhang, J. Xie, and V. K. Varadan, "Soluble functionalized carbon nanotube/poly(vinyl alcohol) nanocomposite as the electrode for glucose sensing," Smart Mater. Struct., vol. 15, no. 1, pp. 123–128, Feb. 2006.

[7] S. LeBlanc, "Thermoelectric generators: Linking material properties and systems engineering for waste heat recovery applications," Sustain. Mater. Technol., vol. 1, pp. 26–35, Dec. 2014.

[8] D. M. Rowe, “Thermoelectrics, an environmentally-friendly source of electrical power,” Renew. Energy, vol. 16, no. 1–4, pp. 1251–1256, Jan. 1999.

[9] T. M. Tritt and M. A. Subramanian, “Thermoelectric Materials, Phenomena, and Applications: A Bird’s Eye View,” MRS Bull., vol. 31, no. 03, pp. 188–198, Jan. 2011.

[10] O. Bubnova and X. Crispin, “Towards polymer-based organic thermoelectric generators,” Energy Environ. Sci., vol. 5, no. 11, p. 9345, Oct. 2012.

[11] S. Riffat and X. Ma, “Thermoelectrics: a review of present and potential applications,” Appl. Therm. Eng., vol. 23, no. 8, pp. 913–935, Jun. 2003.

[12] S. J. Kim, J. H. We, and B. J. Cho, “A wearable thermoelectric generator fabricated on a glass fabric,” Energy Environ. Sci., vol. 7, no. 6, p. 1959, May 2014.

[13] L. C. Ding, B. G. Orr, K. Rahaoui, S. Truza, A. Date, and A. Akbarzadeh, “Thermoelectric Generators as Alternative Source for Electric Power,” World Acad. Sci. Eng. Technol. Int. J. Electr. Comput. Energ. Electron. Commun. Eng., vol. 9, no. 12, pp. 1363–1367, 2015.

[14] E. Kanimba, M. Pearson, J. Sharp, D. Stokes, S. Priya, and Z. Tian, “A comprehensive model of a lead telluride thermoelectric generator,” Energy, vol. 142, pp. 813–821, Jan. 2018.

[15] G. J. Snyder and E. S. Toberer, “Complex thermoelectric materials.,” Nat. Mater., vol. 7, no. 2, pp. 105–14, Feb. 2008.

[16] X. F. Zheng, C. X. Liu, Y. Y. Yan, and Q. Wang, “A review of thermoelectrics research – Recent developments and potentials for sustainable and renewable energy applications,”

Renew. Sustain. Energy Rev., vol. 32, pp. 486–503, Apr. 2014.

[17] M. Martín-González, O. Caballero-Calero, and P. Díaz-Chao, “Nanoengineering thermoelectrics for 21st century: Energy harvesting and other trends in the field,” Renew. Sustain. Energy Rev., vol. 24, pp. 288–305, Aug. 2013.

[18] D. K. Aswal, R. Basu, and A. Singh, “Key issues in development of thermoelectric power generators: High figure-of-merit materials and their highly conducting interfaces with metallic interconnects,” Energy Convers. Manag., vol. 114, pp. 50–67, 2016.

[19] Z. G. Chen, G. Han, L. Yang, L. Cheng, and J. Zou, “Nanostructured thermoelectric materials: Current research and future challenge,” Prog. Nat. Sci. Mater. Int., vol. 22, no. 6, pp. 535–549, 2012.

[20] D. M. Rowe, In “CRC Handbook of Thermoelectrics,” CRC Press, 1995.

[21] A. J. Minnich, M. S. Dresselhaus, Z. F. Ren, and G. Chen, “Bulk nanostructured thermoelectric materials: current research and future prospects,” Energy Environ. Sci., vol. 2, no. 5, p. 466, May 2009.

[22] M. He, F. Qiu, and Z. Lin, “Towards high-performance polymer-based thermoelectric materials,” Energy Environ. Sci., vol. 6, no. 5, p. 1352, Apr. 2013.

[23] M. He, J. Ge, Z. Lin, X. Feng, X. Wang, H. Lu, Y. Yang, and F. Qiu “Thermopower enhancement in conducting polymer nanocomposites via carrier energy scattering at the organic–inorganic semiconductor interface,” Energy Environ. Sci., vol. 5, no. 8, p. 8351, 2012.

[24] C. Xiao, Z. Li, K. Li, P. Huang, and Y. Xie, “Decoupling Interrelated Parameters for

Designing High Performance Thermoelectric Materials," Acc. Chem. Res., vol. 47, no. 4, pp. 1287–1295, Apr. 2014.

[25] H. Alam and S. Ramakrishna, "A review on the enhancement of figure of merit from bulk to nano-thermoelectric materials," Nano Energy, vol. 2, no. 2, pp. 190–212, Mar. 2013.

[26] P. Sahoo, Y. Liu, J. P. A. Makongo, X. L. Su, et al., "Enhancing thermopower and hole mobility in bulk p-type half-Heuslers using full-Heusler nanostructures," Nanoscale, vol. 5, no. 19, p. 9419, 2013.

[27] C. Wood, "Materials for thermoelectric energy conversion," Reports Prog. Phys., vol. 51, no. 4, pp. 459–539, Apr. 1988.

[28] G. Chen, M. S. Dresselhaus, G. Dresselhaus, J. P. Fleurial, and T. Caillat, "Recent developments in thermoelectric materials," Int. Mater. Rev., vol. 48, no. 1, pp. 45–66, Feb. 2003.

[29] A. Shakouri, "Recent Developments in Semiconductor Thermoelectric Physics and Materials," Annu. Rev. Mater. Res., vol. 41, no. 1, pp. 399–431, Aug. 2011.

[30] Y. Pei, H. Wang, and G. J. Snyder, "Band Engineering of Thermoelectric Materials," Adv. Mater., vol. 24, no. 46, pp. 6125–6135, Dec. 2012.

[31] J. Mao, Z. Liu, and Z. Ren, "Size effect in thermoelectric materials," npj Quantum Mater., vol. 1, no. 1, p. 16028, Dec. 2016.

[32] R. Venkatasubramanian, E. Siivola, T. Colpitts, and B. O'Quinn, "Thin-film thermoelectric devices with high room-temperature figures of merit," Nature, vol. 413, no. 6856, pp. 597–602, Oct. 2001.

[33] E. P. Tomlinson, M. J. Willmore, X. Zhu, S. W. A. Hilsmier, and B. W. Boudouris, "Tuning the Thermoelectric Properties of a Conducting Polymer through Blending with Open-Shell Molecular Dopants," ACS Appl. Mater. Interfaces, vol. 7, no. 33, pp. 18195–18200, 2015.

[34] G. S. Nolas, J. Poon, and M. Kanatzidis, "Recent Developments in Bulk Thermoelectric Materials," MRS Bull., vol. 31, no. 03, pp. 199–205, Mar. 2006.

[35] M. Rull-Bravo, A. Moure, J. F. Fernández, and M. Martín-González, "Skutterudites as thermoelectric materials: revisited," RSC Adv., vol. 5, no. 52, pp. 41653–41667, May 2015.

[36] X. Zhang and L. D. Zhao, "Thermoelectric materials: Energy conversion between heat and electricity," J. Mater., vol. 1, no. 2, pp. 92–105, Jun. 2015.

[37] W. Liu, X. Yan, G. Chen, and Z. Ren, "Recent advances in thermoelectric nanocomposites," Nano Energy, vol. 1, no. 1, pp. 42–56, Jan. 2012.

[38] L. Wang, Y. Liu, Z. Zhang, B. Wang, J. Qiu, D. Hui, and S. Wang, "Polymer composites-based thermoelectric materials and devices," Compos. Part B Eng., vol. 122, pp. 145–155, Aug. 2017.

[39] G. Chen, W. Xu, and D. Zhu, "Recent advances in organic polymer thermoelectric composites," vol. 5, no. 18, pp. 4350–4360, May 2017.

[40] Q. Zhang, Y. Sun, W. Xu, and D. Zhu, "Organic Thermoelectric Materials: Emerging Green Energy Materials Converting Heat to Electricity Directly and Efficiently," Adv. Mater., vol. 26, no. 40, pp. 6829–6851, Oct. 2014.

[41] M. Culebras, C. Gómez, and A. Cantarero, “Review on Polymers for Thermoelectric Applications,” Materials, vol. 7, no. 9, pp. 6701–6732, Sep. 2014.

[42] N. Dubey and M. Leclerc, “Conducting polymers: Efficient thermoelectric materials,” J. Polym. Sci. Part B Polym. Phys., vol. 49, no. 7, pp. 467–475, Apr. 2011.

[43] R. Kroon, D. A. Mengistie, D. Kiefer, J. Hynynen, J. D. Ryan, L. Yu, and C. Muller, “Thermoelectric plastics: from design to synthesis, processing and structure–property relationships,” Chem. Soc. Rev., vol. 45, no. 22, pp. 6147–6164, Nov. 2016.

[44] N. Hu, Z. Masuda, C. Yan, G. Yamamoto, H. Fukunaga, and T. Hashida, “The electrical properties of polymer nanocomposites with carbon nanotube fillers,” Nanotechnology, vol. 19, no. 21, May 2008.

[45] R. Verdejo, M. M. Bernal, L. J. Romasanta, and M. A. Lopez-Manchado, “Graphene filled polymer nanocomposites,” J. Mater. Chem., vol. 21, no. 10, pp. 3301–3310, Feb. 2011.

[46] R. Gangopadhyay and A. De, “Conducting Polymer Nanocomposites: A Brief Overview,” Chem. Mater. vol. 12, no. 3, pp. 608-622, March 2000.

[47] M. Piao, G. Kim, G. P. Kennedy, S. Roth, and U. Dettlaff-Weglikowska, “Preparation and characterization of expanded graphite polymer composite films for thermoelectric applications,” Phys. status solidi, vol. 250, no. 12, pp. 2529–2534, Dec. 2013.

[48] J. Luo, B. Krause, and P. Pötschke, “Melt-mixed thermoplastic composites containing carbon nanotubes for thermoelectric applications,” AIMS Mater. Sci., vol. 3, no. 3, pp. 1107–1116, 2016.

[49] K. I. Winey, T. Kashiwagi, and M. Mu, “Improving Electrical Conductivity and Thermal

Properties of Polymers by the Addition of Carbon Nanotubes as Fillers," MRS Bull., vol. 32, no. 04, pp. 348–353, Apr. 2007.

[50] L. M. Veca, M. J. Meziani, W. Wang, F. Lu, et al., "Carbon Nanosheets for Polymeric Nanocomposites with High Thermal Conductivity," Adv. Mater., vol. 21, no. 20, pp. 2088–2092, May 2009.

[51] S. N. Leung, M. O. Khan, and H. E. Naguib, "Development of novel graphene and carbon nanotubes based multifunctional polymer matrix composites," 2014, vol. 1593, no. 1, pp. 240–243.

[52] M. O. Khan, S. N. Leung, E. Chan, H. E. Naguib, F. Dawson, and V. Adinkrah, "Effects of microsized and nanosized carbon fillers on the thermal and electrical properties of polyphenylene sulfide based composites," Polym. Eng. Sci., vol. 53, no. 11, pp. 2398–2406, Nov. 2013.

[53] Z. Han and A. Fina, "Thermal conductivity of carbon nanotubes and their polymer nanocomposites: A review," Prog. Polym. Sci., vol. 36, no. 7, pp. 914–944, Jul. 2011.

[54] C. Gao and G. Chen, "Conducting polymer/carbon particle thermoelectric composites: Emerging green energy materials," Compos. Sci. Technol., vol. 124, pp. 52–70, Mar. 2016.

[55] Q. Wei, M. Mukaida, K. Kirihara, Y. Naitoh, and T. Ishida, "Recent Progress on PEDOT-Based Thermoelectric Materials," Materials, vol. 8, no. 2, pp. 732–750, Feb. 2015.

[56] R. Yue and J. Xu, "Poly(3,4-ethylenedioxythiophene) as promising organic thermoelectric materials: A mini-review," Synth. Met., vol. 162, no. 11, pp. 912–917, 2012.

[57] Q. Yao, L. Chen, X. Xu, and C. Wang, “The High Thermoelectric Properties of Conducting Polyaniline with Special Submicron-fibre Structure,” Chem. Lett., vol. 34, no. 4, pp. 522–523, Apr. 2005.

[58] Y. Sun, Z. Wei, W. Xu, and D. Zhu, “A three-in-one improvement in thermoelectric properties of polyaniline brought by nanostructures,” Synth. Met., vol. 160, no. 21–22, pp. 2371–2376, Nov. 2010.

[59] N. T. Kemp, A. B. Kaiser, C. J. Liu, B. Chapman, et al., “Thermoelectric power and conductivity of different types of polypyrrole,” J. Polym. Sci. Part B Polym. Phys., vol. 37, no. 9, pp. 953–960, May 1999.

[60] L. Liang, G. Chen, and C. Y. Guo, “Polypyrrole nanostructures and their thermoelectric performance,” Mater. Chem. Front., vol. 1, no. 2, pp. 380–386, Feb. 2017.

[61] L. Liang, C. Gao, G. Chen, and C. Y. Guo, “Large-area, stretchable, super flexible and mechanically stable thermoelectric films of polymer/carbon nanotube composites,” J. Mater. Chem. C, vol. 4, no. 3, pp. 526–532, Jan. 2016.

[62] S. Ghosh, T. Maiyalagan, and R. N. Basu, “Nanostructured conducting polymers for energy applications: towards a sustainable platform,” Nanoscale, vol. 8, no. 13, pp. 6921–6947, Mar. 2016.

[63] Y. Du, S. Z. Shen, W. Yang, R. Donelson, K. Cai, and P. S. Casey, “Simultaneous increase in conductivity and Seebeck coefficient in a polyaniline/graphene nanosheets thermoelectric nanocomposite,” Synth. Met., vol. 161, no. 23–24, pp. 2688–2692, Jan. 2012.

[64] Y. Du, S. Z. Shen, K. Cai, and P. S. Casey, “Research progress on polymer–inorganic thermoelectric nanocomposite materials,” Prog. Polym. Sci., vol. 37, no. 6, pp. 820–841, Jun. 2012.

[65] B. T. McGrail, A. Sehirlioglu, and E. Pentzer, “Polymer Composites for Thermoelectric Applications,” Angew. Chemie Int. Ed., vol. 54, no. 6, pp. 1710–1723, Feb. 2015.

[66] J. Zhang, K. Zhang, F. Xu, S. Wang, and Y. Qiu, “Thermoelectric transport in ultrathin poly(3,4-ethylenedioxythiophene) nanowire assembly,” Compos. Part B Eng., vol. 136, pp. 234–240, Mar. 2018.

[67] J. Maiz, M. M. Rojo, B. Abad, A. A. Wilson, et al., “Enhancement of thermoelectric efficiency of doped PCDTBT polymer films,” RSC Adv., vol. 5, no. 82, pp. 66687–66694, 2015.

[68] D. Wang, Y. Su, D. Chen, L. Wang, X. Xiang, and D. Zhu, “Preparation and characterization of poly(3-octylthiophene)/carbon fiber thermoelectric composite materials,” Compos. Part B Eng., vol. 69, pp. 467–471, Feb. 2015.

[69] C. Meng, C. Liu, and S. Fan, “A promising approach to enhanced thermoelectric properties using carbon nanotube networks.,” Adv. Mater., vol. 22, no. 4, pp. 535–9, Jan. 2010.

[70] P. J. Taroni, I. Hoces, N. Stingelin, M. Heeney, and E. Bilotti, “Thermoelectric Materials: A Brief Historical Survey from Metal Junctions and Inorganic Semiconductors to Organic Polymers,” Isr. J. Chem., vol. 54, no. 5–6, pp. 534–552, Jun. 2014.

[71] M. Aghelinejad and S. N. Leung, “Enhancement of thermoelectric conversion efficiency

of polymer/carbon nanotube nanocomposites through foaming-induced microstructuring," J. Appl. Polym. Sci., vol. 134, no. 28, p. 45073, Jul. 2017.

[72] M. Aghelinejad and S. N. Leung, "Thermoelectric Nanocomposite Foams Using Non-Conducting Polymers with Hybrid 1D and 2D Nanofillers," Materials, vol. 11, no. 9, p. 1757, Sep. 2018.

[73] M. Zebarjadi, K. Esfarjani, M. S. Dresselhaus, Z. F. Ren, and G. Chen, "Perspectives on thermoelectrics: from fundamentals to device applications," Energy Environ. Sci., vol. 5, no. 1. 2012, pp. 5147–5162, 2012.

[74] H. Pang, Y. Y. Piao, Y. Q. Tan, G. Y. Jiang, J. H. Wang, and Z. M. Li, "Thermoelectric behaviour of segregated conductive polymer composites with hybrid fillers of carbon nanotube and bismuth telluride," Mater. Lett., vol. 107, pp. 150–153, Sep. 2013.

[75] K. Zhang, S. Wang, X. Zhang, Y. Zhang, Y. Cui, and J. Qiu, "Thermoelectric performance of p-type nanohybrids filled polymer composites," Nano Energy, vol. 13, pp. 327–335, Apr. 2015.

[76] S. N. Patel, A. M. Glaudell, K. A. Peterson, et al., "Morphology controls the thermoelectric power factor of a doped semiconducting polymer," Sci. Adv., vol. 3, no. 6, p. e1700434, Jun. 2017.

[77] X. Hu, G. Chen, X. Wang, and H. Wang, "Tuning thermoelectric performance by nanostructure evolution of a conducting polymer," J. Mater. Chem. A, vol. 3, no. 42, pp. 20896–20902, Oct. 2015.

[78] L. Liang, G. Chen, and C. Y. Guo, "Enhanced thermoelectric performance by self-

assembled layered morphology of polypyrrole nanowire/single-walled carbon nanotube composites," Compos. Sci. Technol., vol. 129, pp. 130–136, Jun. 2016.

[79] A. Dey, O. P. Bajpai, A. K. Sikder, S. Chattopadhyay, and M. A. Shafeeuulla Khan, "Recent advances in CNT/graphene based thermoelectric polymer nanocomposite: A proficient move towards waste energy harvesting," Renew. Sustain. Energy Rev., vol. 53, pp. 653–671, Jan. 2016.

[80] G. M. Nasr, A. S. Abd El-Haleem, A. Klingner, A. M. Alnozahy, and M. H. Mourad, "The DC Electrical Properties of Polyvinyl Alcohol / Multi-Walled Carbon Nanotube Composites," J. Multidiscip. Eng. Sci. Technol., vol. 2, no. 5, pp. 884–889, 2015.

[81] J. Aguilar and J. Bautista-Quijano, "Influence of carbon nanotube clustering on the electrical conductivity of polymer composite films," Express Polym. Lett, vol. 4, no. 5, pp. 292-299, 2010.

[82] J. L. Blackburn, A. J. Ferguson, C. Cho, and J. C. Grunlan, "Carbon-Nanotube-Based Thermoelectric Materials and Devices," Adv. Mater., vol. 30, no. 11, p. 1704386, Mar. 2018.

[83] J. Hone, I. Ellwood, M. Muno, A. Mizel, M. L. Cohen, A. Zettl, A. G. Rinzler, and R. E. Smalley, "Thermoelectric Power of Single-Walled Carbon Nanotubes," Phys. Rev. Lett., vol. 80, no. 5, pp. 1042–1045, Feb. 1998.

[84] D. Dragoman and M. Dragoman, "Giant thermoelectric effect in graphene," Appl. Phys. Lett., vol. 91, no. 20, p. 203116, Nov. 2007.

[85] Y. Xu, Z. Li, and W. Duan, "Thermal and Thermoelectric Properties of Graphene," Small,

vol. 10, no. 11, pp. 2182–2199, Jun. 2014.

[86] C. Yu, Y. S. Kim, D. Kim, and J. C. Grunlan, “Thermoelectric behavior of segregated-network polymer nanocomposites,” Nano Lett., vol. 8, no. 12, pp. 4428–4432, Mar. 2008.

[87] G. Gorrasi, V. Bugatti, C. Milone, et al., “Effect of temperature and morphology on the electrical properties of PET/conductive nanofillers composites,” Compos. Part B Eng., vol. 135, pp. 149–154, Feb. 2018.

[88] Q. Ren, J. Wang, W. Zhai, and S. Su, “Solid State Foaming of Poly(lactic acid) Blown with Compressed CO_2 : Influences of Long Chain Branching and Induced Crystallization on Foam Expansion and Cell Morphology,” Ind. Eng. Chem. Res., vol. 52, no. 37, pp. 13411–13421, Sep. 2013.

[89] K. Zhang, Y. Zhang, and S. Wang, “Enhancing thermoelectric properties of organic composites through hierarchical nanostructures,” Sci. Rep., vol. 3, no. 1, p. 3448, Dec. 2013.

[90] C. A. Hewitt, A. B. Kaiser, S. Roth, M. Craps, R. Czerw, and D. L. Carroll, “Multilayered carbon nanotube/polymer composite based thermoelectric fabrics,” Nano Lett., vol. 12, no. 3, pp. 1307–1310, 2012.

[91] Y. Choi, Y. Kim, S. G. Park, Y. G. Kim, et al., “Effect of the carbon nanotube type on the thermoelectric properties of CNT/Nafion nanocomposites,” Org. Electron. physics, Mater. Appl., vol. 12, no. 12, pp. 2120–2125, 2011.

[92] J. H. Choi, C. M. Hyun, H. Jo, J. H. Son, J. E. Lee, and J. H. Ahn, “Thermoelectric elastomer fabricated using carbon nanotubes and nonconducting polymer,” Jpn. J. Appl.

Phys., vol. 56, no. 9, p. 095101, Sep. 2017.

[93] M. Liebscher, T. Gartner, L. Tzounis, M. Micusik, et al., “Influence of the MWCNT surface functionalization on the thermoelectric properties of melt-mixed polycarbonate composites,” Compos. Sci. Technol., vol. 101, pp. 133–138, 2014.

[94] C. A. Hewitt, A. B. Kaiser, S. Roth, M. Craps, R. Czerw, and D. L. Carroll, “Varying the concentration of single walled carbon nanotubes in thin film polymer composites, and its effect on thermoelectric power,” Appl. Phys. Lett., vol. 98, no. 18, p. 183110, 2011.

[95] D. H. Sung, G. H. Kang, K. Kong, M. Kim, H. W. Park, and Y. B. Park, “Characterization of thermoelectric properties of multifunctional multiscale composites and fiber-reinforced composites for thermal energy harvesting,” Compos. Part B Eng., vol. 92, pp. 202–209, 2016.

[96] C. A. Hewitt, D. S. Montgomery, R. L. Barbalace, R. D. Carlson, and D. L. Carroll, “Improved thermoelectric power output from multilayered polyethylenimine doped carbon nanotube based organic composites,” J. Appl. Phys., vol. 115, no. 18, p. 184502, May 2014.

[97] C. A. Hewitt, A. B. Kaiser, M. Craps, R. Czerwet, et al., “Temperature dependent thermoelectric properties of freestanding few layer graphene/polyvinylidene fluoride composite thin films,” Synth. Met., vol. 165, pp. 56–59, Feb. 2013.

[98] L. Zhao, X. Sun, Z. Lei, J. Zhao, J. Wu, et al., “Thermoelectric behavior of aerogels based on graphene and multi-walled carbon nanotube nanocomposites,” Compos. Part B Eng., vol. 83, pp. 317–322, Dec. 2015.

[99] G. P. Moriarty, J. N. Wheeler, C. Yu, and J. C. Grunlan, “Increasing the thermoelectric power factor of polymer composites using a semiconducting stabilizer for carbon nanotubes,” Carbon N. Y., vol. 50, no. 3, pp. 885–895, 2012.

[100] S. Han and D. D. L. Chung, “Carbon fiber polymer–matrix structural composites exhibiting greatly enhanced through-thickness thermoelectric figure of merit,” Compos. Part A Appl. Sci. Manuf., vol. 48, pp. 162–170, 2013.

[101] L. J. Lee, C. Zeng, X. Cao, X. Han, J. Shen, and G. Xu, “Polymer nanocomposite foams,” Compos. Sci. Technol., vol. 65, no. 15–16, pp. 2344–2363, Dec. 2005.

[102] M. Antunes and J. I. Velasco, “Multifunctional polymer foams with carbon nanoparticles,” Prog. Polym. Sci., vol. 39, no. 3, pp. 486–509, Mar. 2014.

[103] C. Okolieocha, D. Raps, K. Subramaniam, and V. Altstädt, “Microcellular to nanocellular polymer foams: Progress (2004–2015) and future directions – A review,” Eur. Polym. J., vol. 73, pp. 500–519, Dec. 2015.

[104] S. P. Nalawade, F. Picchioni, and L. P. B. M. Janssen, “Supercritical carbon dioxide as a green solvent for processing polymer melts: Processing aspects and applications,” Prog. Polym. Sci., vol. 31, no. 1, pp. 19–43, Jan. 2006.

[105] E. Reverchon and S. Cardea, “Production of controlled polymeric foams by supercritical CO_2,” J. Supercrit. Fluids, vol. 40, no. 1, pp. 144–152, 2007.

[106] N. Babcsán, I. Mészáros, and N. Hegman, “Thermal and Electrical Conductivity Measurements on Aluminum Foams,” Materwiss. Werksttech., vol. 34, no. 4, pp. 391–394, Apr. 2003.

[107] S. Liu, J. Duvigneau, and G. J. Vancso, “Nanocellular polymer foams as promising high performance thermal insulation materials,” Eur. Polym. J., vol. 65, pp. 33–45, Apr. 2015.

[108] D. Schmidt, V. I. Raman, C. Egger, C. du Fresne, and V. Schädler, “Templated cross-linking reactions for designing nanoporous materials,” Mater. Sci. Eng. C, vol. 27, no. 5–8, pp. 1487–1490, Sep. 2007.

[109] B. Notario, J. Pinto, E. Solorzano, J. A. A. De Saja, M. Dumon, and M. A. A. Rodríguez-Pérez, “Experimental validation of the Knudsen effect in nanocellular polymeric foams,” Polymer, vol. 56, pp. 57–67, Jan. 2015.

[110] D. Miller, P. Chatchaisucha, and V. Kumar, “Microcellular and nanocellular solid-state polyetherimide (PEI) foams using sub-critical carbon dioxide I. Processing and structure,” Polymer, vol. 50, no. 23, pp. 5576–5584, 2009.

[111] C. Forest, P. Chaumont, P. Cassagnau, B. Swoboda, and P. Sonntag, “Polymer nano-foams for insulating applications prepared from CO_2 foaming,” Prog. Polym. Sci., vol. 41, no. C, pp. 122–145, Feb. 2015.

[112] M. Alvarez-Lainez, M. A. Rodriguez-Perez, and J. A. DE Saja, “Thermal conductivity of open-cell polyolefin foams,” J. Polym. Sci. Part B Polym. Phys., vol. 46, no. 2, pp. 212–221, Jan. 2008.

[113] M. Antunes, J. I. Velasco, V. Realinho, A. B. Martínez, M. Á. Rodríguez-Pérez, and J. A. de Saja, “Heat Transfer in Polypropylene-Based Foams Produced Using Different Foaming Processes,” Adv. Eng. Mater., vol. 11, no. 10, pp. 811–817, Oct. 2009.

[114] H. D. Gesser and P. C. Goswami, “Aerogels and related porous materials,” Chem. Rev.,

vol. 89, no. 4, pp. 765–788, Jun. 1989.

[115] X. Lu, R. Caps, J. Fricke, C. T. Alviso, and R. W. Pekala, “Correlation between structure and thermal conductivity of organic aerogels,” J. Non. Cryst. Solids, vol. 188, no. 3, pp. 226–234, Aug. 1995.

[116] L. Chen, D. Rende, L. S. Schadler, and R. Ozisik, “Polymer nanocomposite foams,” J. Mater. Chem. A, vol. 1, no. 12, p. 3837, 2013.

[117] S. Baseghi, H. Garmabi, J. N. Gavgani, and H. Adelnia, “Lightweight high-density polyethylene/carbonaceous nanosheets microcellular foams with improved electrical conductivity and mechanical properties,” J. Mater. Sci., vol. 50, no. 14, pp. 4994–5004, Apr. 2015.

[118] W. Yang, W. Zou, Z. Du, H. Li, and C. Zhang, “Enhanced conductive polymer nanocomposite by foam structure and polyelectrolyte encapsulated on carbon nanotubes,” Compos. Sci. Technol., vol. 123, pp. 106–114, Feb. 2016.

[119] Y. S. S. Jun, S. Sy, W. Ahn, H. Zarrin, et al., “Highly conductive interconnected graphene foam based polymer composite,” Carbon N. Y., vol. 95, pp. 653–658, Dec. 2015.

[120] M. A. Worsley, P. J. Pauzauskie, T. Y. Olson, J. Biener, J. H. Satcher, and T. F. Baumann, “Synthesis of Graphene Aerogel with High Electrical Conductivity,” J. Am. Chem. Soc., vol. 132, no. 40, pp. 14067–14069, Oct. 2010.

[121] L. Zhao, J. Zhao, X. Sun, Q. Li, J. Wu, and A. Zhang, “Enhanced thermoelectric properties of hybridized conducting aerogels based on carbon nanotubes and pyrolyzed resorcinol–formaldehyde resin,” Synth. Met., vol. 205, pp. 64–69, 2015.

[122] R. Ansari, “Polypyrrole Conducting Electroactive Polymers: Synthesis and Stability Studies,” E-Journal Chem., vol. 3, no. 4, pp. 186–201, 2006.

[123] K. Kurachi and H. Kise, “Preparation of Polypyrrole/Polyethylene Composite Films by the Vapor-Phase Oxidative Polymerization of Pyrrole,” Polym. J., vol. 26, no. 12, pp. 1325–1331, Dec. 1994.

[124] J. J. López Cascales and T. F. Otero, “Molecular dynamic simulation of the hydration and diffusion of chloride ions from bulk water to polypyrrole matrix,” J. Chem. Phys., vol. 120, no. 4, pp. 1951–1957, Jan. 2004.

[125] A. Kaynak and R. Beltran, “Effect of synthesis parameters on the electrical conductivity of polypyrrole-coated poly(ethylene terephthalate) fabrics,” Polym. Int., vol. 52, no. 6, pp. 1021–1026, Jun. 2003.

[126] N. Mateeva, H. Niculescu, J. Schlenoff, and L. R. Testardi, “Correlation of Seebeck coefficient and electric conductivity in polyaniline and polypyrrole,” J. Appl. Phys., vol. 83, no. 6, p. 3111, 1998.

[127] O. Bubnova, Z. U. Khan, A. Malti, S. Braun, et al., “Optimization of the thermoelectric figure of merit in the conducting polymer poly(3,4-ethylenedioxythiophene),” vol. 10, no. 6, pp. 429–433, 2011.

[128] C. Yu, K. Choi, L. Yin, and J. C. Grunlan, “Light-weight flexible carbon nanotube based organic composites with large thermoelectric power factors,” ACS Nano, vol. 5, no. 10, pp. 7885–7892, Oct. 2011.

[129] T. V Vernitskaya and O. N. Efimov, “Polypyrrole: a conducting polymer; its synthesis,

properties and applications," Russ. Chem. Rev., vol. 66, no. 5, pp. 443–457, May 1997.

[130] K. Tada, K. Satake, and M. Onoda, "In Situ Polymerization of Polypyrrole in Alcohols: Controlling Deposition Rate and Electrical Conductivity," Jpn. J. Appl. Phys., vol. 41, Part 1, no. 11A, pp. 6586–6590, Nov. 2002.

[131] M. Li, W. Li, J. Liu, and J. Yao, "Preparation and characterization of PPy with methyl orange as soft template," J. Mater. Sci. Mater. Electron., vol. 24, no. 3, pp. 906–910, Mar. 2013.

[132] T. Dai, X. Yang, and Y. Lu, "Controlled growth of polypyrrole nanotubule/wire in the presence of a cationic surfactant," Nanotechnology, vol. 17, no. 12, pp. 3028–3034, Jun. 2006.

[133] D. Kopecký, M. Varga, J. Prokes, M. Vrnata, et al., "Optimization routes for high electrical conductivity of polypyrrole nanotubes prepared in presence of methyl orange," Synth. Met., vol. 230, pp. 89–96, Aug. 2017.

[134] J. Wu, Y. Sun, W. B. Pei, L. Huang, W. Xu, and Q. Zhang, "Polypyrrole nanotube film for flexible thermoelectric application," Synth. Met., vol. 196, pp. 173–177, Oct. 2014.

[135] ASTM D729, "Standard Test Methods for Density and Specific Gravity (Relative Density) of Plastics by Displacement," Am. Soc. Test. Mater., p. 6, 2008.

[136] A. Fallis, "TCi system for non-destructive determination of thermal properties of materials," J. Chem. Inf. Model., vol. 53, no. 9, pp. 1689–1699, 2013.

[137] S. L. Kodjie, L. Li, B. Li, W. Cai, C. Y. Li, and M. Keating, "Morphology and Crystallization Behavior of HDPE/CNT Nanocomposite," J. Macromol. Sci. Part B Phys.,

vol. 45, no. 2, pp. 231–245, Mar. 2006.

[138] A. Wong, Y. Guo, and C. B. Park, “Fundamental mechanisms of cell nucleation in polypropylene foaming with supercritical carbon dioxide-Effects of extensional stresses and crystals,” J. Supercrit. Fluids, vol. 79, pp. 142–151, 2013.

[139] G. D. Zhan, J. D. Kuntz, A. K. Mukherjee, P. Zhu, and K. Koumoto, “Thermoelectric properties of carbon nanotube/ceramic nanocomposites,” Scr. Mater., vol. 54, no. 1, pp. 77–82, Jan. 2006.

[140] T. Evgin, H. D. Koca, N. Horny, A. Turgut, et al., “Effect of aspect ratio on thermal conductivity of high density polyethylene/multi-walled carbon nanotubes nanocomposites,” Compos. Part A Appl. Sci. Manuf., vol. 82, pp. 208–213, Mar. 2016.

[141] C. M. Ye, B. Q. Shentu, and Z. X. Weng, “Thermal conductivity of high density polyethylene filled with graphite,” J. Appl. Polym. Sci., vol. 101, no. 6, pp. 3806–3810, Sep. 2006.

[142] H. Ding, Y. Guo, and S. N. Leung, “Development of thermally conductive polymer matrix composites by foaming-assisted networking of micron- and submicron-scale hexagonal boron nitride,” J. Appl. Polym. Sci., vol. 133, no. 4, Jan. 2016.

[143] A. Ameli, P. U. Jung, and C. B. Park, “Electrical properties and electromagnetic interference shielding effectiveness of polypropylene/carbon fiber composite foams,” Carbon N. Y., vol. 60, pp. 379–391, Aug. 2013.

[144] G. H. Motlagh, A. N. Hrymak, and M. R. Thompson, “Improved through-plane electrical conductivity in a carbon-filled thermoplastic via foaming,” Polym. Eng. Sci., vol. 48, no.

4, pp. 687–696, Apr. 2008.

[145] K. Zhang, J. Qiu, and S. Wang, “Thermoelectric properties of PEDOT nanowire/PEDOT hybrids,” Nanoscale, vol. 8, no. 15, pp. 8033–8041, 2016.

[146] M. Aghelinejad and S. N. Leung, “Electrical conductivity and humidity sensing properties of PVA/CNT nanocomposites,” Annual Technical Conference - ANTEC, Conference Proceedings, 2016.

[147] P. Xue, K. H. Park, X. M. Tao, W. Chen, and X. Y. Cheng, “Electrically conductive yarns based on PVA/carbon nanotubes,” Compos. Struct., vol. 78, no. 2, pp. 271–277, Apr. 2007.

[148] M. S. P. Shaffer and A. H. Windle, “Fabrication and Characterization of Carbon Nanotube/Poly(vinyl alcohol) Composites,” Adv. Mater., vol. 11, no. 11, pp. 937–941, Aug. 1999.

[149] D. M. Nerkar, M. R. Rajwade, S. E. Jaware, and G. G. Padhye, “Preparation and electrical characterization of free standing PVA-PPy-$FeCl_3$ composite polymer films,” Archives of Applied Science Research, vol. 7, no. 10, 2009.

[150] M. Morad, M. M. Fadlallah, M. A. Hassan, and E. Sheha, “Evaluation of the effect of V_2O_5 on the electrical and thermoelectric properties of poly(vinyl alcohol)/graphene nanoplatelets nanocomposite,” Mater. Res. Express, vol. 3, no. 3, p. 035015, Mar. 2016.

[151] I. H. Kim, D. H. Baik, and Y. G. Jeong, “Structures, electrical, and dielectric properties of PVDF-based nanocomposite films reinforced with neat multi-walled carbon nanotube,” Macromol. Res., vol. 20, no. 9, pp. 920–927, Sep. 2012.

[152] D. Zhang, J. Yang, Q. Jiang, Z. Zhou, et al., "Combination of Carrier Concentration Regulation and High Band Degeneracy for Enhanced Thermoelectric Performance of Cu_3SbSe_4," ACS Appl. Mater. Interfaces, vol. 9, no. 34, pp. 28558–28565, Aug. 2017.

[153] D. L. Medlin and G. J. Snyder, "Interfaces in bulk thermoelectric materials: A review for Current Opinion in Colloid and Interface Science," Curr. Opin. Colloid Interface Sci., vol. 14, no. 4, pp. 226–235, Aug. 2009.

[154] J. Wang, K. Cai, S. Shen, and J. Yin, "Preparation and thermoelectric properties of multi-walled carbon nanotubes/polypyrrole composites," Synth. Met., vol. 195, pp. 132–136, Sep. 2014.

[155] C. J. An, Y. H. Kang, A. Y. Lee, K. S. Jang, Y. Jeong, and S. Y. Cho, "Foldable Thermoelectric Materials: Improvement of the Thermoelectric Performance of Directly Spun CNT Webs by Individual Control of Electrical and Thermal Conductivity," ACS Appl. Mater. Interfaces, vol. 8, no. 34, pp. 22142–22150, Aug. 2016.

[156] B. Paul, A. K. V, and P. Banerji, "Embedded Ag-rich nanodots in PbTe: Enhancement of thermoelectric properties through energy filtering of the carriers," J. Appl. Phys., vol. 108, no. 6, p. 064322, Sep. 2010.

[157] M. Aghelinejad and S. N. Leung, "Fabrication of open-cell thermoelectric polymer nanocomposites by template-assisted multi-walled carbon nanotubes coating," Compos. Part B Eng., vol. 145, pp. 100–107, Jul. 2018.

[158] A. Ameli, M. Nofar, C. B. Park, P. Pötschke, and G. Rizvi, "Polypropylene/carbon nanotube nano/microcellular structures with high dielectric permittivity, low dielectric

loss, and low percolation threshold," Carbon N. Y., vol. 71, pp. 206–217, May 2014.

[159] P. C. Ma, N. A. Siddiqui, G. Marom, and J. K. Kim, "Dispersion and functionalization of carbon nanotubes for polymer-based nanocomposites: A review," Compos. Part A Appl. Sci. Manuf., vol. 41, no. 10, pp. 1345–1367, Oct. 2010.

[160] S. Kirkpatrick, "Percolation and Conduction," Rev. Mod. Phys., vol. 45, no. 4, pp. 574–588, Oct. 1973.

[161] V. D. Punetha, S. Rana, H. J. Yoo, et al., "Functionalization of carbon nanomaterials for advanced polymer nanocomposites: A comparison study between CNT and graphene," Prog. Polym. Sci., vol. 67, pp. 1–47, Apr. 2017.

[162] X. Sun, H. Sun, H. Li, and H. Peng, "Developing Polymer Composite Materials: Carbon Nanotubes or Graphene?," Adv. Mater., vol. 25, no. 37, pp. 5153–5176, Oct. 2013.

[163] K. T. S. Kong, M. Mariatti, A. A. Rashid, and J. J. C. Busfield, "Enhanced conductivity behavior of polydimethylsiloxane (PDMS) hybrid composites containing exfoliated graphite nanoplatelets and carbon nanotubes," Compos. Part B Eng., vol. 58, pp. 457–462, Mar. 2014.

[164] S. Kumar, L. L. Sun, S. Caseres, B. Li, et al., "Dynamic synergy of graphitic nanoplatelets and multi-walled carbon nanotubes in polyetherimide nanocomposites," Nanotechnology, vol. 21, no. 10, p. 105702, Mar. 2010.

[165] D. Yoo, J. Kim, S. H. Lee, W. Cho, et al., "Effects of one- and two-dimensional carbon hybridization of PEDOT:PSS on the power factor of polymer thermoelectric energy conversion devices," J. Mater. Chem. A, vol. 3, no. 12, pp. 6526–6533, Mar. 2015.

[166] E. Pop, V. Varshney, and A. K. Roy, “Thermal properties of graphene: Fundamentals and applications,” MRS Bull., vol. 37, no. 12, pp. 1273–1281, Dec. 2012.

[167] D. L. Nika, E. P. Pokatilov, A. S. Askerov, and A. A. Balandin, “Phonon thermal conduction in graphene: Role of Umklapp and edge roughness scattering,” Phys. Rev. B, vol. 79, no. 15, p. 155413, Apr. 2009.

[168] T. Kuilla, S. Bhadra, D. Yao, N. H. Kim, S. Bose, and J. H. Lee, “Recent advances in graphene based polymer composites,” Prog. Polym. Sci., vol. 35, no. 11, pp. 1350–1375, Nov. 2010.

[169] Z. Xu and M. J. Buehler, “Nanoengineering Heat Transfer Performance at Carbon Nanotube Interfaces,” ACS Nano, vol. 3, no. 9, pp. 2767–2775, Sep. 2009.

[170] J. Yang, H. L. Yip, and A. K. Y. Jen, “Rational Design of Advanced Thermoelectric Materials,” Adv. Energy Mater., vol. 3, no. 5, pp. 549–565, May 2013.

[171] M. Aghelinejad, Y. Zhang, and S. N. Leung, “Processing parameters to enhance the electrical conductivity and thermoelectric power factor of polypyrrole/multi-walled carbon nanotubes nanocomposites,” Synth. Met., vol. 247, 2019.